EXPLORATORY ELECTROMAGNETIC THRUSTER RESEARCH

PHASE II

by

A. C. Ducati, R. G. Jahn, E. Muehlberger
and R. P. Treat

prepared for

NATIONAL AERONAUTICS AND SPACE ADMINISTRATION

Contract NAS w-1513

Plasmadyne
a division of GEOTEL, INC.
Santa Ana, California

NASA CR TR-105204

FINAL REPORT
FR-059-1513

EXPLORATORY ELECTROMAGNETIC THRUSTER RESEARCH

PHASE II

by

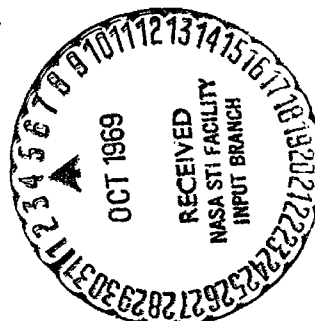A. C. Ducati, R. G. Jahn, E. Muehlberger ·
and R. P. Treat

prepared for

NATIONAL AERONAUTICS AND SPACE ADMINISTRATION
Washington D. C.

June 1969

Plasmadyne
a division of GEOTEL, INC.

Santa Ana, California

FOREWORD

This is the annual report on work carried out during the period
1 February 1968 to 1 February 1969 by Plasmadyne, a division of Geotel,
Inc. on Phase II of "Exploratory Electromagnetic Thruster Research,"
Contract NAS w-1513 originating in the Electrothermal and Electromagnetic
Section, Washington, D. C. under the direction of Jerome P. Mullin.

Adriano C. Ducati was the Principal Investigator in charge of the
direction of the work and preparation of the report. Section 2.2 is presented
by R. G. Jahn and the Appendix is presented by R. P. Treat. Erich
Muehlberger was active in the experimental effort, Ernest Dageford con-
tributed to the improvement of the thrust stand, and Rene' Bregozzo to the
improvement of the vacuum facility and optical systems.

TABLE OF CONTENTS

LIST OF ILLUSTRATIONS

LIST OF ILLUSTRATIONS
(continued)

LIST OF ILLUSTRATIONS
(continued)

1.0 INTRODUCTION

This report describes work done to evaluate the performance of MPD thrusters. A large fraction of the effort is concerned with the effect of environmental conditions on the plume. It is becoming clear that a sizable portion of the arc power is expended externally in the plume, and that ambient gas is rapidly entrained in the jet in a region very close to the thruster. This combination of conditions can affect the thrust produced in a different manner for a test environment than for the environment expected in space. An increased effort on studies of the plume region is therefore considered appropriate.

A vacuum chamber made of insulating material is used to eliminate conducting paths for stray electrical currents and to avoid influencing the magnetic field in the region of the plume. Weak ambient magnetic fields were introduced by wrapping coils around the outside of the test chamber so that the effects of a changing ambient field could be observed. This was found to be a useful diagnostic tool.

For completeness, much of the information presented in the Semiannual Report (Reference 1) is reproduced here, sometimes in abbreviated form. Reference 1 actually covers work performed through August and part of September, and therefore includes the largest portion of the years work. The effort during the last quarter was largely concerned with improving the thrust balance and initiating comparative tests in a metal chamber. The new material is primarily in these two areas.

2.0 STUDIES OF THRUSTER PERFORMANCE

These studies fall into two main groups: examination of conditions in the plume region, and analysis of arc behavior in the vicinity of the electrodes. Sections concerned with the plume are presented first.

2.1 Visual Observation of the Plume

It is believed that a large amount of qualitative information regarding the operation of MPD thrusters can be obtained from a study of the geometry of the plume. There is growing evidence that a significant fraction of the energy added to the gas is added in a region external to the thruster where the electrical discharge pattern is visible in the form of luminous gas excited by collisions with electrons This region is particularly significant in determining the importance of ambient gas entrainment effects. Due to the ease of observation in the visual range, we have limited the initial study to the examination of visual patterns. These may differ from the geometries that would appear in other ranges of the spectrum or by the measurement of other characteristics in the jet region. A great deal of conceptual information can be obtained by studying photographs of the plume; or preferably, by direct observation of the plume.

It has been well established that the visual appearance of the plume is affected by changes in environmental conditions (see References 2 through 5). Figure 1 shows some typical configurations of the jet plume under varying conditions. These have appeared in the literature during recent years. Unfortunately, the best photographic records of plumes miss many details detectable through direct observation. This is largely due to the tremendous range of luminosities throughout the jet. Although color photographs give more information than black and white, they are costly to reproduce and are still lacking in detail. It follows that some verbal description must be given to supplement photographic records. Figure 2 depicts separate zones that have been detected visually in a hydrogen plume. With the present state of knowledge the identification is not definite enough to justify names for these zones. A tentative description, however, may be useful. Region 1 is a bright central region usually referred to as the cathode jet, while region 2 is a less luminous region that we are beginning to associate with the electron beam (to be discussed later). Surrounding this is region 3 which is another luminous region characterized by a shift toward pink coloration. Region 7 is normally referred to as the anode jet and is believed to be excitation caused by electrons returning to the anode. Regions 4 and 6 are less clearly defined and represent luminosity surrounding the central regions and lining the outer region respectively. Region 5 appears to be simply an intermediate region where there is little excitation.

Figure 2. Schematic of Jet Plume Identifying Zones of Different Luminosity and Color as Detected by the Naked Eye

Figure 1. Photographs of Some Typical MPD Arc Jet Configurations as Shown in Recent Literature

A series of tests has been conducted using hydrogen as the propellant to show the influences of changes in the environmental conditions on the appearance of the jet plume. The thruster illustrated in Figure 3 was used in these experiments and its position in the insulating tank is indicated in Figure 4 with the letter "F" (front of tank). For the position "F", which is the only one used in these series of tests, five series of pictures have been taken simultaneously from windows "T" (top), "F_1" (front), "B" (back), "S" (left side) and "F_2" (front right). These pictures do not show all the visible details of the plume so further description will be required. Using a mass flow of 1 mg/sec and an external magnetic field of about 1000 gauss the arc operates at about 100 to 150 volts with a current from 20 to 50 amperes. Its appearance from various points of view is illustrated in the first five images in the first column (zero current) of Figure 5. When the magnetic field of the thruster is increased to 2500 gauss, the plume assumes the appearance shown in the second five images in the first column of Figure 5. At this point a coil of about 20 turns at a diameter of 3 meters was wound around the external part of the insulating tank. With the thruster operating as described before, currents of 2.5, 5, 10, 15, 20, 25, 35, 50, and 100 amperes were passed through the coil with the results illustrated in Figure 5. Let us examine the first series of pictures with a magnetic field of less than 1500 gauss. Without any field applied to the tank, the jet appears as a pink glow around the anode zone measuring about 20 cm in both diameter and length. At the end of this pink glow a faint, well collimated luminosity about 10 cm in diameter extends for more than 1 meter downstream in the tank and bends toward the right side of the tank. This is shown in the first image of the first column of Figure 5. Continued impingement of this beam on the same spot of the tank for a long time produces a permanent burning of the invested surface of the tank (see page 18) and from the outside, an appreciable increase of the spot temperature is felt. When a current of 2.5 amperes is applied to the tank coil, the position of the beam changes as illustrated. It is noted that when no current is applied to the tank a diffuse bluish fog-like glow is evenly distributed in all the internal volume of the tank. As soon as the current is applied to the tank coil the bluish glow seems to be collected toward the axis of the tank. This effect increases with increasing current. The series of pictures shows that under the action of the tank magnetic field (values between 0.1 to 10 gauss) the curvature of the luminous beam toward the tank is reduced gradually until the beam acquires a direction parallel to the axis of the tank for the higher values of field strength. It is interesting to note that in this case the fog-like glow that initially was evenly distributed in the tank volume appears to be concentrated along the axis of the tank. The sequences of the last five lines of Figure 5, where the arc magnetic field is increased to 2500 gauss while all the other conditions remain unvaried, follow a similar pattern especially at the high values of the tank magnetic field. In this case it is apparent that the luminous beam, so well defined at low values of the arc magnetic field strength, is more diffused but still present and influenced by the tank magnetic field. The fog-like glow in the tank follows the same

4
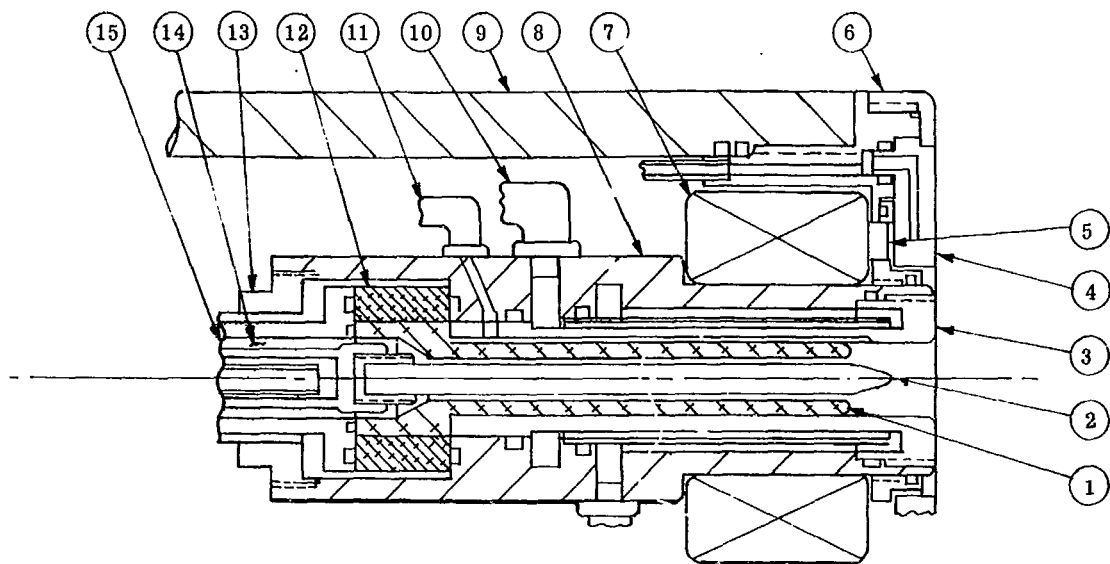
1. Insulator (rapid interchangeable)
2. Cathode (rapid interchangeable)
3. Anode (rapid interchangeable)
4. Front shield (water-cooled)
5. Flexible diaphragm
6. End cap
7. External magnetic field coil
8. Anode housing
9. Insulated thruster arm housing
10. Cooling water inlet
11. Arc chamber pressure tap
12. Insulator
13. Lock nut
14. Propellant injection passage
15. Cathode housing

Figure 3. Typical Design of Plasma Accelerator Used During Tests
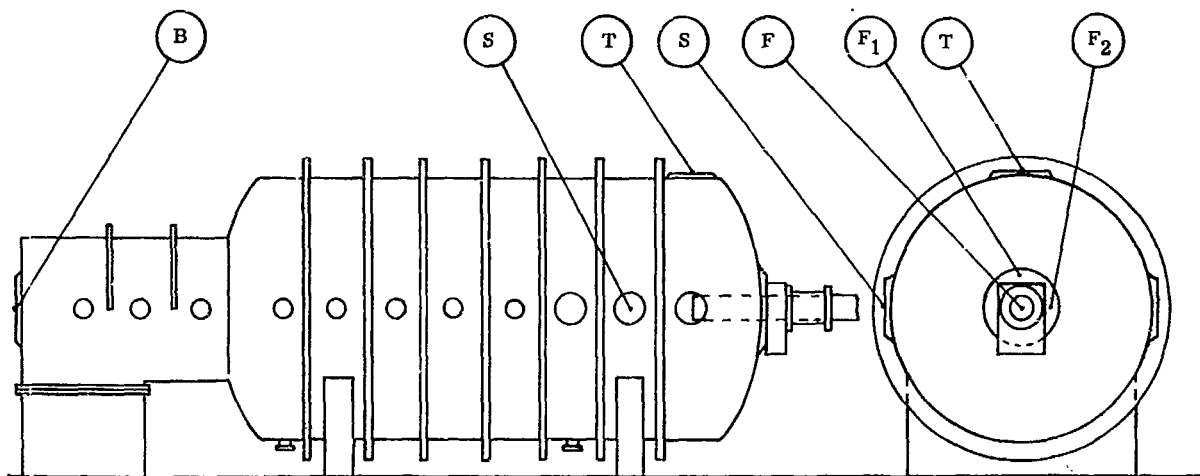
Figure 4. Schematic of Vacuum Tank Showing Thruster Position and
Camera Viewing Points

5
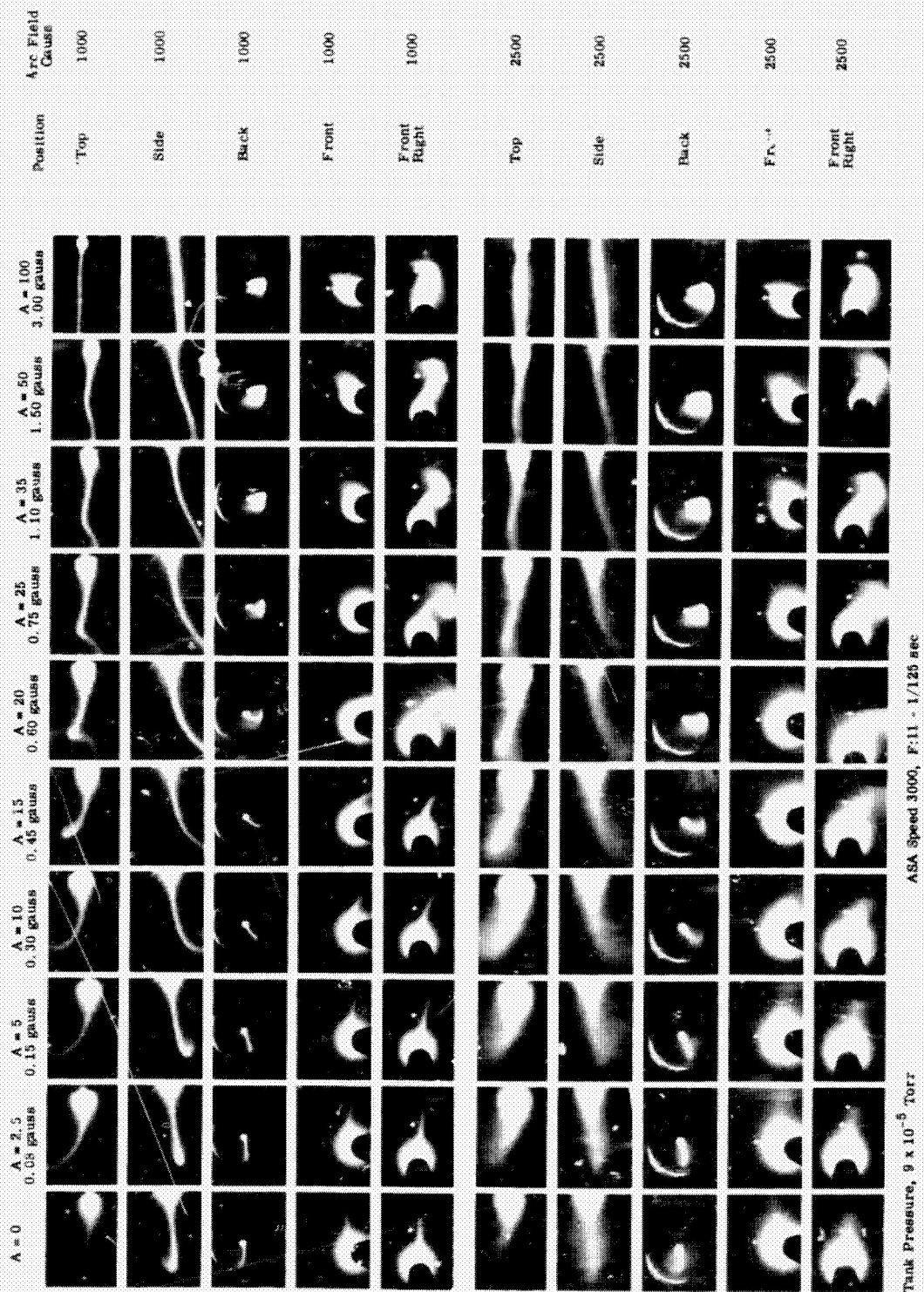
Figure 5. Effect of Changing Tank Field on Jet Geometry From 5 Viewing Positions

Tank Pressure, 9×10^{-5} Torr

ASA Speed 3000, F:11 · 1/125 sec

A = 0	A = 2.5 0.08 gauss	A = 5 0.15 gauss	A = 10 0.30 gauss	A = 15 0.45 gauss	A = 20 0.60 gauss	A = 25 0.75 gauss	A = 35 1.10 gauss	A = 50 1.50 gauss	A = 100 3.00 gauss	Position	Arc Field Gauss
										Top	1000
										Side	1000
										Back	1000
										Front	1000
										Front Right	1000
										Top	2500
										Side	2500
										Back	2500
										Front	2500
										Front Right	2500

patterns with the difference that its intensity at low levels of tank magnetic field is higher. The identification of the luminous beam has been attempted using the procedures described in the following section.

It is interesting to note that when the field of the tank is strong enough, a straight beam 10 to 20 cm in diameter is produced along the axis of the tank. An aluminum plate inserted along the path of this beam is easily melted. It was found that the luminosity of the beam changes slightly from day to day even when the experimental conditions were apparently unvaried. However, further investigation showed that the visibility of the jet is affected by even slight variations in the vacuum level of the tank. More exactly, the luminosity increases rapidly with increasing pressure. The range of pressures tested is from 5×10^{-5} to 4×10^{-5} torr. To observe this effect, a gas was separately injected into the tank and the amount of flow varied to change the tank pressure. The series of pictures in Figures 6 and 7 show the effect of changing the pressure about two orders of magnitude (from 5×10^{-5} to 5×10^{-3} torr). The increase in luminosity was so marked that the photographic exposure had to be decreased in two steps (at 1×10^{-4} and 1×10^{-3} respectively) to avoid excessive overexposure. Figure 8 shows side views of the jet for a number of values of tank pressures. The maximum change in configuration seems to be obtained when the tank pressure is around 10 to 50 microns. A further increase in pressure decreases both the luminosity and the length of the beam as illustrated in the picture sequence of Figure 8.

At this point a test was made to see if further information could be obtained by the injection of different gases to change the pressure level in the tank. Hydrogen, helium, nitrogen, and argon were used. The most important results obtained with this test (which unfortunately cannot be illustrated here due to the high cost of color reproduction) are: a) the discovery of a strong variation of the arc voltage with the environmental pressure and with the type of gas used (the maximum effect was obtained using nitrogen), b) the change of the color and of the luminosity of the fog-like glow in the tank with the kind of gas injected (pink for hydrogen, green for helium, rose for nitrogen, and blue for argon), and c) the apparent penetration of the color corresponding to the gas injected in the thin central zone of the jet (generally called cathode jet). These three qualitative results seem sufficiently important to justify a more complete analysis concerned with the mechanism of the acceleration process and of some still unexplained anomalies.

The observations indicate that a sizable fraction of the arc power is expended externally in the plume. It is expected that it will be possible to estimate the size of the fraction when a more systematic series of tests have been made in which a second type of gas is alternately introduced as the propellant and as the environmental gas. It is evident that this analysis can be greatly improved if spectroscopic, photographic and visual methods are used together and correlated with other basic diagnostic instrumentation. A series
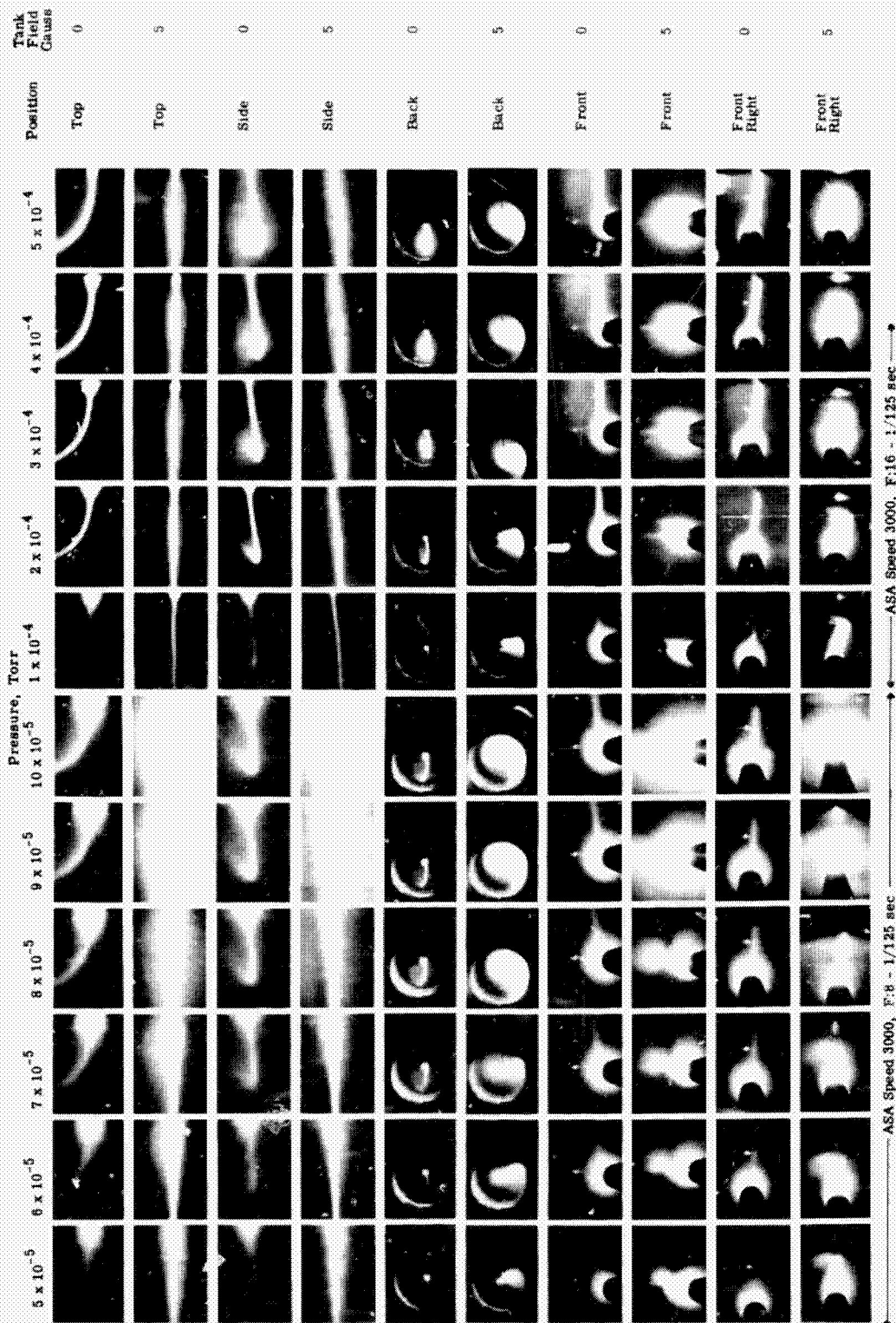
Figure 6. Effect of Tank Pressure on Jet Luminosity From 5 Viewing Positions

8
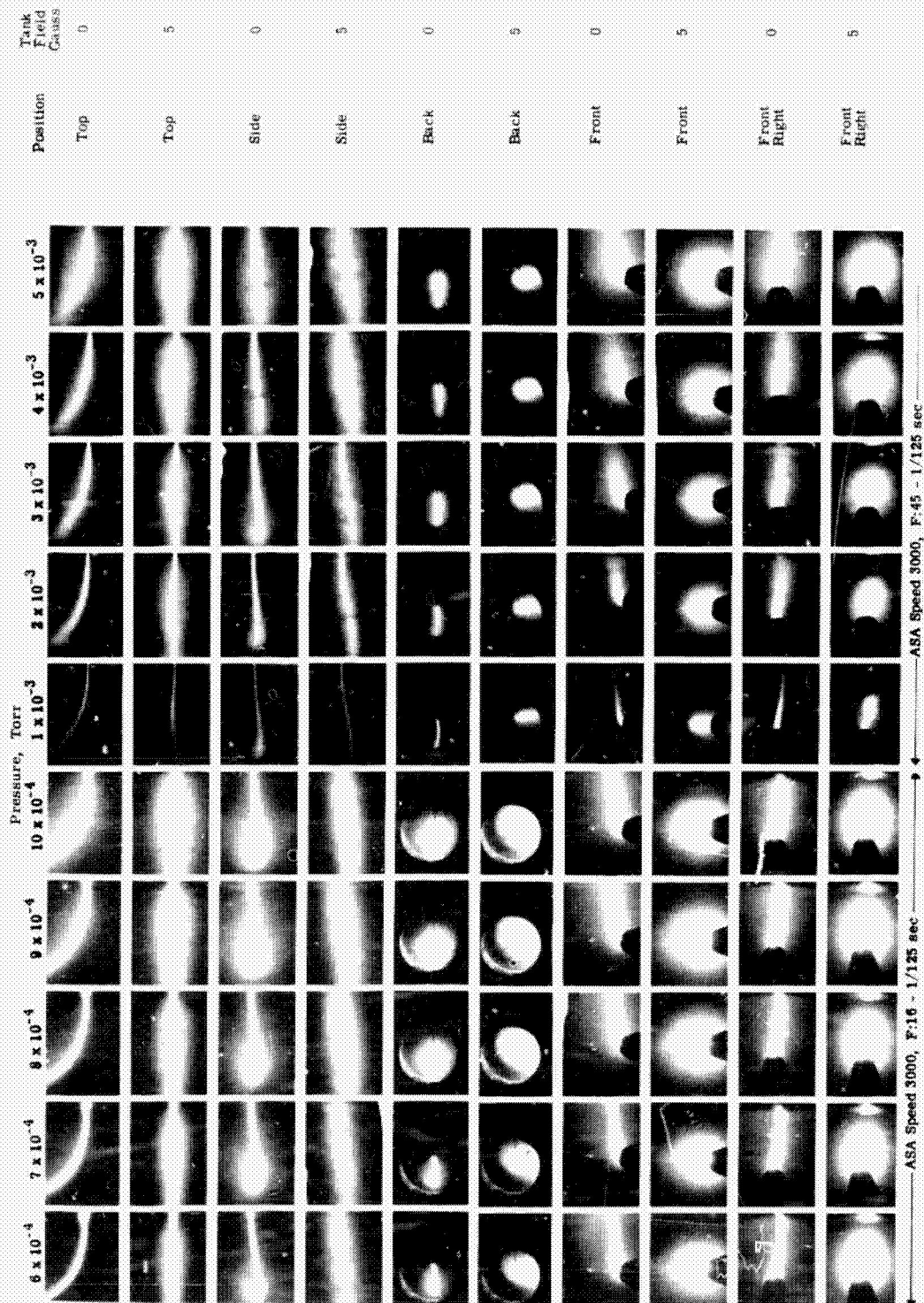
Figure 7. Effect of Tank Pressure on Jet Luminosity From 5 Viewing Positions

9
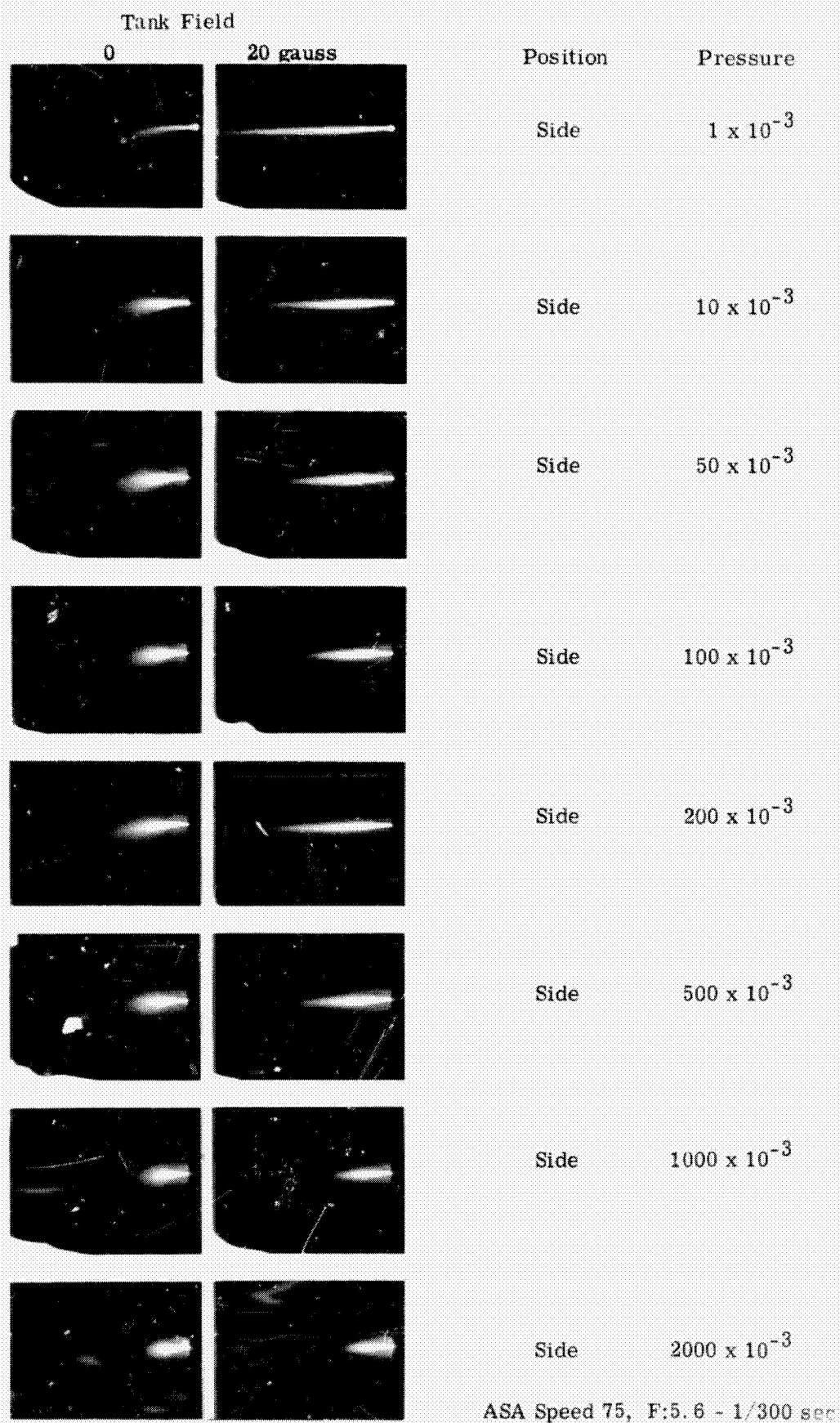
Figure 8.   Effect of Increased Tank Pressure on Jet Luminosity From
One Viewing Position

of measurements using electrical probes at various points in the tank has been initiated and the first quantitative results are now being reduced and will be integrated in the near future with a new series of tests now in progress (these include the study of the rotational mode of the arc of which some details are given in Section 2.4). As soon as the new thrust stand with high sensitivity is operative, thrust data will be obtained for the above described tests. This should provide a better understanding of their importance in the development of this type of accelerator.

Plans are also being made to survey the plume region with a pressure probe. The probe is to be rotatable about two axes to permit flow direction as well as an indication of flow velocity to be obtained. An effort will be made to obtain rapid response so that moderate frequency oscillations in the flow pattern can be detected.

The observation of the plume is expected to be a continuing effort with the goal of providing an improved data base for use in testing various analytical and conceptual models of the thruster performance.

2.2   Experiments for the Identification of a Cathode Jet

Figure 16 of Reference 2 shows a view from a top window of the insulating tank looking downward at the top of the thruster. The same picture is reproduced in this report in black and white as Figure 9a, while Figures 9b and 9c show the same plume as observed respectively from the back and side of the tank.

a.   b.   c.
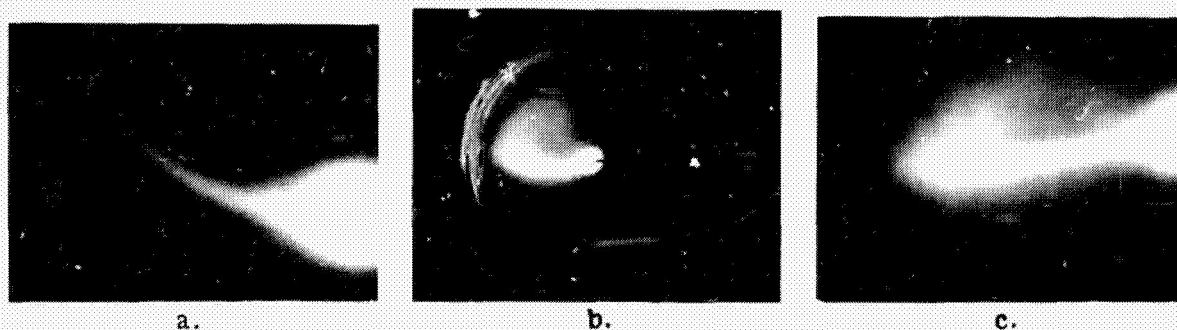
Figure 9.   Three Views of Beam From MPD Arc

The device is operating with a hydrogen flow of 1 mg/sec and a power of a few kw. This was one of the first observations of the exhaust plume of a normal thruster operating in the insulating tank. The most striking feature of this jet is the constant bending toward the right side of the thruster (observed from the top as illustrated in Figure 9a). It is not yet clear if the straight jet that we observed in a metal tank many years ago (Reference 3, page 263, Figure 187) is of the same species; but this may be resolved by further experiments.

Rotation of the thruster around its axis and changes in various operating parameters of the thruster did not change the arc of curvature. However, significant effects were noted when the various magnetic fields were changed. At very high values of the arc magnetic field a diffuse appearance was obtained; permanent magnets brought close to the zone of the jet from outside of the insulating tank produced distinct effects of attraction or repulsion; and a few turns of conducting wire wound around the tank produced strong effects on the jet geometry when small currents were circulated in it. Changing the polarity of this coil or of the arc magnetic field produced distinct changes in the curvature of the beam suggesting that it is of an electronic nature (Reference 2, page 26). The beam is long, tenuous and well-collimated, and has a luminous region which emerges along the centerline from the more intense portion of the plume near the orifice and projects far downstream in a gentle curve toward the tank sidewall. Analysis of the observations seems to clearly identify the phenomenon as an electron beam; however, its origin is still uncertain. In the following part of this section the procedure used to tentatively identify the character of the beam is described.

At the outset it is important to distinguish between the subject phenomenon and the more familiar "cathode jet" commonly observed in magnetoplasmadynamic arc operation over a broad range of conditions. The latter is a sharply defined, intense jet in the center of the plume, clearly emanating from the emission spot on the cathode surface, and tightly constrained by the axial external field. For example, if the emission spot should migrate around the cathode surface, that cathode jet may be seen to precess about the centerline along the surface of revolution defined by the field line through the cathode spot. In contrast, the more diffuse beam that interests us here is found to be sensitive to the bias field in only a secondary way, and over a substantial range of this parameter it executes essentially the same trajectory through the tank, and strikes the wall at the same location.

For the more detailed description and analysis to follow, we refer to operation under the following nominal conditions: The accelerator consists of a 1/4-inch tungsten cathode centered within a 5/8-inch straightbore, tungsten-clad orifice in a 1-1/2-inch face diameter, water-cooled, copper anode (Figure 3). The cathode tip is a blunted cone of 3/8-inch length, withdrawn 1/2-inch upstream of the anode face. The bias coil consists of 28 turns of mean diameter 2-1/8 inches coaxial with the cathode, with centerplane 1-1/4 inches upstream of the anode face. At its centerpoint, this coil provides a nominal field of 1000 gauss, in the downstream direction. Arc voltage and current are set at 150 volts and 50 amperes, respectively, and the hydrogen mass flow at 1.0 milligram per second. At this throughput, the fiberglass vacuum tank, which is 8 feet in diameter and 18 feet long, can be maintained at a background pressure of 1×10^{-4} torr by its 52-inch diffusion pump.

Under these conditions, the subject beam appears as a diffuse, pink-blue column 2 or 3

inches thick, bent into the configuration shown in Figure 9. The major element of its trajectory is a nearly circular, clockwise arc in the horizontal projection of radius 26 inches, extending almost 1/2 revolution from its emergence from the main plume to its intercept with the tank wall (Figure 9a). Superimposed on this is a nearly circular deflection in the projection plane transverse to the thruster axis, of radius 62 inches, clockwise in the upstream view (Figure 9b), which combines with the major horizontal curve to yield a hook-like projection in the vertical plane containing the axis (Figure 9c). Near its intersection with the wall, the beam appears to broaden somewhat, and then to splay out along the surface in all directions.

In view of the low pressures and correspondingly large mean free paths prevailing over most of the long trajectory, it seems reasonable to suspect a nearly collisionless beam of charged particles, undergoing deflection in the prevailing magnetic field. Important to realize in this regard is that the field from the small bias coil is essentially dipolar, and decays to negligible magnitude over most of the beam trajectory, leaving only the earth's magnetic field to impose the observed beam deflection. Specifically, for the test conditions quoted, the bias field falls below the earth's field 1½ inches from the orifice, at which point the major beam deflection is just beginning. Assignment of the beam deflection to the earth's field is also suggested by the prominence of the effect in this dielectric vacuum tank, in contrast to steel tanks which tend to shield the beam from external fields.

To check this hypothesis, a large coil has been appropriately wound on the outside of the vacuum tank, for the purpose of cancelling the earth-field component. In the Santa Ana area, the earth's field has a horizontal intensity of 0.257 gauss, an inclination of 15° east of true north, and a dip angle of 59° to the horizontal.[6] The resultant magnitude is almost precisely 0.50 gauss. Since the axis of the vacuum tank points due south from the arc orifice, the inclined coil plane is set nearly orthogonal to the vertical plane through the tank axis, as shown in Figure 10. With three turns, of mean radius about 80 inches, some 53 amperes should just cancel the earth's field at the coil center. Experimentally, it is found that 45 amperes is the optimum value, at which condition the beam is essentially
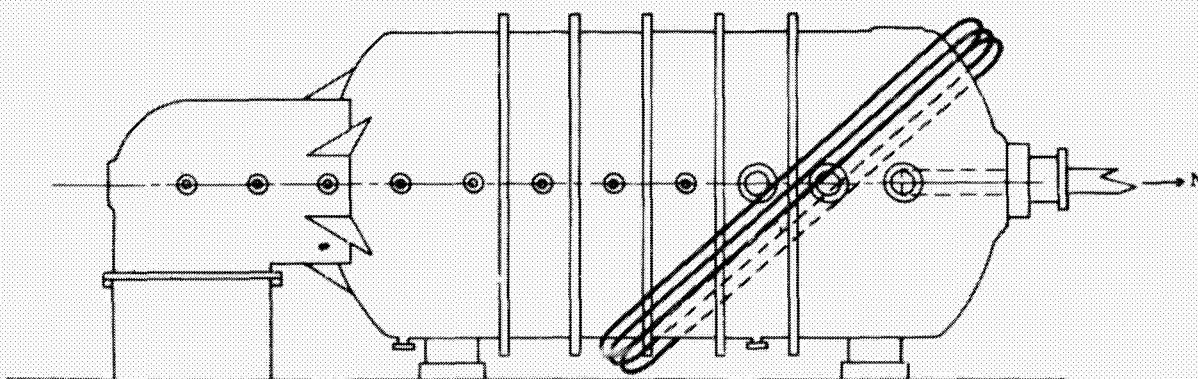
Figure 10. Exterior Coil to Buck Earth's Magnetic Field

13

straightened, and projects well down the tank centerline before diffusion into invisibility (Figure 11c). Doubling of the optimum bucking-coil current deflects the beam to the opposite tank wall in a trajectory essentially symmetric to that seen in the earth's field (Figure 11e). The discrepancy between the calculated and observed current values is readily

a. b. c.

d. e.
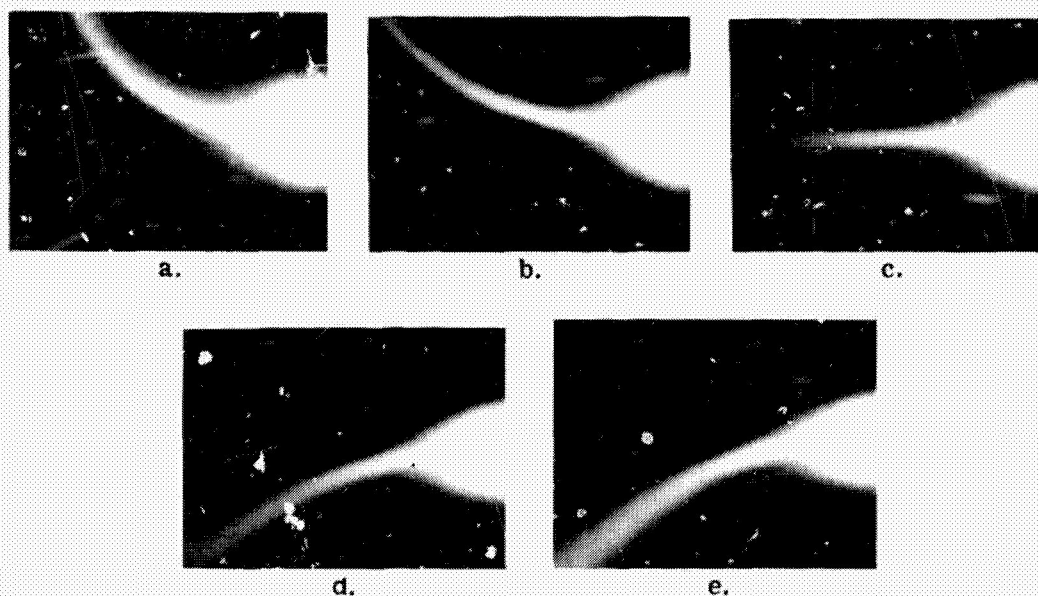
Figure 11. Effect of Bucking Field on Beam Trajectory (Top View)

closed by inclusion of the small contribution of the arc bias coil in this region, and by allowance for the nonuniformity of the bucking-coil field over the beam trajectory. The influence of the earth's field on the beam thus seems established.

The sense of deflection in these fields indicates that the beam consists of negatively charged particles emerging from the accelerator, and since there is no precedent for negative hydrogen ions in this environment, we henceforth presume that the particles involved are electrons. It then is instructive to estimate the energy of these electrons from the dimensions of their trajectories in known fields. The arc bias field is difficult to employ for this purpose since it is so highly nonuniform, but for the reason mentioned above, if we only consider elements of the trajectory beyond 15 inches from the orifice, this field component may be neglected, at least to first order.

With no other field than that of the earth prevailing, we deal with the classical situation of a charged particle injected with a given velocity vector, $\underline{v}$, into a uniform, but inclined field, $\vec{B}_e$. The resulting trajectory is a helix of radius

$$R = \frac{mv_\perp}{qB_e} \qquad (1)$$

transcribed with a circular period

14

$$\tau = \frac{2\pi m}{qB_e}$$
$$\tag{2}$$

and having a turn spacing

$$s = v_{\shortparallel}\, \tau \tag{3}$$

where $v_{\perp}$ and $v_{\shortparallel}$ are the components of $\vec{v}$ perpendicular and parallel to $\vec{B}$, respectively, and q and m are the charge and mass of the particle, all in the mks system. Under the nominal operating conditions, only about one-half turn of the helix is completed before the trajectory intersects the tank wall. Insertion of the observed radius, projected on the helix base plane, in (1) yields a value for the particle velocity of 5.73×10^6 m/sec; division of the observed trajectory length by the half-period gives the value 5.80×10^6 m/sec with both estimates considered accurate to ± 10 percent.

An independent estimate of particle energy can be made by superimposing another uniform component of magnetic field, and observing the change in the beam configuration. The most convenient implementation has been to wind an evenly-spaced solenoid on the outside of the vacuum tank, coaxial with it, to provide a reasonably uniform north-south component of magnitude comparable with, but less than the resultant earth field (Figure 12). The first order effects of this field component, B_s, are to change $v_{\shortparallel}$, and thus the helix turn spacing, and to tip the helix base plane. Axial views of the trajectory for three values of B_s are shown in Figure 13. Briefly, it is found that 0.15 gauss is just sufficient to cancel the earth's north component (plus the small contribution from the arc bias coil) yielding a transverse plane projection that is radially straight, i.e., the helix degenerates into a circle of zero pitch, in a plane containing the tank axis. Analysis of the curvature introduced into this projection by changes of ± 0.15 gauss from this value then yields indicated velocities of 5.62×10^6 m/sec and 6.68×10^6 m/sec, respectively, these estimated accurate to ± 15 percent.

Considering the relative and absolute accuracies of the various methods, we select a mean value of $v = 5.93 \times 10^6$ m/sec ± 10 percent, to which corresponds the convenient particle energy value

$$\epsilon = \frac{1}{2} mv^2 = 100 \text{ e.v. } \pm 20\%. \tag{4}$$

In comparison with the arc terminal parameters quoted above, this corresponds to 2/3 of the full arc voltage, and raises fundamental questions about the origin of this high energy electron beam in the magnetoplasmadynamic arc environment.

Some indication of the source of the electron beam might be derived from systematic variation of the arc operating parameters about the nominal conditions, but this is not readily accomplished. For a given electrode geometry and gas type, the arc voltage, current, bias field and gas flow rate are functionally interlocked in a particular arc mode;

15
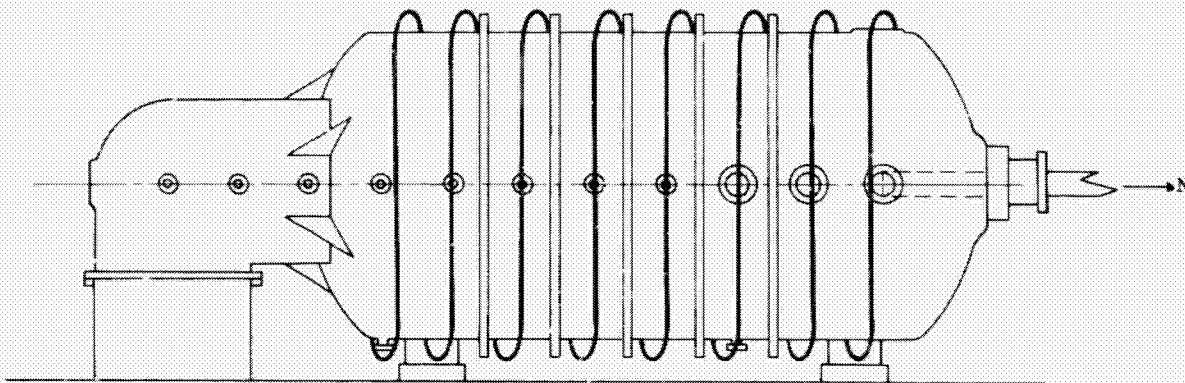
Figure 12. Exterior Coil to Change North-South Beam Field Component
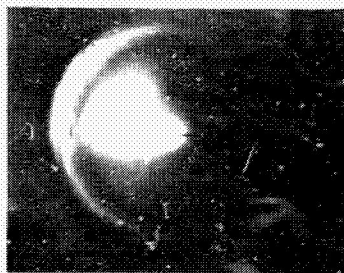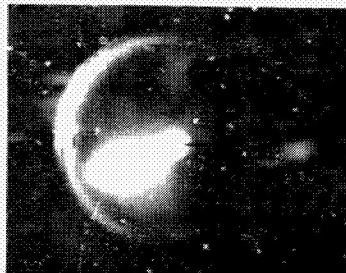
a. $B_S = 0$ b. $B_S = 0.15$ gauss   c. $B_S = 0.30$ gauss

Figure 13. Effect of Axial Field on Electron Beam (Upstream View)

variation in one of these parameters predicates first order change in at least one other. A common example is the increase in arc voltage with bias field at constant current. Occasionally, for obscure causes possibly involving the cathode emission pattern, an arc will elect a different mode of operation and display a different functional relation among its terminal parameters, whereon it is possible to duplicate all but just one of the nominal conditions. In such rather irregular events, it has been possible to ascertain, for example, that a drop in arc voltage from 150 to 110 volts produces a beam helix of correspondingly smaller radius and pitch, and that a drop in arc current from 50 to 20 amperes does not affect the beam geometry, per se. Similarly the principal effect of a bias field increase from 1000 to 3000 gauss is found to be a brightening of the main plume near the orifice, with little change in the character of the long beam emerging from it. Based on these isolated examples of the effect of single parameter change, the observed behavior of the beam under continuous variation of arc parameters in a given mode of operation appears consistent, e.g., an increase in beam helix size appropriate to the arc voltage increase predicated by the larger bias field, etc.

Variation of tank background pressure produces striking changes in the luminosity of the beam (see Section 2.1). Over the range from 10^{-4} to 10^{-3} torr, the visible brightness of the beam increases by orders of magnitude, suggesting that the luminosity is provided by background particles, excited by inelastic impact of the electrons in the beam. Above 5×10^{-3} torr, the beam appears to have difficulty penetrating the background gas, first disappearing at its tail near the tank wall, and, by 3×10^{-2} torr, retracting completely within the confines of the near plume. Above this pressure, no visible beam emerges but the near plume appears slightly displaced radially in the same direction as the beam deflection at lower pressures, as if by reaction to containment of the beam within itself. Obstruction of the beam in this pressure range is in agreement with simple mean free path calculations for 100-volt electrons in molecular hydrogen, using established total cross sections.[7] Background of argon and nitrogen have also been bled into the tank, both of which define the beam more brilliantly in their characteristic hues, and both of which extinguish it in roughly the same high pressure range.

One conceivable source of the observed beam would be a jet of "runaway" electrons whose existence in the magnetoplasmadynamic arc environment has been suggested in other connections.[3] The plasma properties in the arc chamber, as best they are known, satisfy at least marginally the Spitzer[8] and Dreicer[9] criteria for the onset of the runaway phenomenon, provided the medium contains only fully stripped ions and electrons. For the energies available here, this restricts the possibility to pure hydrogen; yet, when the arc is supplied with a 50 percent mixture of argon and hydrogen mass flow, or when it ingests argon or nitrogen from the tank background, its beam intensifies, rather than extinguishes. Further, the beam may be observed at arc power below 2 kw, where it is doubtful that even pure hydrogen is fully dissociated and ionized.

Thus it seems that the acceleration of the beam electrons must occur in a legitimately low density region of the arc, say $n < 10^{12}$ cm^{-3}, where their mean free path is long compared to the acceleration path length. Based on arc chamber pressure measurements of 0.7 torr, this would seem to indicate some portion of the plume well outside the orifice. Yet it is difficult to conceive of an electric field configuration which can deliver two-thirds of the arc potential in this region, and equally difficult to explain the excellent beam collimation, presumably provided by the bias magnetic field, in a region where the electron gyro radius is not substantially smaller than the beam width.

The remaining alternative is to postulate an unusually low density corridor for electron acceleration from the cathode tip out through the anode orifice well into the plume, possibly sustained by a pumping action of the jet or of the electron beam itself. Some suggestion that such a strong positive radial pressure gradient exists is provided by the immediate appearance in the core of the plasma of the foreign gases purposely injected into the tank during the backpressure experiments described above. In this concept the device would resemble an electron gun, or electrostatic sprayer, with pointed cathode and ring anode, and the current conduction near the cathode and anode might involve separate streams of electrons and ions, as first suggested by Stratton.[10]

Regardless of the details of its origin, the observed electron beam, if not properly obviated, could complicate the operation of a magnetoplasmadynamic arc as a space thruster. On the one hand, if the beam were to circle about some local or external magnetic field and return to the anode or to some other portion of the spacecraft, surface damage could result. As evidence of the vigor of this beam, its region of normal intersection with the vacuum tank wall has become visibly charred (see Figure 14). Attempts to probe it

Figure 14. Beam Impact Zone Showing Charring of Insulating Tank Inner Wall

electrostatically have suffered from rapid heating of the probe to incandescence. Even when straightened by the bucking field its impact on probe supports far down the tank produces visibly glowing hot-spots after only a few seconds. On the other hand, if the field geometry were to keep the beam from returning to the spacecraft, some neutralization provision might be required to balance the negative charge loss. In either case, the beam involves disproportionately large power drain, since at its apparent specific impulse, its power to thrust ratio is very high.

Clearly the relative importance of any of these effects depends on the fraction of total arc current involved in this beam, and this is a difficult measurement to make accurately by any of the usual magnetic or electric probing methods because of the very small current density, relatively large background fields and charge densities, and the hostile thermal environment. That the current density is small follows first from elementary space-charge considerations. For example, assuming that the current distribution across the beam is reasonably smooth, that the background ionization provides negligible space-charge neutralization, and that the beam spreading is mainly electrostatic rather than thermal, the observed ratio of beam length to diameter indicates a total beam current of less than 10^{-3} amperes, and corresponding electron density between 10^5 and 10^6 cm^{-13}.[11] A rudimentary Langmuir probe survey has been made through the beam near its impingement on the wall, and this shows a departure from ion saturation current in the neighborhood of 70 to 80 volts, and indicates a high energy electron current component of a few milliamps. Without more detailed studies, it seems reasonably assured then that the beam carries only a small portion of the total arc current.

For application as a space thruster, the prosaic solution may simply be to avoid domains of operation where the electron beam emerges from the main plume, e.g., by different bias field strengths and configurations, higher chamber pressures, etc. Nevertheless, better understanding of this phenomenon may shed light on other aspects of the arc structure and acceleration mechanisms, and prove useful in dealing with other troublesome aspects of magnetoplasmadynamic arc operation, notably the excessive heat transfer to the anode surface, and the re-entrainment of ejected gas.

2.3   Comparative Tests Conducted in Insulating and Conducting Tanks

The tests conducted in the insulating vacuum chamber show thruster behavior that has not been previously observed. To distinguish between effects of environment and effects of thruster design, arrangements were made to repeat tes , using the same thruster in a metal tank. An aluminum tank was used to permit magnetic fields to be introduced which are similar to those generated by coils wrapped around the insulated vacuum chamber. The tests are primarily to permit observation of the effects of electrical conduction in the vacuum chamber.

The arrangement used is illustrated in Figures 15 and 16. It consists of an aluminum tank in series with the insulating tank. The testing procedure is as follows: The thrust stand and thruster is withdrawn far enough to permit the insulating tank valve to be closed. The thrust stand is then moved to the extreme wall of the testing building leaving a space of about 10 feet between it and the insulating tank. The valve with its large flange is removed from the insulating vacuum tank and connected to the metal tank which has two mating flanges on opposite ends. The metal tank is moved laterally and its second flange is attached to the insulating tank where the flange supporting the valve was connected before. At this point the thruster is pushed through the valve seat into the metal chamber.

Tests have started in the metal tank, but there is not yet enough data available to permit meaningful comparisons with and without an insulated tank. It has however been established that an electron beam occurs and behaves in an aluminum tank in much the same way as the beam observed in the insulating tank. This was noted in an initial series of tests made in the metal tank with a magnetic field coil wrapped around the test chamber as shown in Figure 17. The effect is shown in Figure 18 where the beam is seen leaving the metal tank and entering the insulating tank. The characteristic curvature of the beam is seen with the curvature decreasing progressively as the magnetic field strength is increased. This behavior would have been expected from observations in the insulated tank.

To determine the effect of a more intense magnetic field on the beam, the smaller coil pictured in Figure 19 was mounted adjacent to the thruster. Pictures of the plume are shown in Figures 20 and 21. Two views are given for each operating condition simply to include a wider field. Field strengths noted are for external field which is superimposed on a constant field due to the thruster field coil (about 50 gauss at the center). It is seen that the beam becomes very concentrated and well collimated at the high field strengths.

2.4 Experiments on the Rotational Mode of the Arc

It is well-known that in some circumstances the arc can rotate or oscillate at very high frequencies. Recently this mode of operation was suspected of contributing to the acceleration process in magnetoplasmadynamic systems.[12] Various experiments have been conducted for the detection of rotation of an arc spoke in the anode region, but the influence of this mode of operation on the efficiency of acceleration has not yet been established. Based on a theoretical analysis which is given in the Appendix, a series of experiments has been designed to establish the characteristics of the rotational mode of the arc operation and later to determine the influence of these modes on the efficiency of propulsion. It is evident that to obtain satisfactory results from the experimental study, it is necessary that the measurements of the rotational and propulsion parameters be conducted simultaneously. For this reason it was decided to provide for optical observation of rotation of the

20
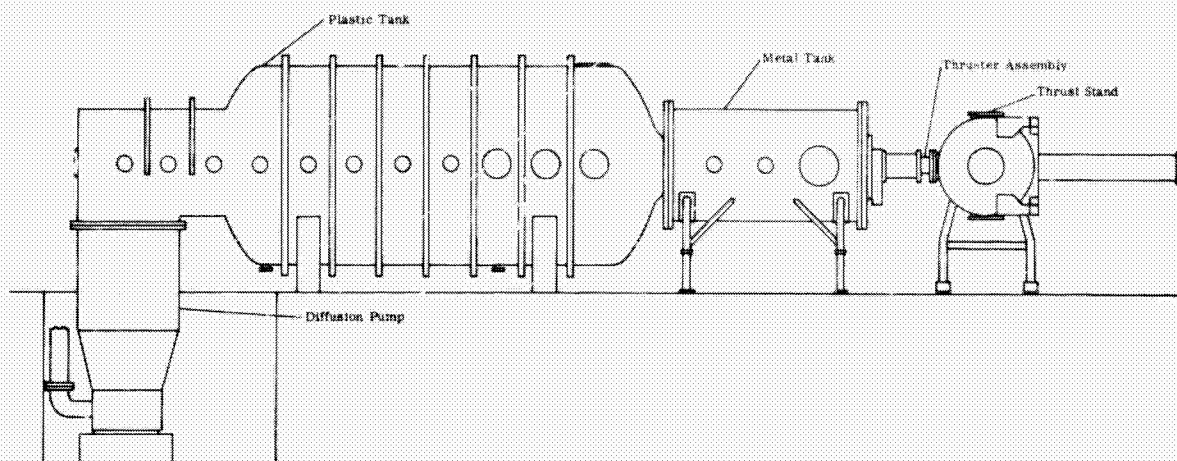
Figure 15. Schematic of Vacuum Test Facility Showing Inserted Metal Tank
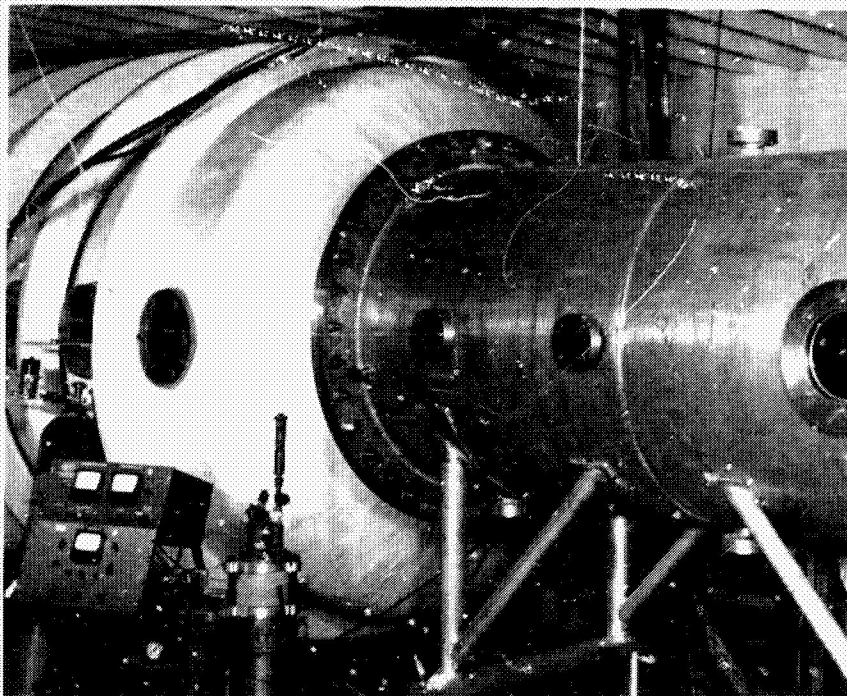
Figure 16. Close-up Photograph of Aluminum Tank Inserted Between
Plastic Tank and Thrust Stand

21
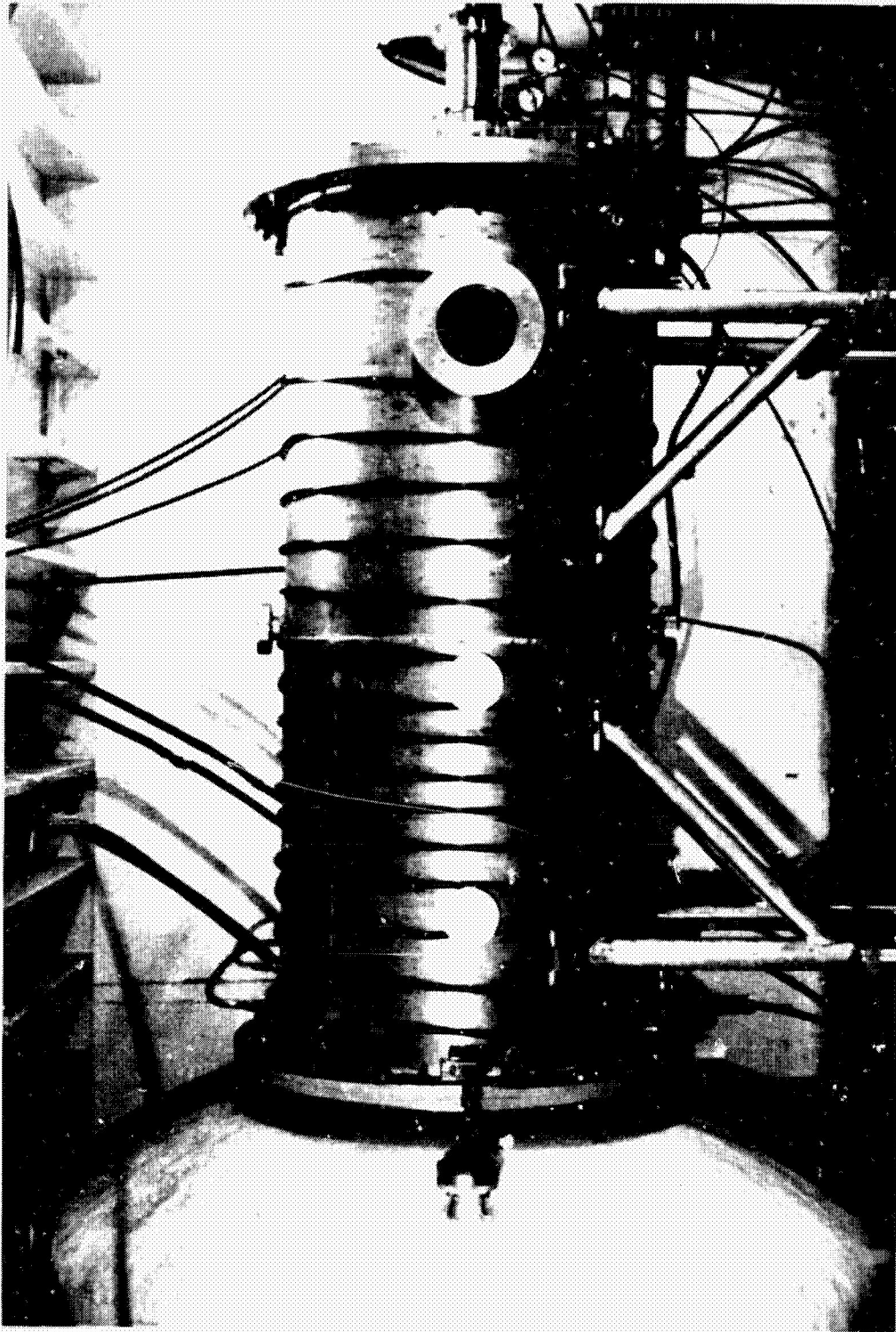
Figure 17. Aluminum Test Chamber With External Magnetic Field Coil Installed

22

a. 10 gauss   b. 20 gauss

c. 30 gauss   d. 40 gauss

e. 350 gauss   f. 450 gauss

Figure 18. Beam Trajectory Across Two-Foot Window Between Tanks
for Different Fields Applied to Metal Tank
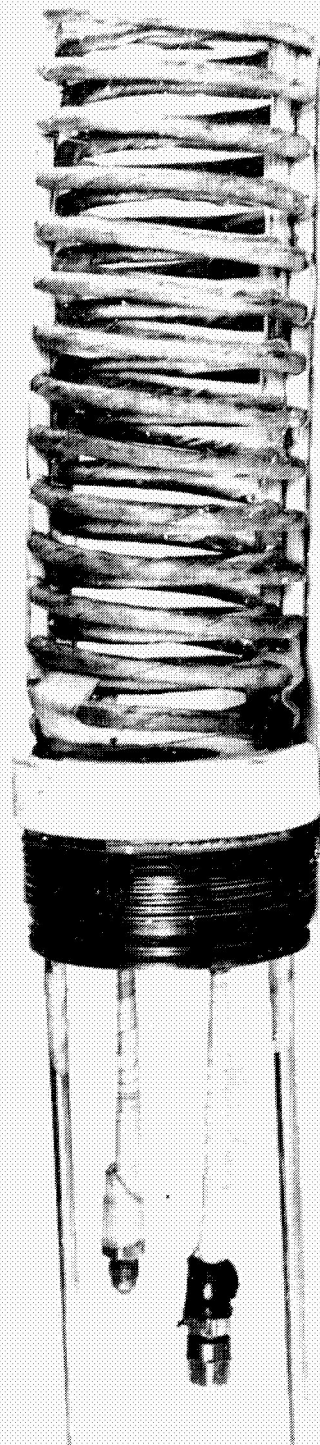
Figure 19. Auxiliary Magnetic Coil Applied After the Thruster Throat

a. Ratio, 1:1
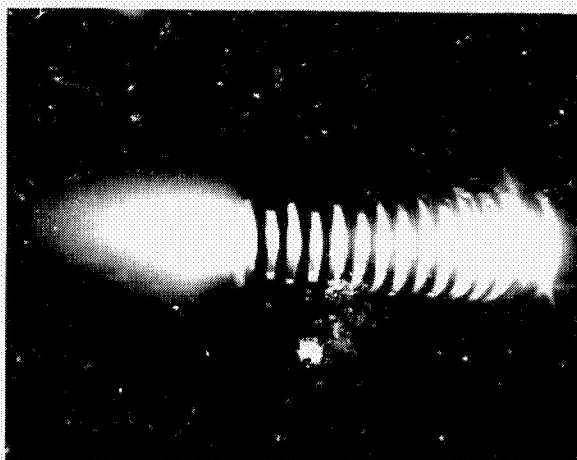
b. Same Condition as a

c. Ratio, 1:3
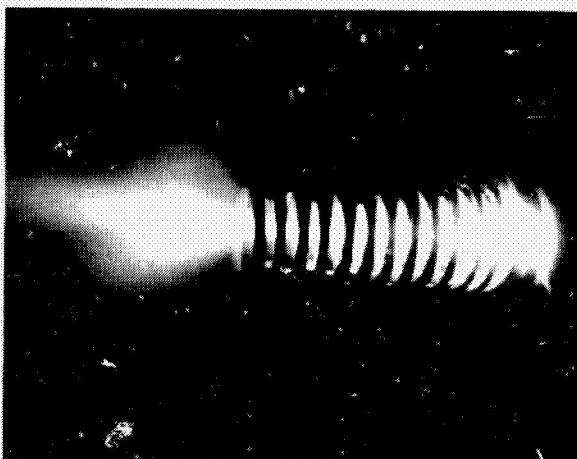
d. Same Condition as c
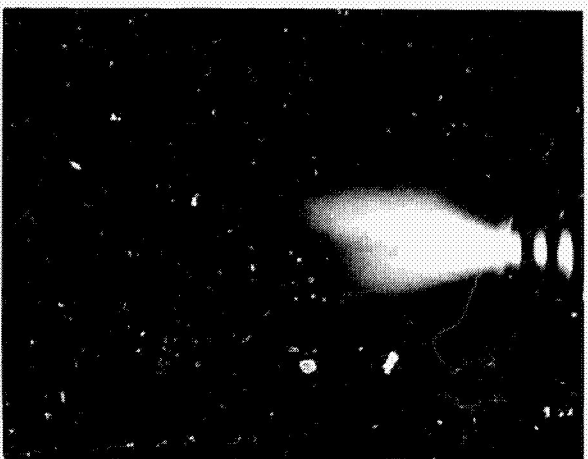
e. Ratio, 1:5
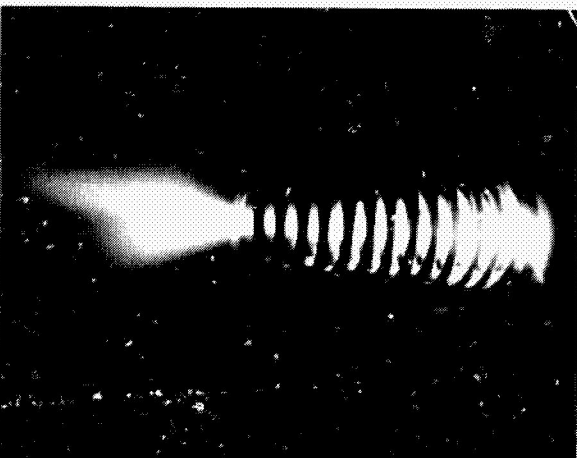
f. Same Condition as e

Figure 20.   Change of Plume Geometry With Different Ratios Between
Arc and Auxiliary Magnetic Fields
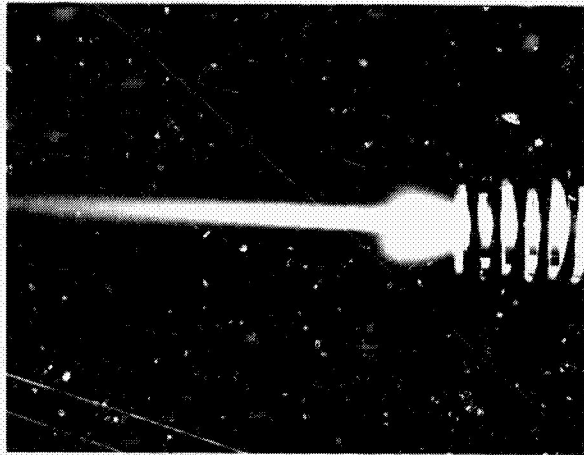
a. Ratio, 1:100
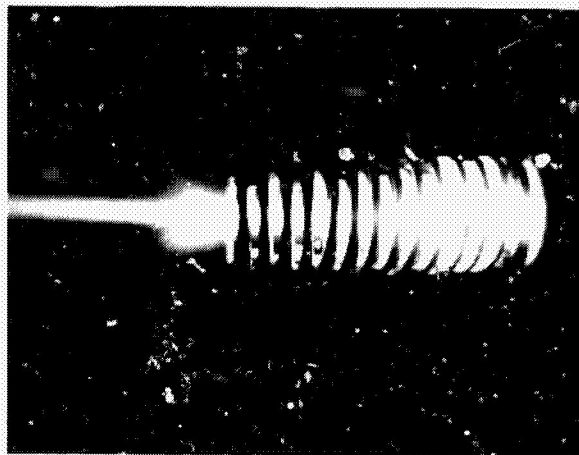
b. Same Condition as a
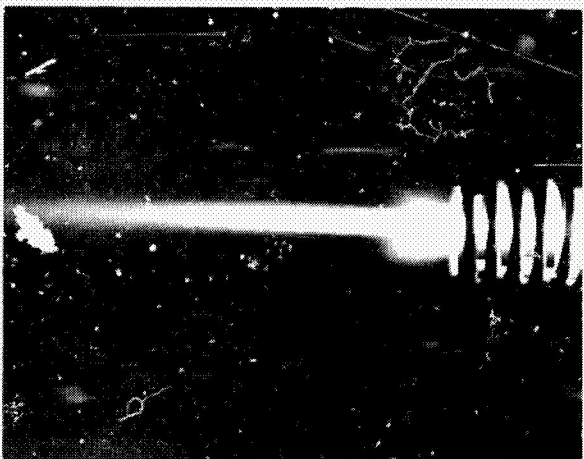
c. Ratio, 1:200
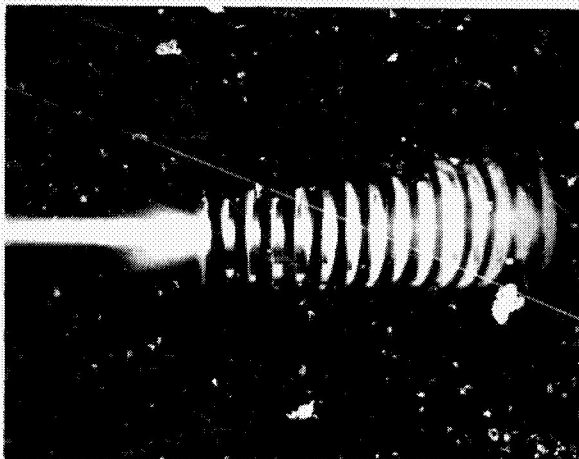
d. Same Condition as c
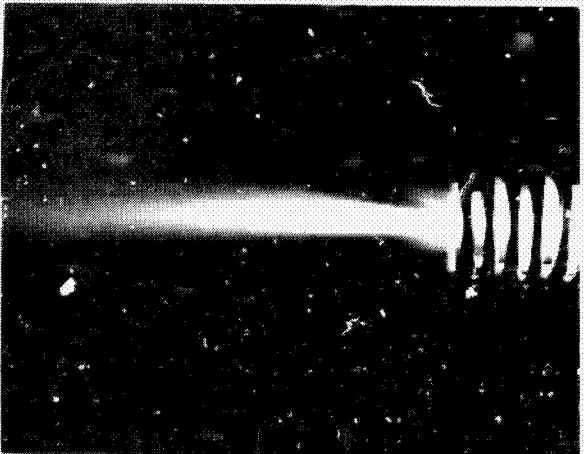
e. Ratio, 1:300
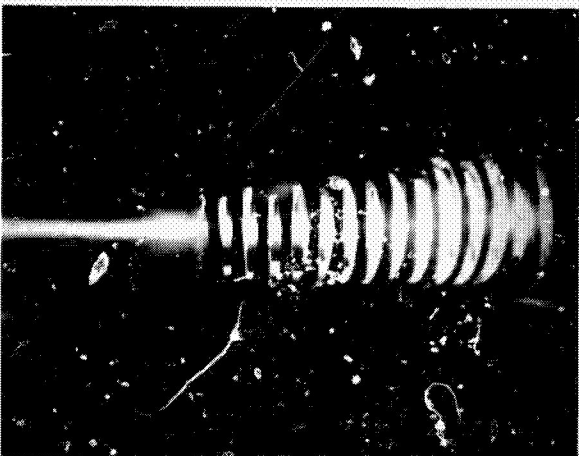
f. Same Condition as e

Figure 21. Change of Plume Geometry With Increased Ratios Between
Arc and Auxiliary Magnetic Fields

arc discharge without interference with the thrust measurements.

Figure 22 shows the simple optical system devised for the measurement of the rotational speed. At the back (B) of the insulating tank, along the axial line, is a 4.5 inch viewing
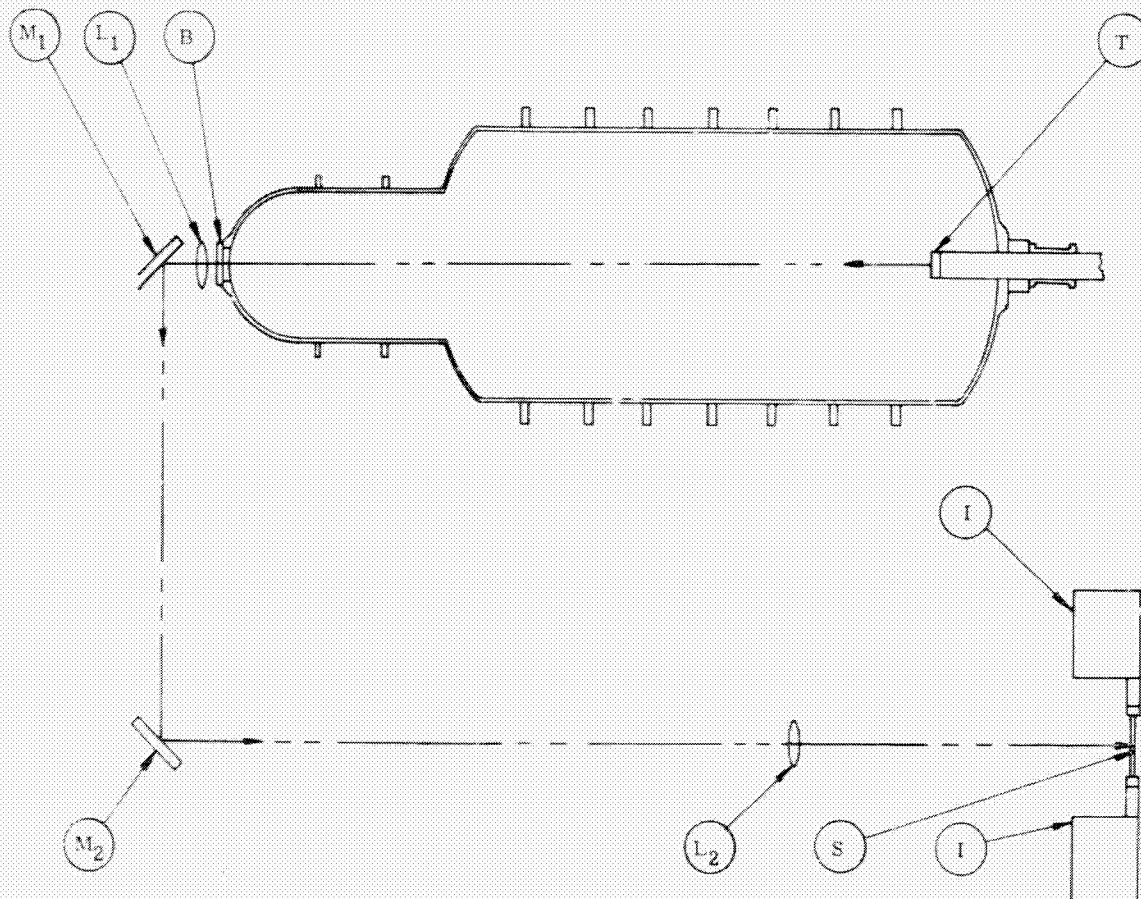
Figure 22. Schematic of Optical System Used for the Projection of the Arc Image

port where a long focal length lens (L$_1$) is fixed. This lens images the thruster throat (T), which is about 7 meters away, on a translucent screen with the aid of two front surface mirrors (M$_1$ and M$_2$) and an additional interchangeable lens (L$_2$). By changing the focal length of L$_2$, it is possible to enlarge the image of the thruster throat to any magnification desired on the screen (S). The screen is conveniently located with all the other instruments (I) necessary for the measurements of the thruster characteristics (top left, Figure 23). In this manner the operator has the operating conditions of the cathodic and anodic space of the arc under constant observation. Information can be obtained visually, photographically, photoelectrically and spectrographically without requiring elaborate instrumentation.

27

Figure 24. Close-up Photograph of Viewing Screen and Dual Optical Detector Used for Measurement of Arc Rotation

Figure 23. Instrumentation Used for Measurement of Thruster Performance Parameters Including Projection of Arc Image on Viewing Screen (top left)

28

To explore the various zones of the arc it has been found convenient to use one or more fiber optic lines connected to sensors and capable of being moved across the image on the surface of the translucent screen. When the absorption of the screen material reduces the sensitivity of detection, the complete screen can be removed and the exploration conducted directly at the image plane. To maintain the optical fibers in the right position a special support has been devised as illustrated in Figure 24. For the detection of the rotational frequency the procedure is as follows: The image of the anode is first sharply focused on the translucent screen. Next, the center of the fiber optics support is moved until it coincides with the cathode spot of the arc. Then the two supports of the fiber optics are brought close together so as to look at practically the same luminous spot (Figure 25). In this position the two optical detectors (photomultipliers) connected at the other end of two fiber optics are regulated to give an identical output potential. These two voltages are fed to a dual beam oscilloscope which can easily detect the frequency of the rotating spot. On the screen of the oscilloscope the separate images from the two photomultipliers will show the same frequency of rotation with practically the same phase because the fiber optics are looking at practically the same spot on the arc image (Figure 25a). As soon as the two fiber optics are separated (Figures 25b through 25f), a difference of phase results depending

a.   b.   c.

d.   e.   f.
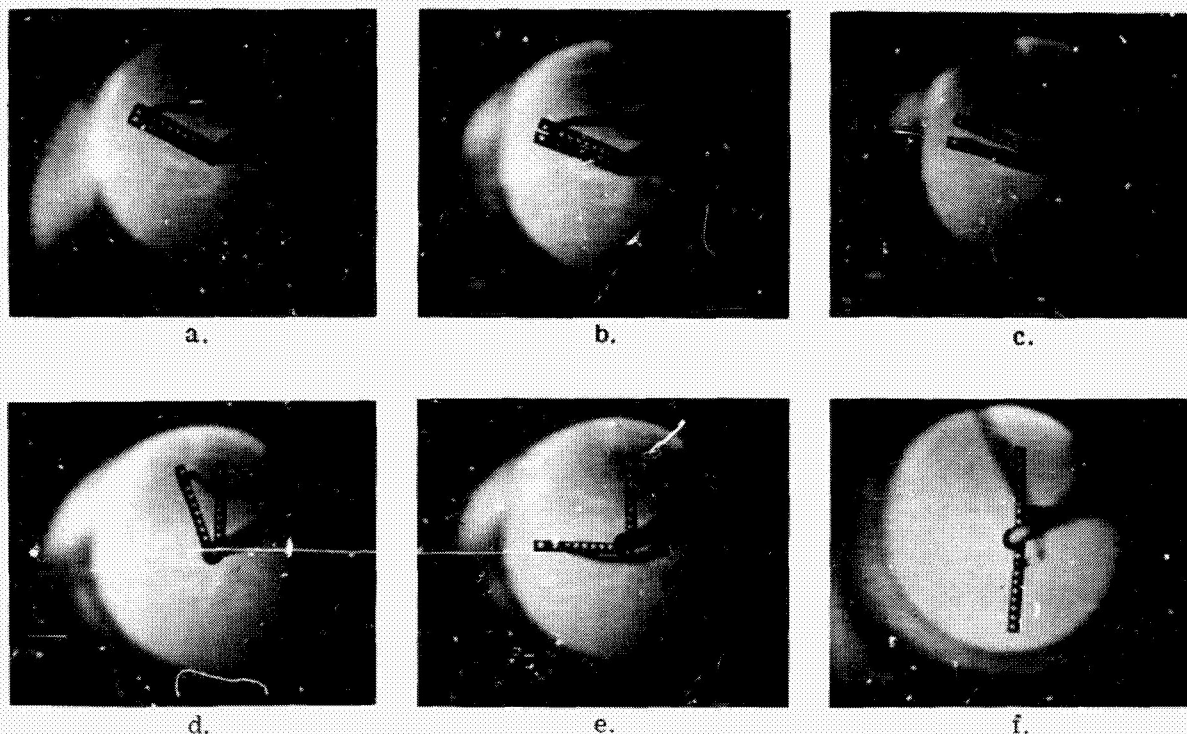
Figure 25. Close-up Photographs of Dual Optical Detector
Showing Various Angular Positions on Arc Image

on the time required by the luminous spot to pass from one fiber sensor to the other. When the two fiber sensors are close together (as in Figure 25a) the resulting image is as shown in Figure 26. When the sensors are at 180' (as in Figure 25f) the resulting image is as shown in Figure 27. However, because of a continuous slight change in the rotational frequency it is difficult with this method to obtain a sharp repetitive image for measuring the rotational frequency. During the first tests we found that the reproducibility does not seem completely reliable. In particular the differences in phase shift are sometimes un-correlated. In spite of these unresolved difficulties, a few frequencies have been found for some arc conditions. These were in excess of 100 kc. Slight variations around this value were obtained by varying the magnetic field and the arc current. Further experiments will be necessary to better establish these values and to find the exact dependence of the rotational speed on the various operative parameters of the arc.

While this simple method of measuring the rotational speed is being improved, the optical system described has been found very useful for the continuous monitoring of the arc image and especially of the electrode behavior in various conditions of operation. It has been noted that some instabilities of the arc appear to be connected with the instability of the cathode spot which often migrates from one point to another of the cathodic region. A correlation between the inclination of the arc jet and the position of the cathodic spot has also been found. Some sources of instability of the jet have been connected to the tempera-ture of the cathode. The effect is maximum when the temperature is just sufficient to support the arc discharge. From this first series of experiments it appears that this simple optical imaging setup can be used in a variety of applications.
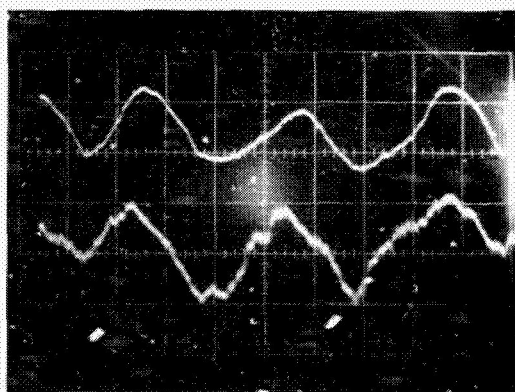
Figure 26. Oscillogram of
Figure 25a
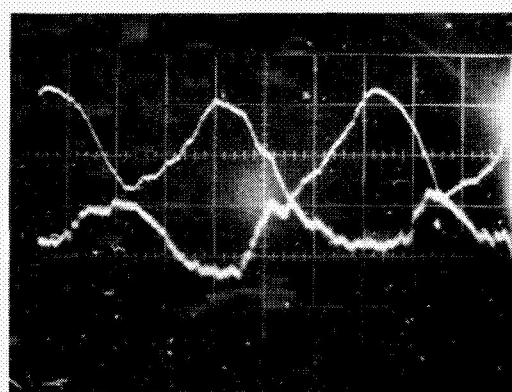
Figure 27. Oscillogram of
Figure 25f

3.0 REFINEMENT OF THE TEST FACILITY

A substantial amount of work has been done in ir proving the vacuum system and the thrust balance and is reported below. Although the work on the vacuum system is summarized here, the reader is referred to Reference 1 for a more detailed description of this activity.

3.1 The Vacuum System

The following are the major improvements that have been made in the vacuum system:

a.   Vacuum valves have been installed at all locations where occasional access is required to the test chamber. Locations include the port for introducing thrusters, ports for inserting probes, connections for the attachment of vacuum gauges and ion gauges, and even some of the windows which are equipped with valves so they can be cleaned without releasing vacuum in the chamber. When thrusters or probes are to be introduced into the chamber, a sliding seal is provided so that sealing is obtained before the valve is opened. This arrangement permits vacuum to be maintained continuously in the chamber. (See Reference 1 for photographs.)

b.   A small diffusion pump has been provided for maintaining a vacuum in the chamber between test periods. It has been found that the small pump produces less backstreaming of oil vapors and a slower rate of deposit of oil on windows and test equipment during down times. Furthermore, it would be much less expensive to provide a condensing baffle for the small pump than for the large pump used during tests.

c.   A technique has been developed for controlling pressure in the chamber using two methods. With the diffusion pump in operation, pressure is controlled by injecting gas into the tank; while at higher pressures, with the diffusion pump stopped, pressure is controlled by a throttle valve in the forepump line. With these methods, pressure may be varied in an essentially continuous way over a range of six orders of magnitude.

d.   Experiments have shown that the backstreaming of oil is undesirably high unless higher forepumping speeds are used than those recommended by the diffusion pump manu-facturer. The use of a second smaller diffusion pump in series with the large pump is suggested as the most economical way of reducing the backstreaming to an acceptable level.

3.2 Ultra-sensitive Thrust Stand

During the past year a major effort has been made to improve the performance of our new precision thrust balance to achieve the original goals of sensitivity and reliability. To date, this effort has been only partially successful, but it seems appropriate at this time to present a detailed review of the various problems that have been encountered, and of the procedures

that have been followed to solve them. This account, which covers the following fifty pages, is essentially a technical report of its own which gives the flavor of the painstaking trial and error techniques required in this work, and hopefully will be of use to others faced with the same task.

Two factors increase the need for good accuracy in the measurement of thrust for this program. First, the goal is to determine differences in apparent performance that result from changes in environmental conditions (such as use of nonconducting versus a conducting test chamber). It is important to be able to repeat thrust measurements with sufficient accuracy that any significant environmental effects will not be masked by random errors. Second, it is desired to perform the tests at the lowest feasible ambient pressure level and in a test chamber that is large compared to the size of the jet. With existing limitations in vacuum system and test chamber size, it follows that a low propellant flow must be selected with a correspondingly low thrust. For these reasons, a special effort has been made to evaluate the performance of the thrust balance and to determine possible ways of improving its sensitivity and accuracy.

Early in the program, it was decided to measure thrust by mounting the thruster directly on a balance rather than attempting to interpret measurements of force acting on a thrust plate located in the jet. Recent measurements of the flow pattern in a test chamber (reported in Reference 13) show that the jet entrains surrounding gas very rapidly. In the confines of a test chamber, an eddy develops with a backflow region surrounding the jet. Since the gas in the eddy has momentum added repeatedly as it recirculates, there is not a clearcut relation between the integrated momentum in the downstream flow and the momentum in the jet at the nozzle exit. This differs from the case of an unconfined jet for which the gas that is entrained may be assumed to have been initially at rest. The entrainment rate has been shown to increase rapidly as gas temperature is increased. To avoid an uncertainty in the meaning of the momentum measurement, it would be necessary to use the thrust plate so close to the nozzle exit that questions regarding interaction effects would arise. This adds to the difficulty of interpreting force measurements on a plate at very low Reynolds numbers and in strongly non-uniform flow.

We have therefore elected to undertake the problem of supplying propellant, coolant and electrical power to a very sensitive thrust balance without disturbing the reading. The task is uniquely difficult because very large currents (up to 500 amperes in the field coil) are required on a thrust platform that must eventually measure thrusts in the neighborhood of 150 mg with good accuracy. Although the difficulties are formidable, there are methods for checking the performance of the instrument, and it should be possible to place a higher degree of confidence in the final results.

The thrust stand used for this program is shown in Figures 28 through 34. A unique feature of the instrument is that it is housed in a separate chamber with an arm extending
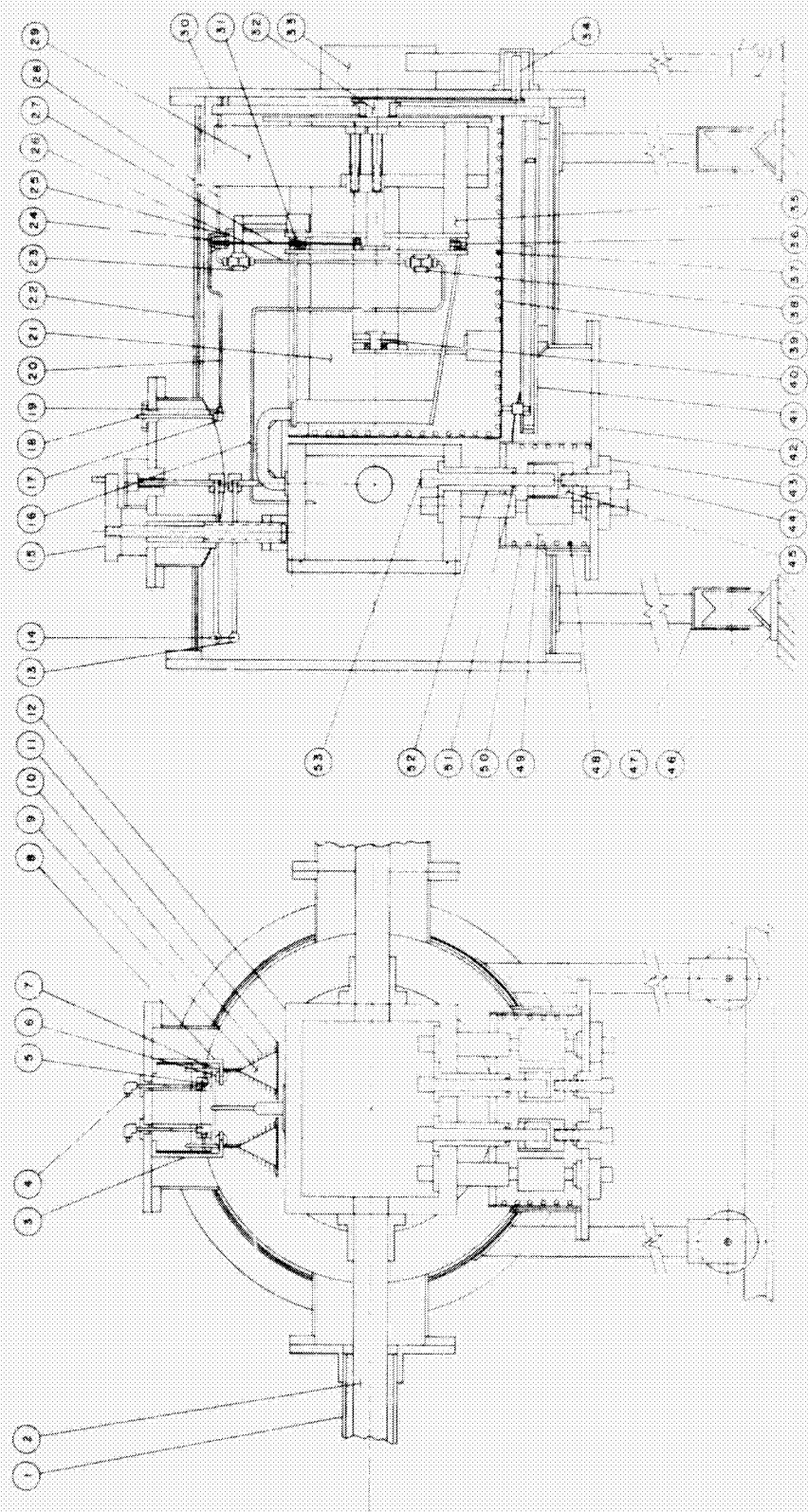
Figure 28. Detailed Drawing of the Complete Thrust Stand

33

LEGEND

1. Plastic tube
2. Aluminum tube assembly
3. Thrust level system
4. Shaft
5. Miter gears
6. Jewel bearing pulley
7. Rack and pinion gear
8. Thrust calibration system
9. Aluminum cone
10. Weights
11. Platen
12. Thruster support housing
13. Linear variable differential transformer armature
14. Linear variable differential transformer mount
15. Locking device
16. Metal tube
17. Pinion gear
18. Rotating shaft
19. Rack gear
20. Lever arm
21. Vacuum oil
22. Outer shell
23. Mounting block
24. Suspension wire fastener
25. Torsion assembly
26. Teflon tube

27. Torsion spring device
28. Metal tube
29. Counterbalance
30. Rear plate
31. Ball bearing and guide pin
32. Shaft and bearing assembly
33. Auxiliary wheel support
34. Lever and adjustment assembly
35. Torsion wire support
36. Bearing and guide pin assembly
37. Copper tubes
38. Rotatable mounting block
39. Inner assembly
40. Shaft and bearing assembly
41. Internal track
42. Bottom mounting plate
43. Electrical insulator
44. Copper bus bar
45. Mercury pot
46. Track assembly
47. Leg assembly
48. Copper tubes
49. Oil bath
50. Vacuum oil structure
51. O-ring seal
52. Electrical insulator
53. Copper bus bar
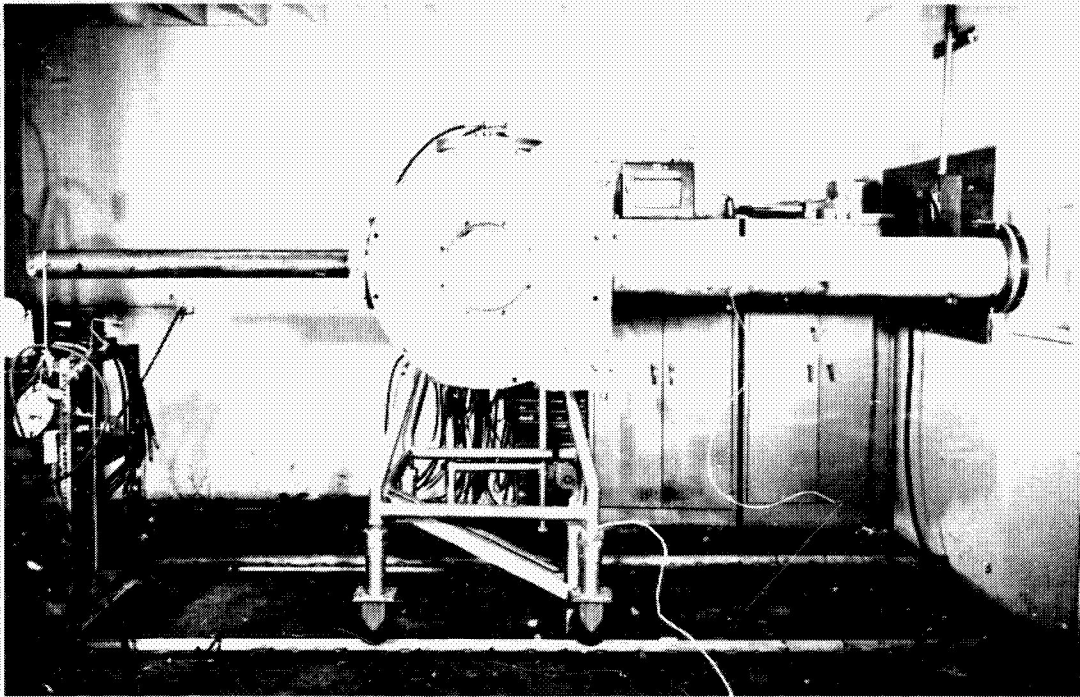
Figure 29. Side View Photograph of Thrust Stand Showing Plastic Tube
Thruster Housing (left) and Balance Arm Assembly (right)
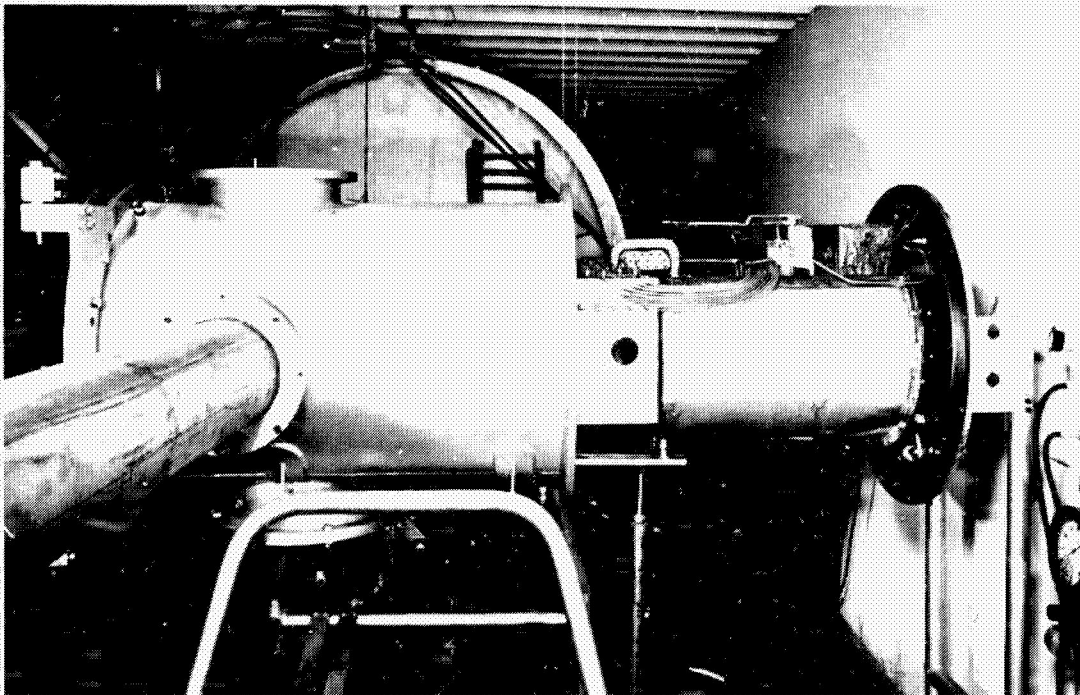
Figure 30. Close-up Photograph of Thrust Stand Balance Showing Multiple
Fluid Connecting Lines with Dampening Oil Bath and Thruster Support Housing
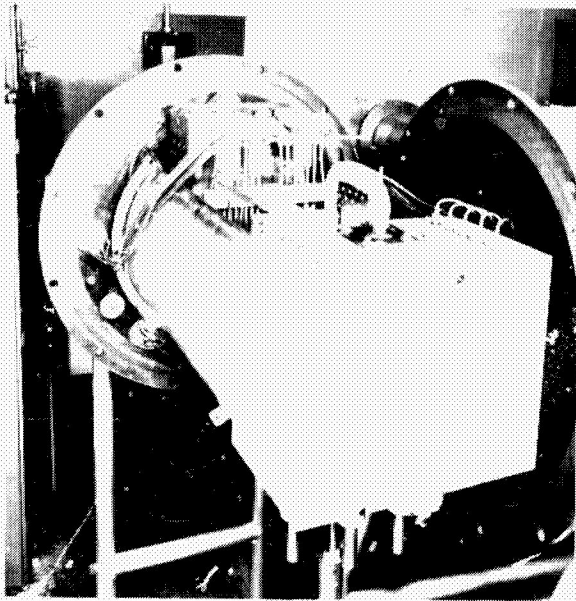
Figure 31. Photograph of Thrust Stand
Showing Entire Thrust
Balance Withdrawn From Main Housing
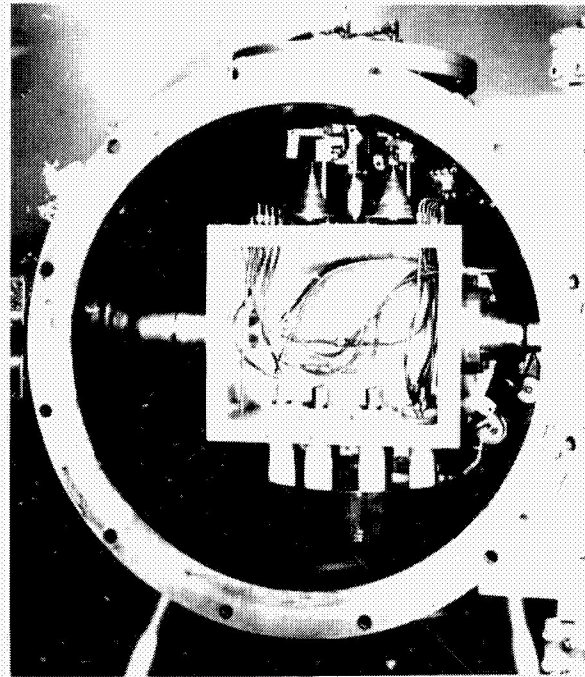
Figure 32. Close-up Photograph of Thruster
Support Housing Showing Internal Electrical
and Fluid Feed Line Connections to Thruster
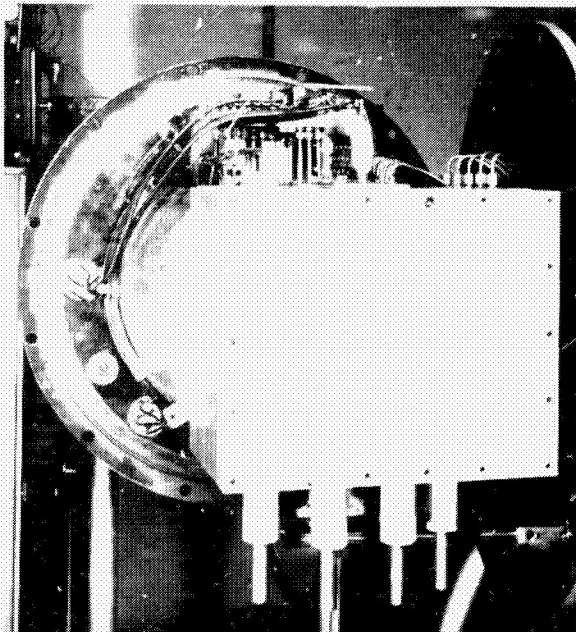
Figure 33. Close-up Photograph of Sealed
Thruster Support Housing Showing External
Electrical and Fluid Feed Line Connections
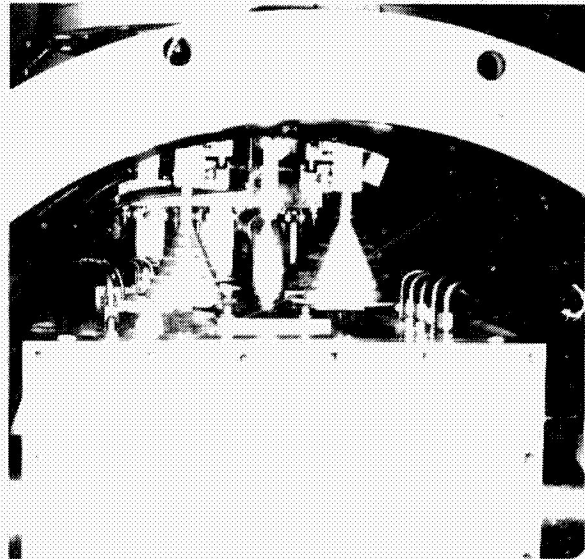
Figure 34. Close-up Photograph of Thrust
Calibration System Showing Balance Cones
With Remote Controlled Weight Application

through into the test chamber. By use of a sliding seal and gate valve, the thruster can be removed for adjustment or modification without losing vacuum. The balance consists of a beam supported on its axis by a 13 inch length of .090'' diameter piano wire. Small ball bearings steady the beam and limit its movement to rotation about a vertical axis. The bearings can be slipped out of place while adjusting the counterweights. An accurate balance is assured by adjusting the weights until the bearings slip into place without disturing the beam. Power for the arc and for the magnetic field coil are supplied through four copper electrodes immersed in pots of mercury. As a precaution against arcing, all portions of the leads, electrodes and mercury pots which are exposed to vacuum are immersed in vacuum oil. The leads connecting the electrodes to the thruster pass through a sealed compartment of the beam which is pressurized with inert gas. Propellant lines, cooling water lines and instrumentation lines connect to the beam through 14 vertical sections of nylon and teflon tubing which attach to the beam near its pivot axis. These flexible sections consist of 1/4 inch diameter tubes 14 inches long. The teflon tubes used for the high pressure cooling water are reinforced with woven stainless steel wire. Remote controls are provided for leveling the instrument, setting the zero and performing a calibration from outside the vacuum chamber. A more detailed description of the unit is given in References 1 and 2. A siz ble effort has been devoted to evaluation of performance of the thrust balance to determine the degree of reliance that can be placed in the measurements, and also to establish possible methods of improving the accuracy by future modifications. The study has included both experimental and analytical work. The problem is quite complex, and the behavior of the instrument still is not completely understood. The work that has been done is described in the paragraphs that follow:

3.2.1 Performance of the Beam Alone

Initial measurements were made with no mercury or oil in the power pots and with no propellant or coolant supplied to the thruster. However, the flexible tubes were connected to the beam. A calibration curve is shown in Figure 35 while a response curve is presented in Figure 36. These curves are intended as a basis for comparison as more of the services are added. The figures show a sensitivity of 91.7 divisions per gram with a scatter of less than 30 milligrams. The beam takes about 2 minutes to settle so that a reading can be made.

It is useful to determine how much of the beam stiffness is due to the torsional wire support, and how much is due to the flexible sections of tubing. To help establish this, measurements were made of stiffness in bending and torsion for samples of the two types of tubing. To do this, the natural frequency was measured for an object of known moment of inertia oscillating in the rotational mode about its center of gravity. The spring force was supplied by samples of the tubing. To measure torsional stiffness, the object was simply suspended from the tubing; while to measure stiffness in bending, the object was mounted on light ball bearings and opposite ends of the tubing were attached to the mounting base and to the
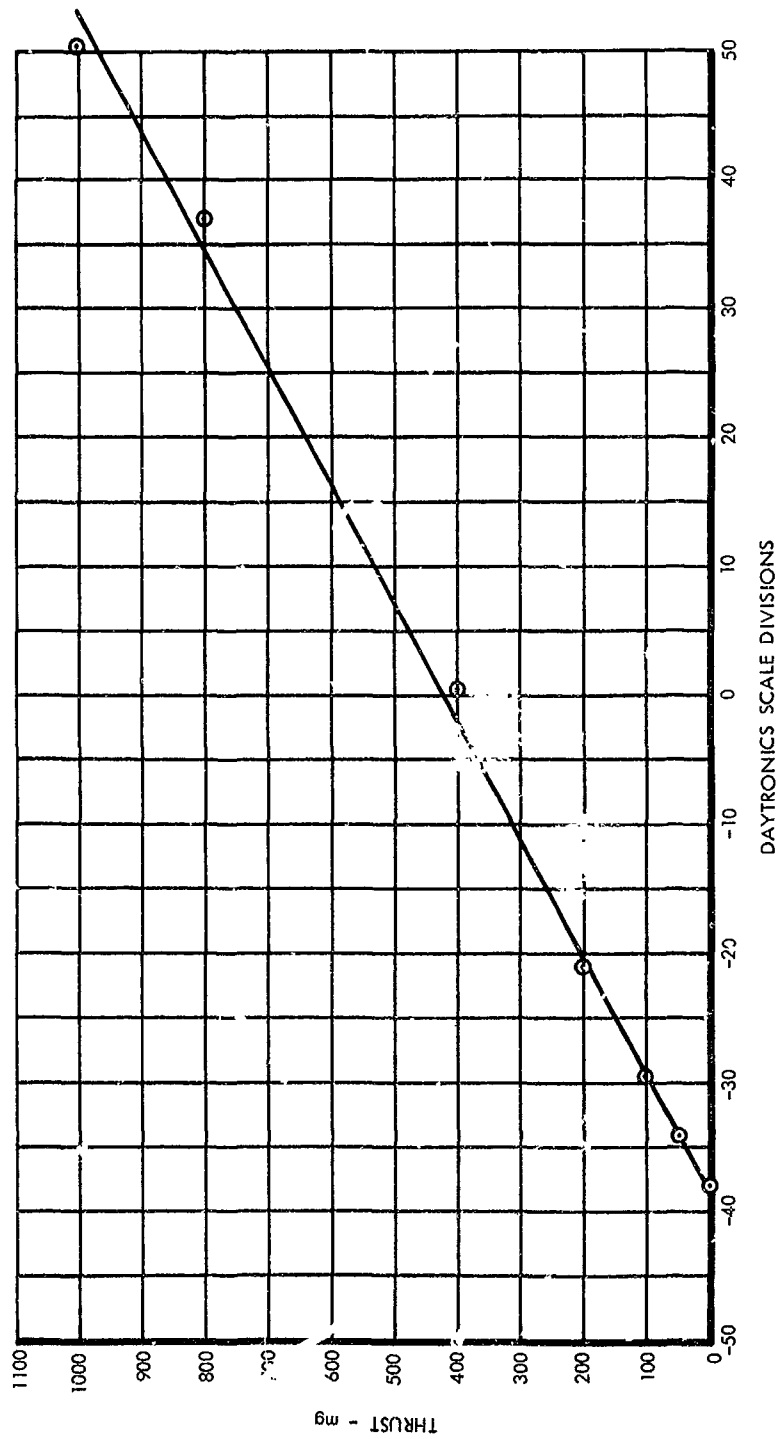
Figure 35. Thrust Balance Calibration Curve Before Filling the
Power Pots With Mercury
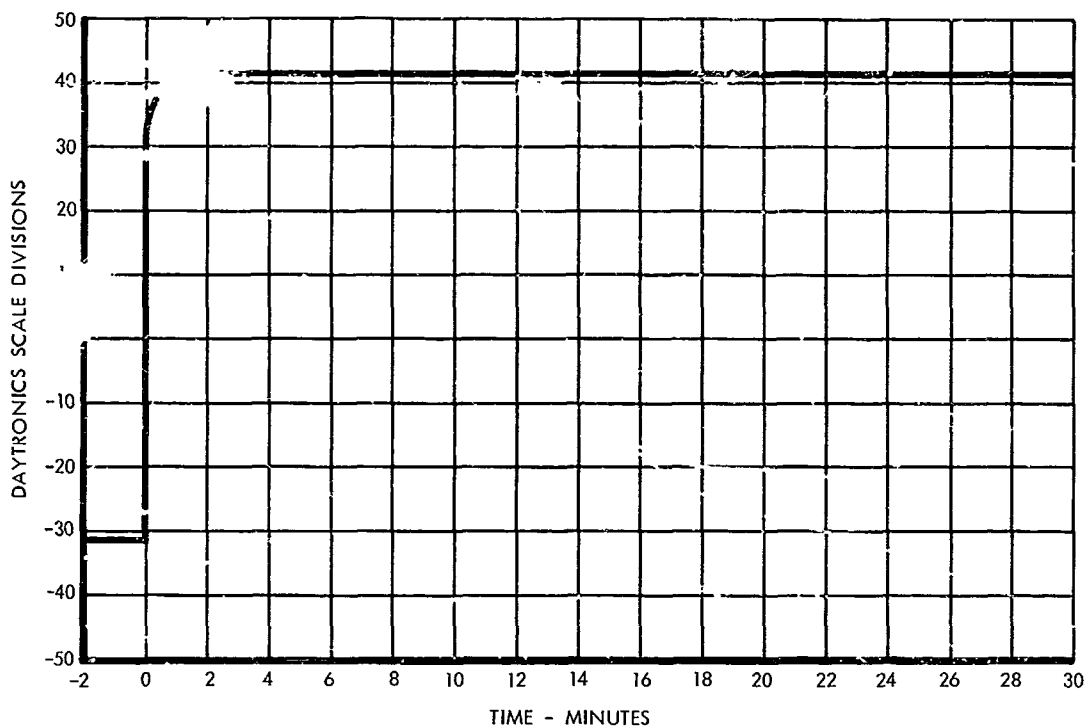
Figure 36. Thrust Balance Response Curve Before Filling the
Power Pots With Mercury

rotating object at equal radial distances from the pivot. Measurements were made at several temperatures, and results are shown in Figure 37.

Using these figures, we can now estimate the stiffness of the 14 tubes connecting to the beam, and of the supporting wire. Since the tubing is offset from the pivot axis, it is subject to flexure in bending as well as torsion. We will use the values for tubing stiffness listed below:

	$EIxx$	GIp
Nylon Tubing	26.7 lb in^2	17.5 lb in^2
Reinforced Teflon Tubing	158 lb in^2	575 lb in^2

It is assumed that the movement in translation is small enough that stretching of the tubing can be neglected, and that the usual beam equations are applicable. The two ends of the tube remain parallel giving an S shaped deflection resulting in the relation:

$$\frac{F}{\Delta y} = 12 \frac{EIxx}{l^3}$$

To express this in terms of torsional stiffness of the beam, the distance (r) of the tube from the pivot axis is introduced, giving
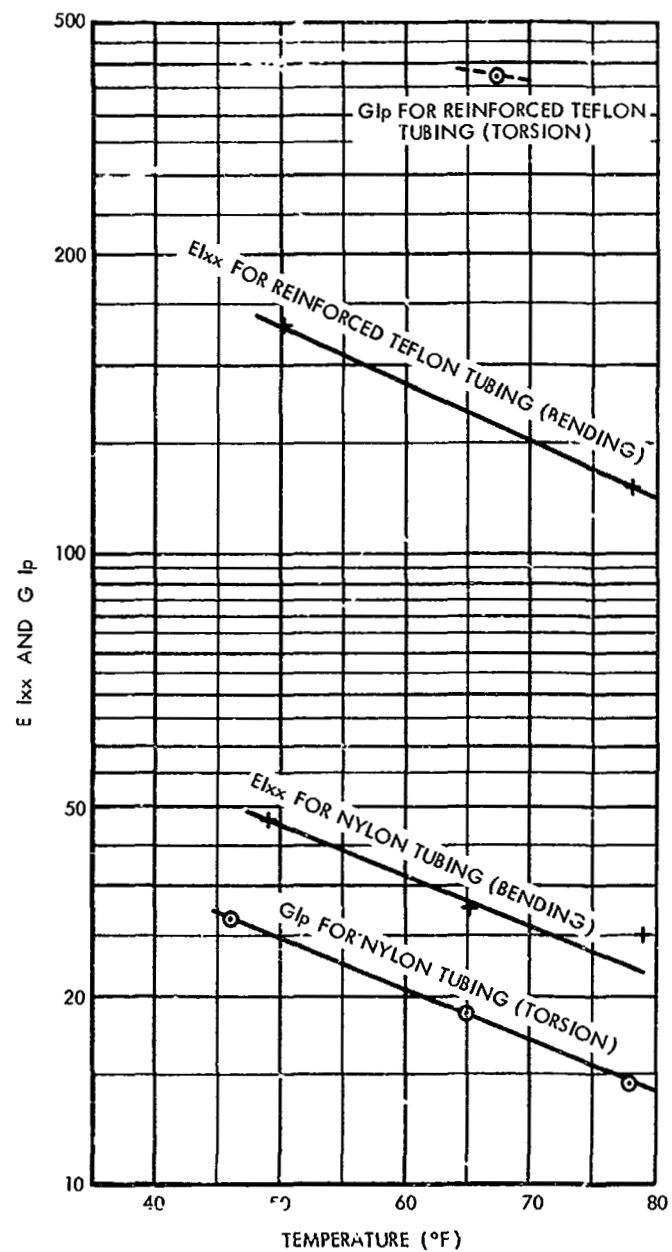
Figure 37. Measured Stiffness of Flexible Tubing Samples

40

$$k = \frac{M}{\phi} = \frac{Fr}{\Delta y/r} = 12 \frac{EIxx \ r^2}{l^3}$$

The arrangement of the tubing is shown in Figure 38, and the stiffness added by bending for each tube position is tabulated below

Tube Position	r (Inches)	l (Inches)	$EIxx$ lb in^2	k $\frac{lb \ in}{radian}$
1	1.25	14	26.7	0.182
2	1.73	14	26.7	0.351
3	2.31	14	26.7	0.623
4	2.93	14	26.7	1.000
5	3.56	14	26.7	1.480
6	4.20	14	26.7	2.063
7	4.85	14	158.0	16.280

Summing on both sides of the centerline, we obtain 11.4 lb in/rad contributed by the nylon tubes, and 32.6 lb in/rad contributed by the reinforced teflon tubes.

The determination of the torsional stiffness of the various members is simpler because rotation is independent of distance from the pivot. We use

$$k = \frac{GIp}{l}$$
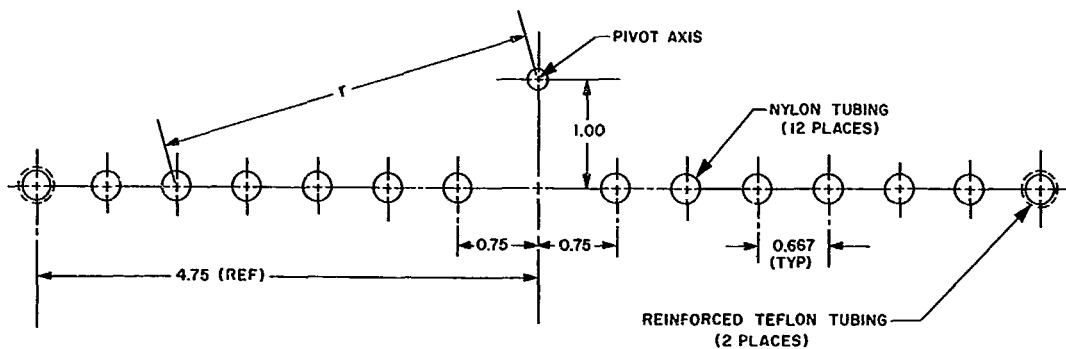
Figure 38. Arrangement of Flexible Tubing Sections With Respect to the Pivot Axis

and take $G = 11.6 \times 10^6$ lbs/in^2 for the supporting wire. Calculated stiffness for all of the members connecting to the beam is summarized below

	Number	Action	k $(\frac{lbs \ in}{rad})$	Percent
Nylon Tubes	12	torsion	15.0	10.2
		bending	11.4	7.8
Reinforced Teflon Tubes	2	torsion	82.1	55.9
		bending	32.6	22.2
Supporting Wire	1	torsion	5.7	3.9
		bending	0	0
		TOTAL	146.9 lb in/rad	

41

This compares with a measured stiffness of 150 lb in/rad based on a deflection of 0.010 inch at the transducer (34-inch radius) when a 1 gram force is applied at the thruster (20-inch radius). A rough check is obtained by calculating the natural period of the beam. The moment of inertia of the beam is estimated to be about 280,000 lb in^2.

$$\text{period} = 2\pi\sqrt{\frac{I}{gK}} = 2\pi\sqrt{\frac{280,000 \text{ lb in}^2}{386\dfrac{\text{in}}{\text{sec}} \quad 147\dfrac{\text{lbs}}{\text{rad}}}} = 13.9 \text{ seconds}$$

which compares to a value of 11 seconds measured before adding mercury to the power pots. The agreement is considered satisfactory in view of the approximations used in estimating the moment of inertia.

The purpose of the preceding calculation is to illustrate that the need for a large number of plastic tubes connecting to a highly sensitive balance results in a condition where the tubing contributes a very substantial fraction of the beam stiffness. This is undesirable because the stiffness of plastic tubing is strongly dependent on temperature, and the sensitivity of the instrument will vary if the tubing temperature is allowed to change during a test. This would be difficult to avoid since the exit cooling water must leave through the tubing. The problem is being handled at present by providing for calibration to determine the sensitivity of the beam during operation. However, another difficulty remains. It is hard to mount all of the flexible tube so that locked in strain is completely eliminated at the zero position. Instead, the torsion wire is adjusted to provide the pre-load necessary to bring the beam to zero. Since stiffness varies with temperature in a different manner for nylon, teflon and steel, a zero shift can be expected if the temperature of the assembly changes. Furthermore, any preload in the cooling water exit tubing can be expected to decrease as water temperature increases. Two approaches are being considered for reducing this problem.

a. A "Thrust Killer" could be installed on he beam to permit tare readings to be taken without disturbing the operating conditions of the thruster. This device was developed at Plasmadyne under an OSR contract, Reference 14. A more recent version is described in Reference 15.

b. The sections of plastic tubing could be replaced by flexible coils or zig-zag arrays of tubing made of stainless steel or Ni Span C.

It may be desirable to use both of these measures.

3.2.2 The Effect of Ground Vibrations

Although the balance is exceptionally sensitive, it was found to be relatively free from the influence of ambient vibrations. This is believed to be largely due to the fact that it is a

slow response device with a period that is long compared to the periods of possible exciting disturbances. The beam is also carefully counterbalanced which should greatly reduce the effect of the translational components of vibration. Figure 39 shows a record of the zero reading with and without operation of the water pump and the vacuum system.
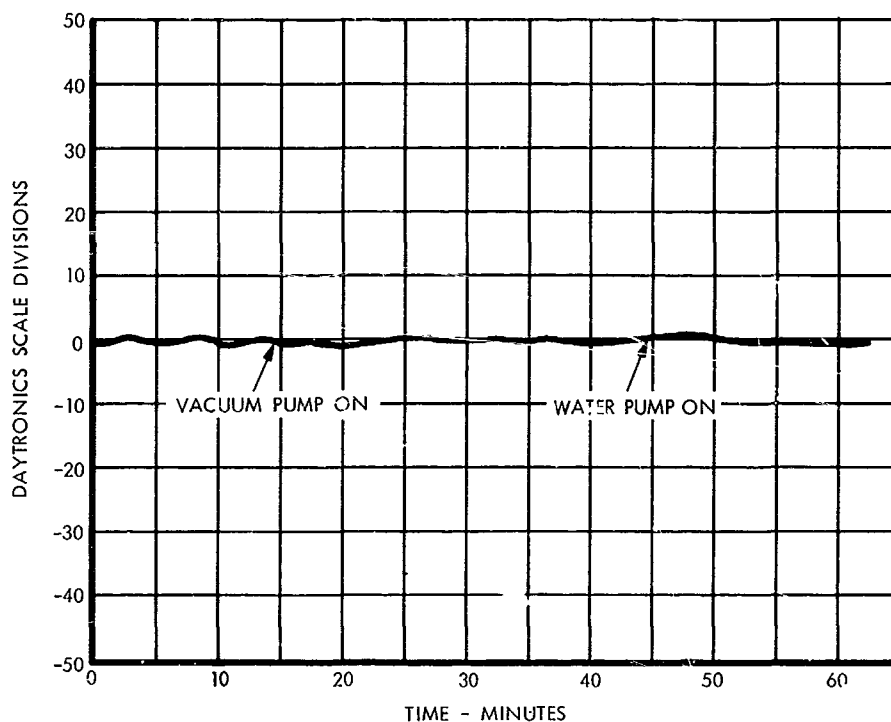
Figure 39. Effect of Operation of the Water Pump and Vacuum System
on the Thrust Balance Zero Reading

3.2.3 The Effect of Flow in the Flexible Tubing

A test was performed in which cooling water was introduced to the magnetic coil and to the thruster, and the performance of the balance was observed. A shift in the zero reading of several hundred milligrams was observed indicating a substantial "bourdon tube" effect. The shift was offset by an adjustment of the torsion wire mount, and the calibration curve given in Figure 40 was obtained. No significant change in sensitivity is shown. The bourdon tube action in the water lines is not too serious because water pressure remains essentially constant during a test. However, pressure is a variable in some of the gas lines, and any bourdon tube action there must either be eliminated or calibrated out. Since plastic tubing is purchased in coil form, it is particularly susceptible to bourdon tube action. However, tubes could be mounted in opposing pairs, or an adjustment could be provided to allow rotation of the tubes so that the bourdon force acts in a direction passing through the beam pivot axis. If a switch is made to a design with metal tubing, the problem

43
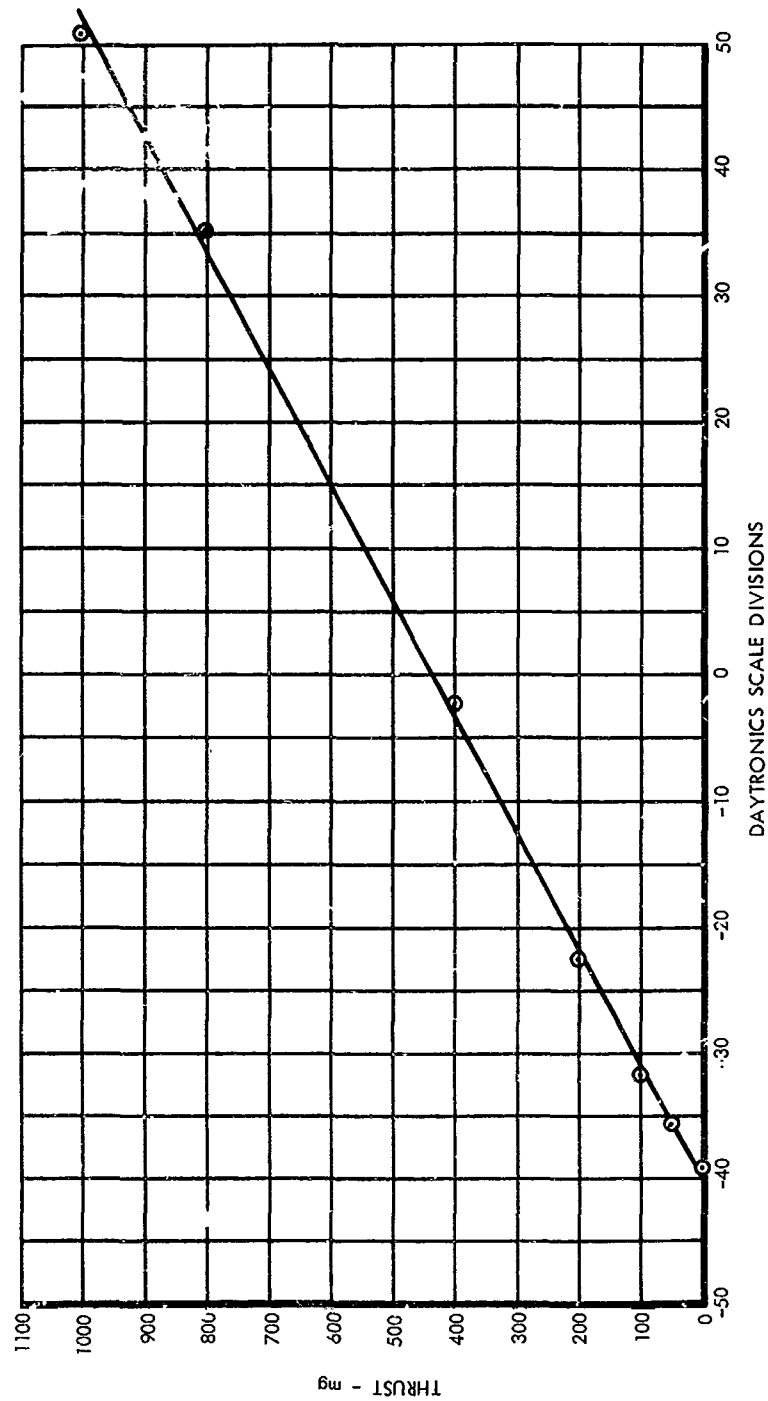
Figure 40. Thrust Balance Calibration Curve With Cooling Water Flowing
Through the Flexible Tubing

44
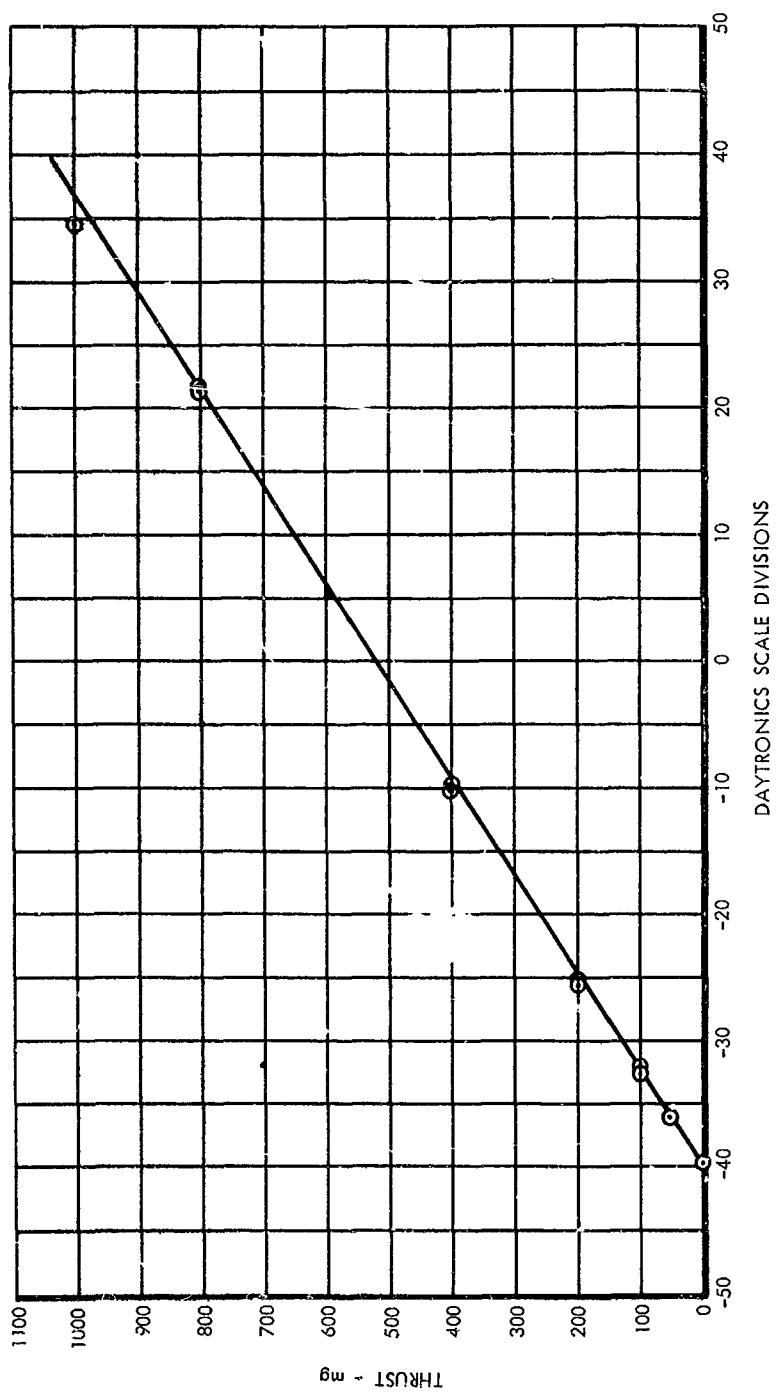
Figure 41. Thrust Balance Calibration Curve With Mercury in the Power Pots

45

is expected to be less serious since metal tubing has a more uniform circular section, and can also be purchased in straight form.

3.2.4 The Effect of the Mercury and Vacuum Oil

After filling the mercury pots and covering the mercury with vacuum oil, the performance of the thrust balance was measured again. The calibration curve, shown in Figure 41, shows a reduction in sensitivity to 59.2 divisions per gram (about 65 percent of the previous value): while the response curve, shown in Figure 42, indicates that nearly 16 minutes are required for the reading to level off (compared to 2 minutes before adding the mercury and oil). The natural period of the beam decreased to between 9 and 10 seconds at the same time. The cause for this change in characteristics has not been definitely established. Normally, the surface tension effects would increase sensitivity slightly. An object on the surface of a liquid is attracted to the nearest wall by surface tension, which has the same effect as a negative spring constant. Thermal effects or changes in the degree of wetting of the electrode or the container would be expected to have a random effect whereas the curves shown in Figures 41 and 42 are fairly typical of a large number of observations. Although the addition of the oil would reduce the response rate, the beam was still found to be underdamped and to show small oscillations of the proper frequency superimposed on the trace shown in Figure 42. A tentative theory which seems to fit the facts is that the change in behavior is caused by a very thin oxide film on the mercury surface. We will now consider this possibility.
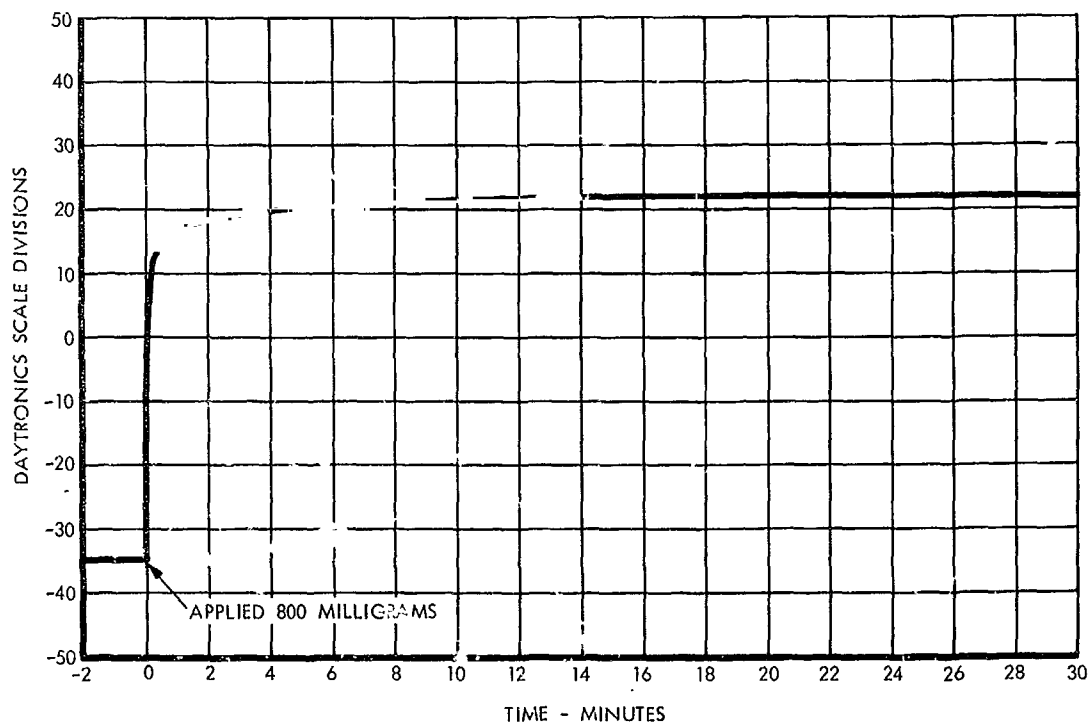
Figure 42. Thrust Balance Response Curve With Mercury in the
Power Pots
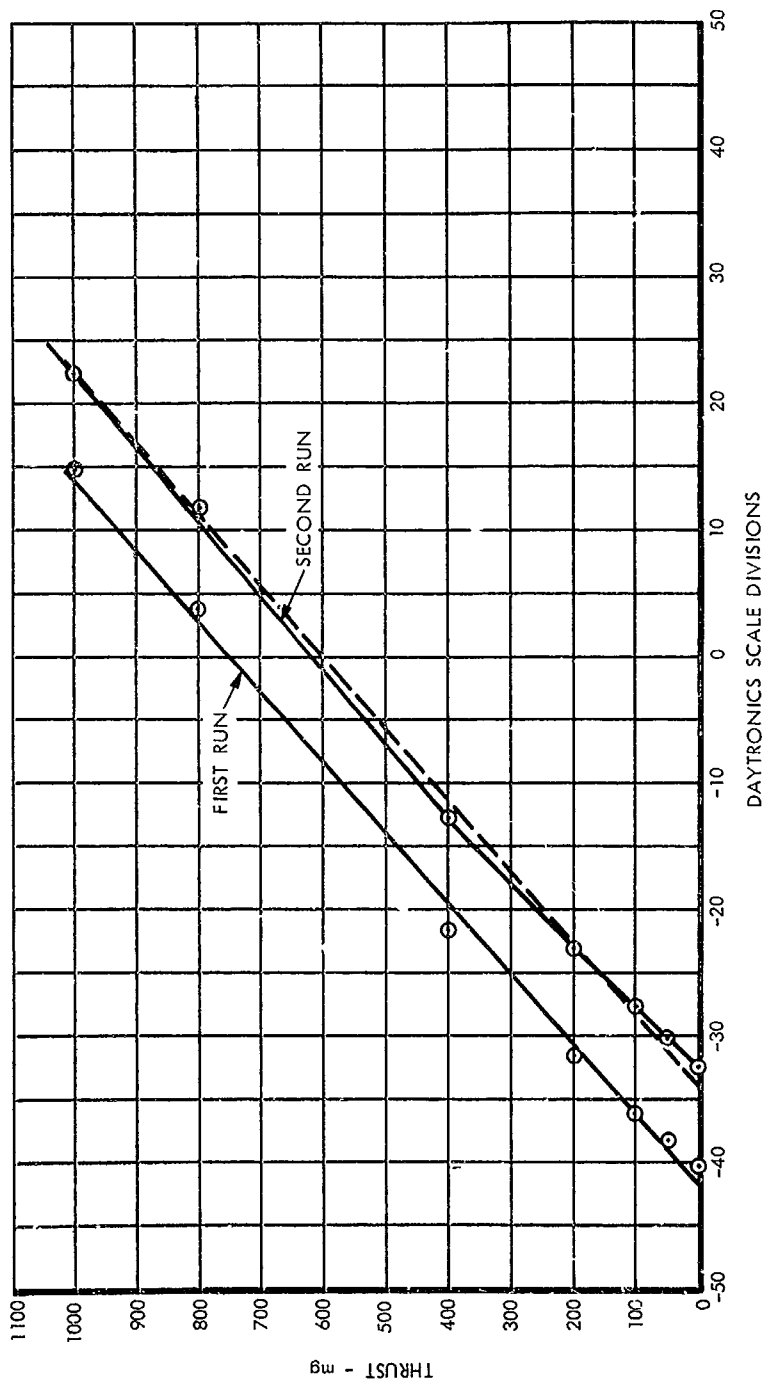
Figure 43. Thrust Balance Calibration Curve With the Vacuum Oil Covering the Power Pots Heated

47

Mercury is subject to the formation of an oxide film on its surface if there are metal impurities in the mercury, and if the surface is exposed to oxygen. Regardless of its initial purity, the mercury in a power pot soon takes other metals into solution from the electrodes and from the container. If the oil covering is not thoroughly outgassed, a reaction between oxygen dissolved in the oil and the metal dissolved in the mercury will form a thin film of oxide on the surface within a matter of hours. The film is a solid that resists movement of the electrode and has the effect of increasing the spring constant and reducing the repeatability. When it is thin, it is not visible until compressed at which time crinkling of the surface is observable as flakes of the oxide buckle and overlap. If an oxide film exists in the power pots, it would be expected to reduce the movement of the beam when a given force is applied. The beam would stop moving with a compressive force in the film. Following this, random vibrations would permit rearrangement of flakes of the film allowing the beam to gradually move further toward its normal equilibrium position. Evidence which is believed to favor the oxide film theory is listed below:

a. The introduction of mercury and oil increased the effective spring constant of the balance even though no other attachments were made to the beam.

b. The introduction of mercury and oil increased the response time by a large factor even though the beam remained underdamped.

c. A repeat test with increased oil temperature (Figures 43 and 44) showed increased rather than decreased response time. Some further reduction in sensitivity is also noted suggesting the possibility of a thicker oxide film at this time.
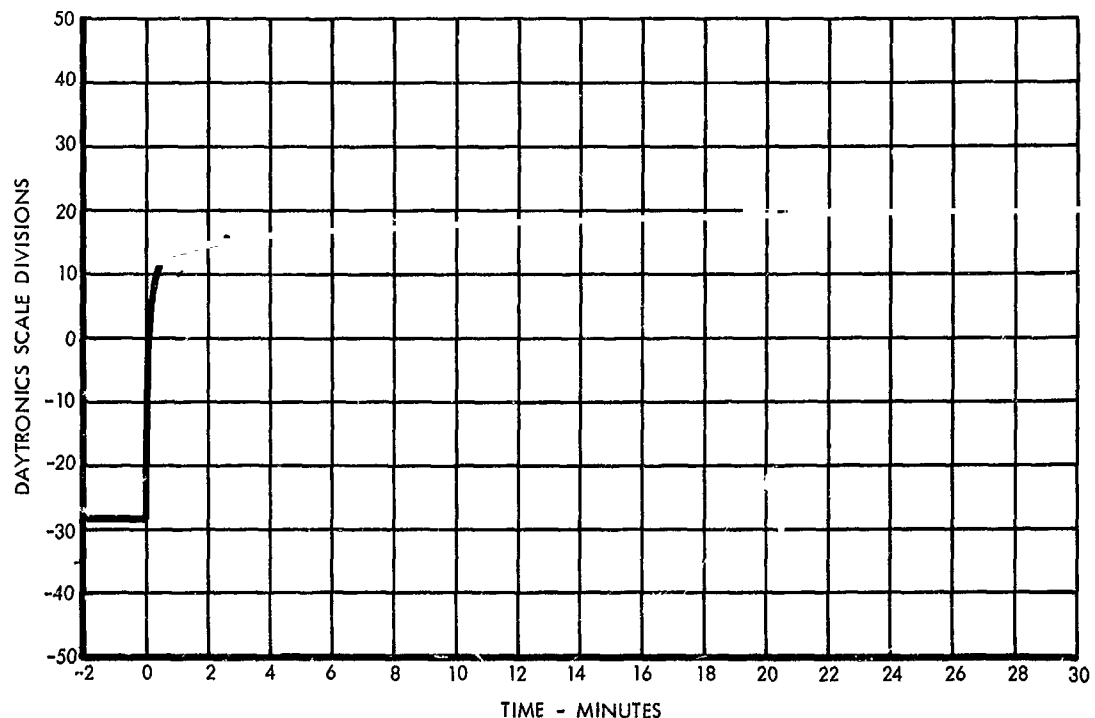
Figure 44. Thrust Balance Response Curve With the Vacuum Oil Covering the Power Pots Heated

48

d. Tests with current passing through the power pots show a much more rapid response (see Figure 45). It may be that convection currents in the mercury stir the oxide film enough to eliminate its restraining action when current is flowing.

Assuming that the oxide is indeed causing the variable sensitivity and excessive response time, the following design changes could be expected to improve performance

a. Arrangements could be made to fill the power pots with clean mercury with a remotely controlled system after completely outgassing the oil and purging the chamber of oxygen.

b. Provision could be made for periodically dumping the mercury into a separate chamber that would allow impurities to collect and be trapped on a separate surface. A variation would involve sweeping devices to clear the surface and trap impurities behind a fence on the surface.

c. A vibrator could be provided to shake the surface of the mercury and allow the oxide flakes to reach an unloaded geometry rapidly.

d. The electrodes could be undercut at the mercury surface to reduce surface film inter-action.

e. Pancake shaped power pots could be stacked vertically on the pivot axis so that electrode movement would consist of a very slight rotation only.

f. Mercury pots could be replaced by thin ribbon-like flexible bus bars. The flexible sections could be submerged in a vacuum oil to avoid the need for an insulating coating which would introduce added temperature dependent stiffness. Electromagnetic interaction between leads could be minimized by arranging the leads in symmetrical pairs. At present, coaxial cable is not considered feasible because of the difficulty of providing adequate flexibility with a repeatable stress-strain relationship. It is also possible in principle to arrange the leads so that interactions with the earth's magnetic field cancel, and this would be desirable feature for the arc power leads. It may also be possible to compensate for the field coil interaction by proper design of the field coil leads. This is because the field coil axis is nearly aligned with the earth's field, and the interaction moment is not par.   arly large.

The main disadvantage of flexible bus bars in place of mercury pots is that the sensitivity of the beam would be greatly reduced by the added stiffness. Although a more sensitive transducer readout could be used, errors due to such things as thermal distortion in the assembly would be magnified. The problem can be reduced by maintaining a uniform temperature in the structural members, by using materials with a low coefficient of expansion, or by adding a spring loaded linkage with a toggle action to produce a negative
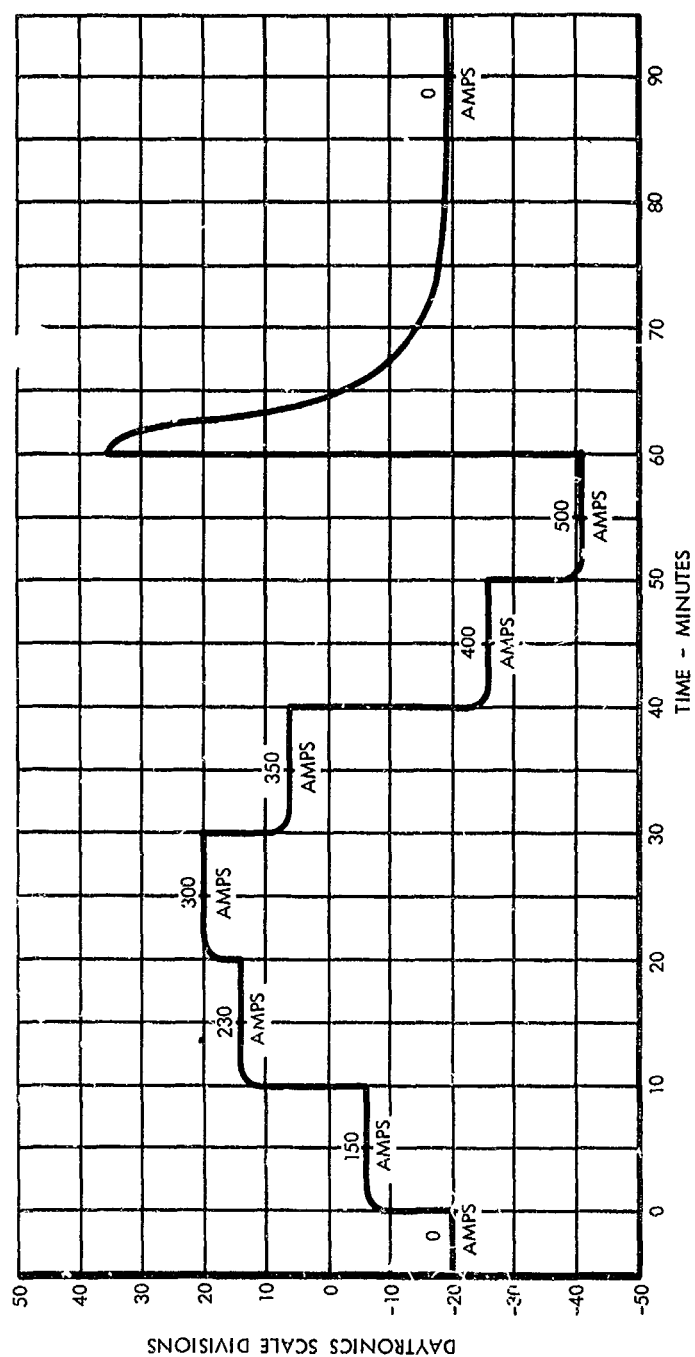
Figure 45. Effect of Field Coil Current on the Thrust Balance Zero Reading

50

spring constant and increase the sensitivity of the beam. It can be shown that there is an optimum amount of toggle action. Too much would make the beam overly sensitive to changes in temperature of the spring elements, a final choice between improved mercury pots and flexible bus bars has not yet been made.

3.2.5 Effect of Current in the Power Leads

The effect of current in the power leads on the performance of the balance is shown in Figures 45 through 48. A very sizable zero shift was found to occur. Although it is possible to use the balance by calibrating it with the coil energized and with the electrodes shorted out with various amounts of current passing through the leads, it is considered essential to understand the effect and to eliminate it if possible. A number of calculations have been made in an effort to evaluate some of the possible disturbing forces. It is interesting to note that the response time is much more rapid when current is flowing through the pots (the electrical current appears to have a favorable effect on the oxide film).
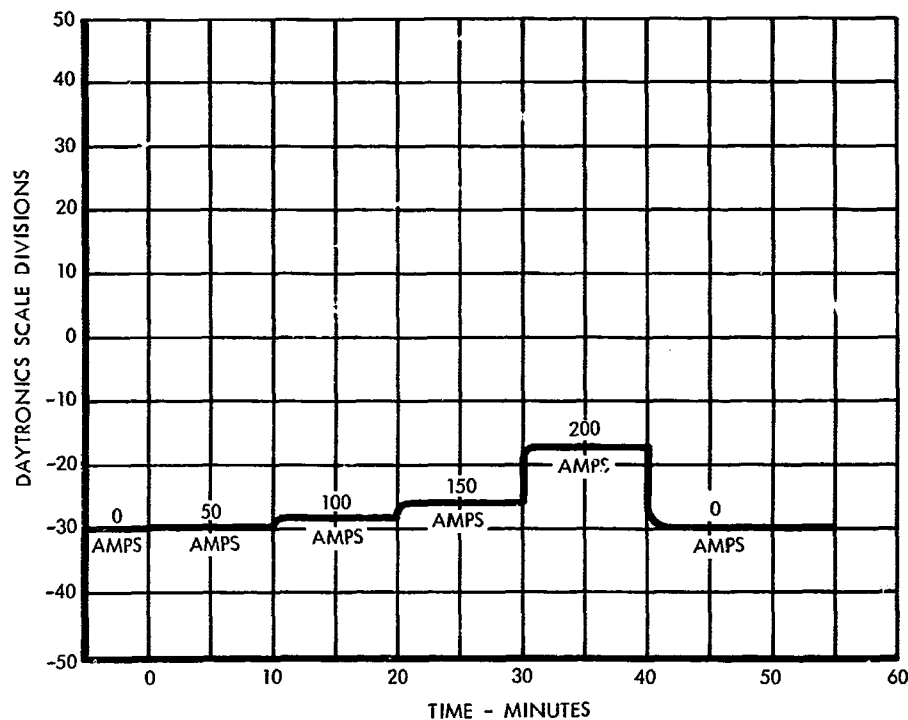
Figure 46. Effect of Arc Current on the Thrust Balance Zero Reading

a. Electromagnetic Interactions

Figure 45 shows a reversal in trend as current in the field coil circuit is increased. This is not too surprising when we consider that there are two types of electromagnetic interactions.

51
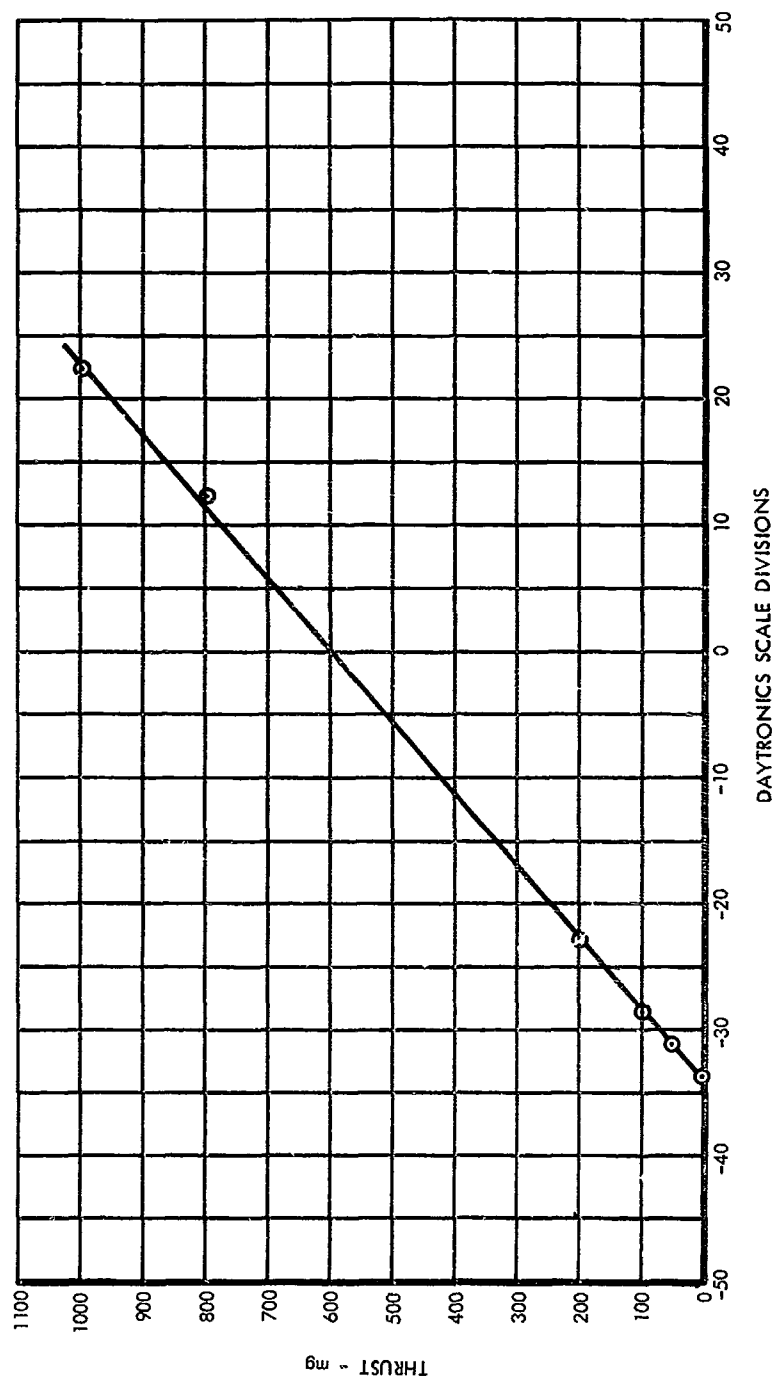
Figure 47. Thrust Balance Calibration Curve With Current in the Field
Coil and Arc Circuits

Unbalanced interactions between leads will introduce a force proportional to the square of the current, while interactions with the earth's magnetic field will vary as the first power of the current. If the two forces are opposed, the net force will act in one direction at low currents when the earth field effects are dominant, and in the opposite direction at high currents when interactions between leads dominate. The net force would vary in a parabolic manner:

$$\text{net force} = aI - bI^2$$
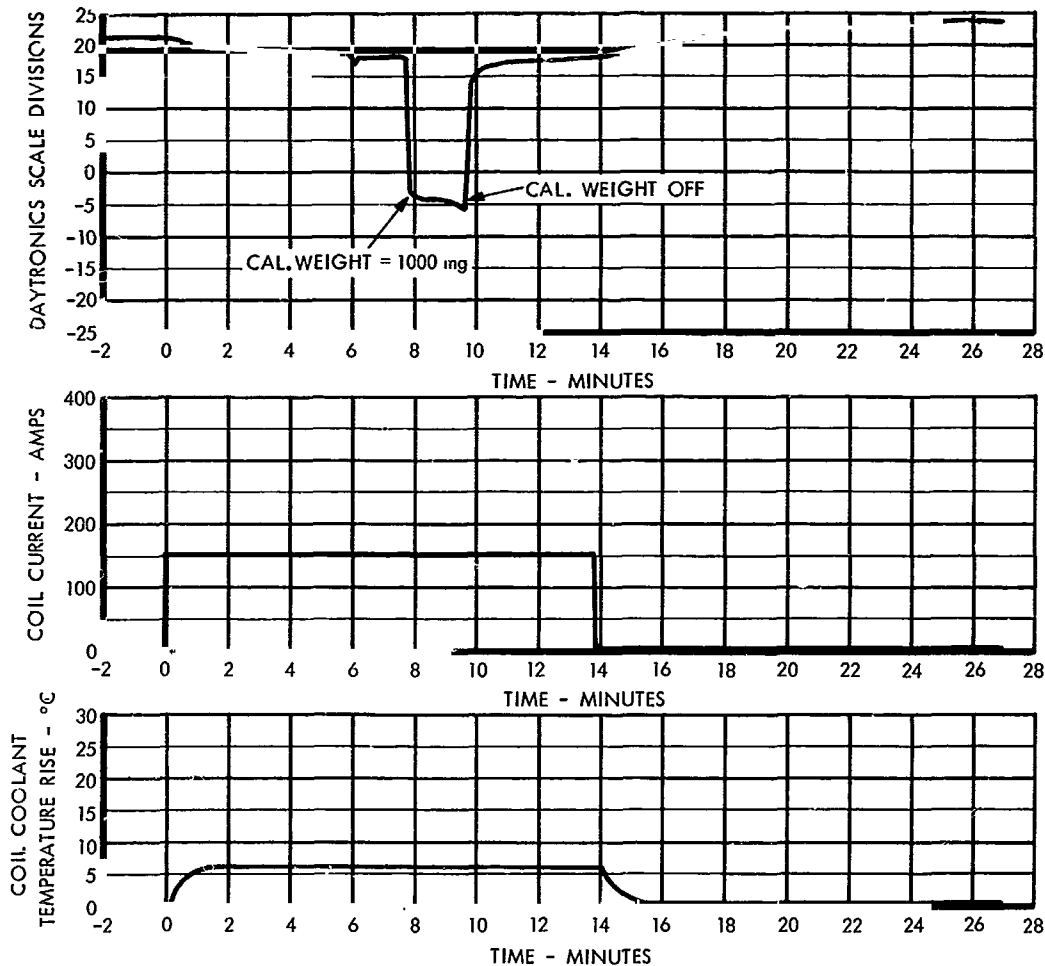
Figure 4C. Thrust Balance Response Curve With Current in the Field Coil

Figure 49 shows the readings given in Figure 45 replotted as a function of current. The dotted line is a parabola selected to approximately fit the data. If the variation were entirely due to electromagnetic interactions, we would expect the test points to fit a parabolic curve of this type. We see that it is possible in principle to account for a large portion of the variation in this way. However, there are sizable departures from the

parabolic variation that must be due to other effects.
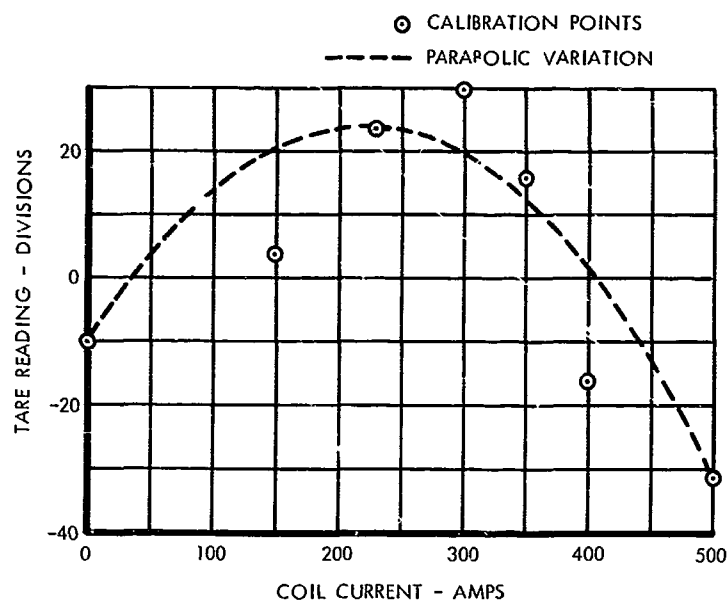
Figure 49. Thrust Balance Tare Reading Versus Coil Current Compared
to a Parabolic Variation

The next step is to estimate the possible magnitude of electromagnetic interactions to see
if the measured forces can plausibly be explained in this way. We will consider first the
action of the earth's field on the magnetic field coil.

Interaction with the Earth's Magnetic Field

In trying to align itself with the earth's field, the field coil can produce a torque on the
beam which would cause an apparent thrust reading. There are 32 turns with an average
diameter of about 6.4 cm. We will consider a case with a current of 300 amps. Only the
horizontal component of the earth's field needs to be considered since the vertical com-
ponent does not produce a moment about the vertical axis of the beam. In the Southern
California area, the horizontal component of the earth's field is about .26 gauss. The
expression for the torque produced on a coil by a uniform field is

$$T = \frac{\pi N r^2 \, BI}{10} \sin \alpha$$

where α is the angle between the centerline of the coil and the horizontal component of the
earth's field. Substituting the values given above we obtain

54

$$T = 8020 \text{ dyne cm sin } \alpha$$

Since α changes as the beam moves, the coil has a small effect on the spring constant of the beam.

$$\frac{dT}{d\alpha} = 8020 \text{ dyne cm cos } \alpha$$

which has a maximum value of 8020 dyne cm/radian or .007 lb in/radian which is negligible compared to other stiffening effects. The zero shift, however, is not as small. The thrust is at a radius of 50.8 cm from the pivot axis. Estimating α to be 15°, we can write

$$\text{apparent thrust} = \frac{8020 \text{ dyne cm}}{50.8 \text{ cm}} \text{ sin } 15°$$

$$= 41 \text{ dynes or 42 milligrams of force}$$

The earth's field will also effect the power leads if they are not coaxial or arranged so that the moments cancel. The outer pair of electrodes are separated about 26 cm, and extend vertically about 20 cm to terminals inside the pressurized enclosure. The torque produced by the action of the earth's field on this portion of the leads may be expressed:

$$T = \frac{BI \text{ hw}}{10} \text{ sin } \alpha$$

The electrodes are aligned more nearly in the north south direction and, from this standpoint, are subject to a stronger effect than the field coil. Estimating $\alpha = 75°$ and again taking I = 300 amps, we write

$$T = \frac{.26 \text{ gauss (300 amps)(20 cm) 26 cm}}{10} \text{ sin } 75°$$

$$= 3920 \text{ dyne cm}$$

$$\text{apparent thrust} = \frac{3920 \text{ dyne cm}}{50.8 \text{ cm}} = 77 \text{ dynes}$$

or 78 milligrams

Adding the two effects, we see that a zero shift of 120 milligrams could be caused by a 300 amp current in the field coil circuit. This figure is too small to completely account for the initial increase in reading shown in Figure 45.

It is difficult to estimate the effect of interaction forces between leads on the thrust reading because the leads are intended to have a symmetrical arrangement with no net force acting on the beam. The force per unit of conductor length repelling two parallel

55

leads in a circuit is given by

$$\frac{\text{orce}}{\text{length}} = \frac{2I^2}{10w}$$

Letting w be 10 cm for the distance between the inner pair of electrodes, again taking a current of 300 amps, and assuming an unbalance equivalent to a 1 cm difference in the mercury level for the two electrodes, the side load may be expressed

$$\text{side load} = \frac{2(300 \text{ amps})^2}{10(10 \text{ cm})} \quad 1 \text{ cm} = 1800 \text{ dyne}$$

or 1840 milligrams

Since this force would act at close to the same radius as the thrust, the above figure may be considered equal to apparent thrust. The calculation shows that even small departures from symmetry in the geometry of the leads could produce the strong reversal in the tare readings shown in Figure 45.

b. Surface Tension Effects in the Mercury Pots

The mercury level in the space surrounding an electrode is either raised or depressed by a two-dimensional capillary tube action. If the electrode is closer to one wall than the other, the fluid on the close side will experience a greater change in level, and this will upset the balance of hydrostatic pressure acting on opposite sides of the electrode. The resulting force will tend to move the electrode toward the closer wall. The effect is equivalent to a negative spring constant, and is normally included in the calibration of the instrument. However, errors can occur if

i   the relative position of the electrode changes during a run due to thermal distortion,

ii the surface tension of the mercury changes due to a change in temperature, or

iii the degree of wetting of the electrode or the container changes during the run.

Figure 50 illustrates the surface tension effect. The arrows represent pressure forces acting on the sides of the electrode. Arrows shown as heavy lines are imbalanced, and result in an apparent thrust. Notice that the apparent thrust has the same magnitude and direction regardless of whether or not the fluid wets the walls. However, if the walls are wet on one side of the mercury gap but not the other, a difference in the apparent thrust results.

Considering a two dimensional model, the change in level due to capillary action can be found by equating the surface tension forces to the pressure forces resulting from the

change in level:

$$2Tl = \rho g \, \Delta h \, wl$$

$$\Delta h = \frac{2T}{\rho g \, w}$$

a. MERCURY DOES NOT WET THE WALLS (ELECTRODE OFF CENTER)
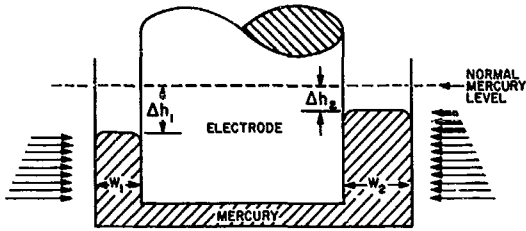
c. ELECTRODE CENTERED, UNEVEN WETTING NO NET SIDE LOAD
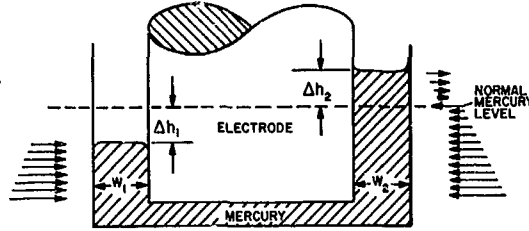
b. MERCURY WETS THE WALLS (ELECTRODE OFF CENTER)

d. ELECTRODE CENTERED, UNEVEN WETTING SIDE LOAD PRODUCED
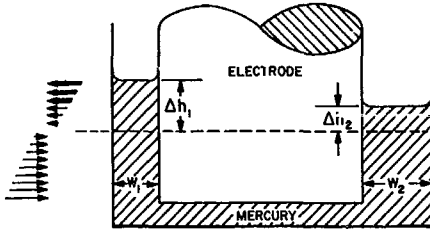
VECTOR LENGTH REPRESENTS GAGE PRESSURE
l = LENGTH OF ELECTRODE NORMAL TO PAPER
$\bar{w} = \frac{1}{2}(w_1 + w_2)$
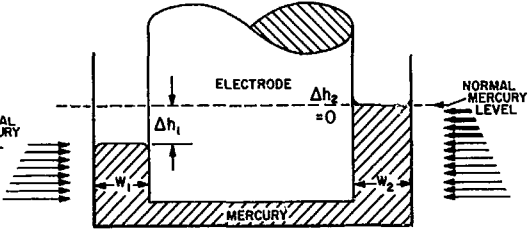
HEAVY ARROWS DENOTE UNBALANCED PRESSURE FORCES

Figure 50. Unbalanced Pressure Forces Acting in a Power Pot

The side force may be expressed as the average unbalanced pressure multiplied by the difference in area covered by fluid on the two sides of the electrode.

$$\text{side force} = (\Delta h_1 - \Delta h_2)l \, \frac{\rho g \, (\Delta h_1 + \Delta h_2)}{2}$$

Substituting the expression for Δh

$$\text{side force} = \frac{2T^2 l}{\rho g} \left(\frac{1}{w_1^2} - \frac{1}{w_2^2} \right)$$

For the case with the electrode nearly in the center, we can substitute

$$w_1 = \bar{w} - \Delta w \text{ and}$$

$$w_2 = \bar{w} + \Delta w$$

and drop second order terms which gives

57

$$\text{apparent thrust} = \frac{81T^2}{\rho g \overline{w}^3} \Delta w.$$

We can take the following figures as representative for the power pots

$$l = 2.54 \text{ cm}$$
$$w = 1.5 \text{ cm}$$
$$\rho = 13.55 \text{ gm/cm}^3 \}$$
$$T = 480 \text{ dynes/cm} \} \quad \text{mercury}$$

Substituting

$$\text{side force} = \frac{8 \ (2.54 \text{ cm}) \ (480 \ \frac{\text{dynes}}{\text{cm}})^2 \ \Delta w}{13.55 \text{ gm/cm}^3 \ 980 \text{ cm/sec}^2 (1.5 \text{ cm})^3} \left(\frac{\text{gm cm}}{\text{dyne sec}^2}\right)$$

$$= 104.6 \frac{\text{dyne}}{\text{cm}} \ \Delta w$$

The power pots are located at a radius of about 50 cm from the pivot, so the effect on the spring constant of the beam may be expressed

$$k = -\frac{104.6 \ \frac{\text{dynes}}{\text{cm}} \ \Delta w \ 50 \text{ cm}}{\left(\frac{\Delta w}{50 \text{ cm}}\right)} = -262,000 \frac{\text{dynes cm}}{\text{radian}}$$

or $-0.232 \ \frac{\text{lb in}}{\text{radian}}$ for each electrode,

and -0.928 lb in/radian for all four electrodes.

Since this value is small compared to the stiffness of elements that connect to the beam, the effect on sensitivity is unimportant. We must, however, consider other errors that might occur. To estimate the error due to thermal distortion, it is assumed that the electrode is offset with respect to the container by a distance corresponding to a 3°F temperature change in 20 inches of steel.

$$\Delta x = 20 \text{ inches } 8.9 \times 10^{-6}/°F \ 3°F = 5.34 \times 10^{-4} \text{ inches}$$

$$\text{side force} = 104.6 \frac{\text{dyne}}{\text{cm}} = 13.6 \times 10^{-4} \text{ cm} = 0.142 \text{ dynes each electroc}$$

or 0.568 dynes and 0.58 mg for the four electrodes.

The power pots are mounted at about the same radius as the thruster so this figure may also be taken as the thrust error.

To estimate the error due to changing surface tension, we assume a change in mercury temperature of 50°F, and an average electrode offset of 1mm, the initial surface tension

58

force is

$$104.6 \ \frac{\text{dynes}}{\text{cm}} \ .1 \ \text{cm} \ = \ 10.46 \ \text{dynes}$$

This force is included in the calibration and does not represent an error. A 50°F change in mercury temperature would result in a .425 percent change in surface tension, so

$$\text{thrust error} \ = \ 10.46 \ \text{dynes} \ .00425 \ = \ .0445 \ \text{dynes each electrode}$$

$$\text{or} \ .178 \ \text{dynes and} \ \underline{.182 \ \text{mg}} \ \text{for the four electrodes}$$

To categorize the error due to irregular wetting, we will assume an initial condition with the electrode centered and no wetting of the walls. A disturbance is then assumed to occur that results in wetting of one side of the electrode only as in Figure 50d. This is the most extreme change that. can be visualized. When it happens, the mercury on the side that wets will rise to the "normal fluid level" and an unbalanced pressure force will act on the electrode.

$$\text{thrust error} \ = \ \text{unbalanced area x (average unbalanced pressure)}$$

$$= \ \Delta h_1 1 \ \text{x} \ \frac{\rho g \ \Delta h_1}{2}$$

substituting the expression for Δh

$$\text{thrust error} \ = \ \frac{2 l \ T^2}{\rho g \ \overline{w}^2}$$

$$= \ \frac{2(2.54 \ \text{cm}) \ (480 \ \frac{\text{dynes}}{\text{cm}} \ )^2}{13.55 \ \text{gm/cm}^3 \ 980 \ \text{cm/sec}^2 (1.5 \ \text{cm})^2} \ \left(\frac{\text{gm cm}}{\text{dynes sec}^2} \right)$$

$$= \ 39.2 \ \text{dynes or} \ \underline{40 \ \text{mg}}$$

This is for one electrode alone, and represents a serious error if this much change in the wetting of the walls should actually occur during a test. However, it seems very unlikely that such an extreme change would occur during the period of a test run. Changes in surface tension effects are tentatively considered to be an unimportant source of error.

c. Convection Currents in the Mercury

Regardless of how carefully the electrodes and mercury containers are constructed, there are likely to be irregularities in the current flow through the mercury. Although copper and mercury amalgamate forming a good electrical contact, there is also a strong tendency for the electrode to become coated with an oil film that prevents actual contact. When an electrode is withdrawn, the mercury coating on its surface is typically quite

spotty indicating that only certain regions offer a good conductive path. If the current flow is strongly unsymmetrical, one sided heating and strong convective currents can be expected.

As an example, we will consider a case with an electrical current path having a geometry equivalent to a mercury conductor one inch in diameter and .5 inch long. Taking the resistivity of mercury as 95.8×10^{-6} ohm cm, and considering a current of 300 amps, the heating rate in the conducting path can be estimated

$$R = 95.8 \times 10^{-6} \text{ ohm cm} \frac{.5 \text{ inch}}{\frac{\pi}{4}(1 \text{ inch})^2} \frac{\text{inch}}{2.54 \text{ cm}} = 24.0 \times 10^{-6} \text{ ohm}$$

$$\text{heating rate} = I^2 R = (300 \text{ amps})^2 \, 24.0 \times 10^{-6} \text{ ohms} = 2.16 \text{ watts}$$

We next examine the temperature gradient that would be required in the mercury if we assume that half of this heat must be dissipated by thermal conduction in the mercury through the sides of the cylindrical conduction path. The thermal conductivity of mercury is taken as .0148 cal/cm sec °C, while the area of the side of the cylinder is 10.11 cm^2.

$$\frac{dT}{dR} = \frac{\text{power}}{kA} = \frac{1/2\,(2.16 \text{ watts})}{.0148 \frac{\text{cal}}{\text{cm sec °C}} \, 10.11 \text{ cm}^2 \, 4.19 \frac{\text{watt secs}}{\text{cal}}}$$

$$= 1.72 \frac{°C}{\text{cm}}$$

The preceding calculation has been performed to provide a logical basis for assuming a difference in the mercury temperature on opposite sides of the electrode. We will choose a temperature difference of 3°C to use for estimating convection current effects.

An indication of the magnitude of the convection current error may be obtained by considering a simplified model. The active portions of the mercury are taken as two rectangular sections 1 inch wide, .6 inch thick and 2 inches high on opposite sides of the electrode. Each section has a mass of about 266 grams. The temperature of one section is taken as 1.5°C above average, while the temperature of the other is taken as 1.5°C below average. The cubic coefficient of expansion for mercury is $.182 \times 10^{-3}/°C$. This allows us to evaluate the buoyant and sinking forces which are equal in magnitude for the two sections.

$$F_b = F_s = 266 \text{ grams} \, .182 \times 10^{-3}/°C \, 1.5°C = 73 \text{ mg}$$

which makes the total force which must be overcome by convection current drag equal to

$$F \text{ drag} = F_b + F_s = 146 \text{ mg}$$

Some fraction of this amount will act as drag on the electrode in the thrust direction, but there is also a likelihood of some additive effect from the four electrodes. The above figure is therefore taken as representative of the thrust error that might be expected from convection current effects in the mercury. The uncertainty in the calculation is fairly large. It is entirely possible that the irregular variations shown in Figure 49 are primarily caused by convection currents.

A number of measures are being considered for reducing the effect of current in the power leads. Although it is not clear at present how much of the initial zero shift with increasing current is due to interaction with the earth's field and how much to some other effect such as convection current in the mercury, an effect as large as appears to occur can certainly be reduced by rearrangement of the leads. The interaction between leads also appears to have a large effect on the zero reading which could undoubtedly be reduced by providing an adjustment. For example, the mercury level could be controlled in one of each pair of electrodes. It appears likely that the effect of convection currents in the mercury is large enough to be of serious concern. This problem may be more serious than the electromagnetic interaction effects simply because it is expected to be less repeatable. When the mercury is stirred up, a change in the wetting c ld follow with resulting changes in the heating and convection current pattern. The problem could be largely eliminated (as would any surface tension effects) by stacking the power pots on the pivot axis. Flexible bus bars would of course provide another solution if a suitable design could be found. In either case, an adjustment in lead position would have to be substituted for the adjustment in mercury level to eliminate lead interaction errors.

3.2.6 The Effect of Inaccuracies in Balancing the Beam

Several types of errors can occur if the beam is not accurately balanced. An unbalance can result from normal inaccuracies in the initial adjustment of the counterbalance weight or from thermal distortion of the beam during operation. An effort has been made to estimate the magnitude of error resulting from unbalance.

The beam is initially balanced using pieces of lead weighing about 1100 grams at a location about 20 cm from the pivot axis. Weights are added or removed until the bearings will slip freely into place at the pivot axis. When the best combination of weights is found, the maximum unbalance can be

$$\text{max unbalance} = 1/2 \ (20 \text{ cm}) \ 1100 \text{ grams} = 11,000 \text{ gm cm}$$

In addition, a change in unbalance can occur due to thermal distortion of the beam. For example, if the temperature of the aluminum tube supporting the thruster increases 5° F during a test, the tubing length will increase an amount

$$\Delta 1 = 51 \text{ inches } 12.9 \times 10^{-6}/° \text{ F } 5° \text{ F } .00329 \text{ inches}$$

61

Taking a 15 pound thruster mounted at the end of a 15 pound tube, and assuming that the remainder of the beam remains at the same temperature, the change in unbalance becomes:

$$\Delta \text{ unbalance } = \frac{3}{2} \text{ .00329 inches 15 lbs } = \text{ .074 lb in}$$

or 85 gm cm

The initial unbalance will produce an error if the pivot axis tilts during a test, while the change in unbalance will produce an error if the pivot axis is not vertical initially.

a. Error Associated with a Change in the Mounting Base Angle

The mounting base angle may change during operation due to thermal distortion of the vacuum chamber and its supporting structure. For example, if the structure is equivalent to a square steel frame and a temperature difference of $2°F$ between the two sides is introduced, the change in angle would be

$$\Delta \phi = 6.7 \times 10^{-6}/°F \ (2°F) = 1.34 \times 10^{-5} \text{ radians}$$

A tilt in a direction normal to the unbalance will introduce a zero shift. With the maximum initial unbalance, the resulting change in thrust reading would be

$$\text{thrust error } = \frac{11,000 \text{ gm cm } 1.34 \times 10^{-5} \text{ radians}}{50.8 \text{ cm}} \ \frac{1000 \text{ mg}}{\text{gm}}$$

$$= 2.9 \text{ mg}$$

On the other hand, a tilt in a direction parallel to the unbalance will produce a change in sensitivity.

$$\Delta k = \frac{M}{\theta} = 11,000 \text{ gm cm } 1.34 \times 10^{-5} \text{ radians}$$

$$= .148 \frac{\text{gm cm}}{\text{radian}}$$

which may be considered negligible compared to the normal beam stiffness.

b. Error Associated with an Initial Tilt in the Pivot Axis

The instrument is mounted in a separate vacuum chamber that is rolled into place on tracks. After positioning and evacuating the chamber the instrument can be leveled by a remote adjustment.

We will assume an error of .0005 radians (1.72 minutes) in the adjustment. If the unbalance changes in a direction normal to the tilt of the pivot axis, a zero shift will occur.

$$\text{thrust error} = \frac{85 \text{ gm cm} \cdot .0005 \text{ radians}}{50.8 \text{ cm}} \quad \frac{1000 \text{ mg}}{\text{gm}}$$

$$= .84 \text{ mg}$$

On the other hand if the unbalance changes in a direction parallel to the direction of axis tilt, a change in sensitivity will occur.

$$\Delta k = \frac{M}{\theta} = 85 \text{ gm cm} \cdot .0005 \text{ radians}$$

$$= .042 \frac{\text{gm cm}}{\text{radian}}$$

Again, the change in sensitivity is found to be negligible compared to the initial stiffness of the beam.

Although the calculated zero shifts are large enough to be of some concern, the errors can be readily reduced by increasing the accuracy of the initial adjustments. Very small errors in the initial balance of the beam can be detected by tilting the instrument slightly and noting the change in reading, while very small errors in the orientation of the pivot axis can be detected by adding weights to or taking weights from the beam and noting the change in reading. Errors due to inaccuracy in balancing the beam are not considered a problem.

3.2.7 Frictional Effects

The early calibration curves made before introducing mercury to the power pots show good repeatability, indicating that frictional effects in the instrument are normally acceptably small. However, it has not been definitely established that frictional effects are unimportant under all conditions. A question exists regarding the behavior of the wire reinforced teflon tubing. The reinforcing consists of a braided outer covering of stainless steel wire. The tubing will take a permanent set when bent if the deflection is large, but seems to behave repeatably under normal conditions that exist on the thrust stand. The question that is unanswered is whether jolts to the instrument can result in a permanent set in the tubing and a corresponding zero shift. This could conceivably occur for example when the field coil is suddenly de-energized. It is planned to perform tests with the flexible tube mounting reproduced on a separate beam. This will permit frictional effects, if they exist, to be distinguished from disturbances associated with the mercury pots.

We conclude from the evaluation of the thrust balance that the instrument, as it is, can be used to measure thrust with an error no greater than 30 mg provided current in the power pots does not exceed 200 amps, and a calibration is performed to determine:

i   the zero reading with the cooling water and the field coil circuit on, and
ii to determine sensitivity with the thruster operating.

63

It is also necessary to allow for the effect on the zero reading of arc current and gas pressure in the propellant line as determined by a separate calibration.

Accordingly, performance of the balance is considered satisfactory at thrusts of 1 gram and above at all except the highest field coil currents. In order to obtain satisfactory measurements at lower thrusts and at higher current values, a number of additional modifications are being considered.

1. A thrust killer (as described in References 14 and 15) could be installed on the thrust platform. A thrust killer is a set of baffles that can be swung into the jet during operation. The baffles are attached to the thruster. They greatly reduce the jet velocity and direct the flow radially outward so that a tare reading can be taken with the thruster in operation. This permits a zero reading as well as sensitivity to be determined under running conditions. Notice that it is not subject to the same difficulties that are experienced in the use of a thrust plate for measuring thrust directly. A thrust killer can be located very close to the thruster (in fact right against it) so that the flow entering the thrust killer is clearly just the flow leaving the nozzle. Interaction forces between the thruster and the thrust killer cancel insofar as the tare reading is concerned because the two are structurally connected.

2. The mercury pots could be undercut at the mercury surface and relocated in a vertical stack at the pivot axis, or replaced completely with flexible bus bars. This would be expected to largely eliminate effects due to oxide film on the mercury, convection currents in the mercury, and possible changes in surface tension forces. Adjustments would also be provided to permit electromagnetic forces on the leads and field coil to be minimized.

3. At least some of the flexible plastic tubes could be replaced by flexible arrays of metal tubing. This would reduce the influence of temperature on the sensitivity of the beam, reduce bourdon tube effects, and eliminate the possibility of frictional effects in the wire reinforced teflon tubing.

In principle, Items 2 and 3 are not required if a thrust killer is used. However, any reduction in extraneous variations in the calibration of the beam will reduce the frequency with which calibration must be performed during a test and increase the confidence that something does not change between the time that a calibration is performed and the time that thruster performance is measured.

3.3 A Change in Approach to the Problem of Measuring Thrust

From the foregoing account it is clear that further improvement in the performance of this thrust balance is an exponentially tedious task. Given the requisite time and effort, such improvement can be achieved, but for most purposes it is already quite adequate. In those

few cases where yet higher sensitivity and stability are required, it now appears that a rather different approach to the problem may be more productive than further refinement of the facility described above.

One of the goals of this program is to establish how closely space conditions can be simulated in the laboratory. To perform experiments with the best vacuum conditions obtainable and with the largest feasible ratio of test chamber size to thruster size, it is necessary to use the smallest thruster size that permits satisfactory measurements to be made. Since a theory is lacking for predicting environmental conditions that will adequately simulate space, a target of 100 watts has been selected for thruster size based on the judgement that it should be possible to develop satisfactory instrumentation for measuring performance in this size range. Thrust levels calculated for a range of powers and specific impulses are tabulated below for an assumed thruster efficiency of 30 percent.

	Specific Impulse	
Power (watts)	2000	4000
	Thrust (mg)	
100	312	156
200	625	312
500	1560	780
1000	3120	1560

We see that the balance must give satisfactory results down to a thrust level of about 150 mg which is considerably lower than has previously been measured with good accuracy with this type of thruster. It is therefore desired to obtain a thrust reading which is accurate within 1 or 2 mg. Although the present balance is exceptionally sensitive, it is evident that a very significant improvement in its performance will be required.

The problem is made difficult by the service lines that must be connected to the thruster. These include:

a. Electrical power for the arc.
b. Electrical power for the magnetic field coil (up to 500 amps with the present design).
c. Low and high pressure cooling water lines.
d. A propellant line, and
e. Various instrumentation lines.

It has been shown in the preceding section that these connections can introduce sizable disturbing forces.

Although a program is being undertaken to reduce these errors by improving the design of the balance, the urgency of obtaining good thrust readings with very small thrusters seems to warrant a back-up approach. In parallel with the activity for further improvement of the balance, a plan is being initiated for redesigning the engine to make it as self sufficient as can feasibly be done, thereby minimizing connecting lines to the thrust platform. It has been found that increased weight on the thrust platform has a minor affect on accuracy compared to the effect of connecting lines. Approaches which will be considered are listed below:

a. The propellant supply could be mounted directly on the thrust platform. It could take the form of a small cryogenic container. Notice that a one liter container of liquid hydrogen would hold about 70 grams of propellant, while the flow rate at the high end of the power range is about 1.5 mg per second. This corresponds to a minimum running time of 13 hours. A 70 gram weight change would not introduce a serious imbalance in the beam, even if the container were located a foot or two from the pivot axis.

b. Power conditioning equipment (such as a transformer and rectifier) could be mounted directly on the thrust platform, permitting power to be introduced through small (high voltage-low current) leads. It is also possible that the magnetic field coil could be re-designed to operate directly at a higher voltage and lower current. As an alternative, the use of permanent magnets to provide the necessary field could be considered when temp-erature conditions permit.

c. A radiation cooled thruster could be used to eliminate cooling water lines. The amount of surface needed for radiation cooling at these low power levels is quite moderate.

In the absence of large connecting leads, the problem of measuring small steady state thrust forces becomes immediately much easier. At the present stage of development it is expected that this approach can provide more rapid improvement than is anticipated from continued refinement of the balance. The design of a small self contained engine for mounting on the thrust stand may also provide information which will be of use in the devel-opment of engine components for flight applications.

4.0 CONCLUSIONS

The major findings resulting from the program are listed below:

1. A comprehensive series of photographs are presented to show the effect on the geometry of the visible plume of variations in environmental conditions. These include changes in the arc field coil strength, changes in the strength of the field due to coils wrapped around the chamber, and changes in the pressure of gas in the test chamber. The experiments show:

a. A well collimated luminous beam extends dowistream from the thruster and bends to the right of the insulated tank. The beam can be observed in the aluminum tank as well as the insulated tank.

b. A magnetic field generated by coils wrapped about the vacuum chamber tends to concentrate the diffuse fog-like glow in the tank into a central beam and to straighten the curvature of the beam.

c. The beam has a strong heating effect on any surface that it strikes, conducting or non-conducting; and

d. An increase in the test chamber pressure produces a marked increase in the luminosity of the plume.

2. The following conclusions have been reached from measurements of the shape of the luminous beam in the earth's magnetic field inside a large coil designed to cancel the earth's field, and inside a large coil designed to produce fields of varying strength.

a. The normal curvature of the beam is caused by the earth's field.

b. The sense of the curvature corresponds to a beam of electrons rather than a beam of positive ions for particles moving in the downstream direction.

c. The tightness of the spiral path corresponds to electron velocities estimated to be:

$$5.93 \times 10^6 \text{ m/sec } \pm 10 \text{ percent}$$

which is equivalent to 100 electron volts or about two thirds of the arc voltage.

d. The estimated particle energy is found to correlate with arc voltage as arc voltage changes due either to a change in operating mode or a change in the strength of the arc field coil. No significant dependence on arc current was observed.

e. The luminosity of the beam increases as pressure in the test chamber is increased, but continued increase in the pressure results in shortening of the visible beam. The observed beam lengths correlate with calculated mean free paths for electrons at this energy level.

These observations support the theory that the beam consists of electrons accelerated by the arc potential difference.

3. From preliminary Langmuir probe surveys and from space charge considerations, it appears that the current in the beam is small (no more than a few milliamps). Nevertheless, the energies involved are large and concentrated enough that the existence of the beam must be viewed as a possible hazard in space applications. In some situations a magnetic field could cause the beam to curve in a circular path resulting in its impingement on the spacecraft.

4. The mechanism for formation of the beam is not understood, but any explanation would seem to require an unusually low density corridor in a region of high potential gradient near the electrodes. The phenomena may provide clues to a better understanding of the arc operation.

5. Tests made using hydrogen as the working fluid but with various other gases introduced directly into the test chamber show that:

a. The arc voltage is strongly dependent on the ambient pressure and on the type of environmental gas used, and

b. The color of the plume depends on the environmental gas. The color change apparently penetrates to the center of the jet.

These observations suggest that the jet mixes very rapidly with the surrounding gas, and strongly indicate that a large fraction of the arc energy is expended in the plume rather than in the arc chamber, or at least in a region that reflects conditions in the plume.

6. An optical system has been developed for studying the rotational and oscillating behavior of the arc. Typical oscilloscope traces show an arc frequency greater than 100 KC. In at least part of the cases, phase shift measurements suggest that the oscillations are rotational in character.

7. An approximate analytical model is presented which gives a theoretical lower bound on the rotational frequency of the arc. Comparison with experiments shows that the theory predicts trends fairly well, and usually does predict a lower frequency than is measured. The discrepancy suggests that the gas does not attain the angular velocity of the arc as is supposed in establishing the lower limit.

8. The possibility is suggested that the moving arc may act to some extent like a motor powered fin or vane transferring electrical energy directly into kinetic energy in the gas. Notice that this action could occur whether the arc motion is purely rotational or the arc experiences axial-Jacob's ladder type oscillations as well (as described in Reference 16). An approach is presented for calculating the fraction of the electrical power that must go into ohmic heating, and the fraction that may be transferred in part as non-dissipative electromagnetic work. More refined experiments are needed to evaluate this possibility.

9. A study of the thrust balance made near the end of the program has shown that, although the instrument is exceptionally sensitive, the intended accuracy goals have not yet been achieved. With the present configuration, the thrust measurements are strongly influenced by extraneous forces associated with the service lines supplied to the thruster. These include the propellant line, the cooling water lines, and the power leads for the arc and the magnetic field coil. As a consequence, the thrust measurements (which were made prior to the study of the thrust balance) cannot be considered sufficiently reliable for presentation. It will be necessary to either improve the balance design or very carefully take into account the effect of the connecting leads in the calibration. To alleviate the problem, a change in approach is suggested. The engine would be constructed as a nearly self sufficient unit which could be mounted on the thrust platform. The assembly would include a propellant supply and power conditioning equipment, and the thruster would be designed to be cooled by radiation. It is believed that the service connections can be reduced to a pair of high voltage low current power leads and a number of light leads for control and instrumentation purposes.

Activities suggested for future studies include the use of more refined instrumentation for surveying conditions in the plume, tests correlating changing operating conditions with thrust measurements using improved thrust measuring techniques and development of a thruster with features that make it relatively free of influences of the environment. In particular, it is believed that the development of a thruster with reverse polarity would provide useful information regarding the behavior of the plume, and might be more readily developed for space application if some of the external interaction effects could be avoided. Also, it appears attractive to shift toward thrusters of smaller size to enable space conditions to be more closely simulated in the test facility. Instrumentation for a more detailed examination of the plume is expected to include electrical probes, an improved pressure probe which is rotatable and at the same time has high sensitivity and fast response, and equipment for spectroscopic analysis of the luminous plume.

APPENDIX 1

Rotating Azimuthally Localized Current Distribution in an MPD Arc

Introduction

It is now clear that the MPD arc is capable of a number of different modes of operation. In particular both axisymmetric and azimuthally localized current distributions have been found. In a previous analysis we have considered the axisymmetric case. The work presented here deals with an azimuthally localized or fin-like distribution. In the coaxial MPD arc with an axial bias magnetic field, the current must cross magnetic field lines to establish a conduction path between the electrodes. In the case of an axisymmetric current distribution it follows from generalized Ohm's law that where a radial electron current density exists then also a Hall current must flow, and the magnitude of the radial current is inversely proportional to the square of the Hall parameter. On the other hand, if the discharge forms in an azimuthally localized region, Hall currents cannot flow because an azimuthally continuous conduction path does not exist. Initially, the electrons attempt to drift azimuthally in the crossed radial electric and axial magnetic field and tend to escape the discharge region leaving behind the heavier ions. This motion sets up a charge separation induced azimuthal field, the Hall field, which in turn influences the conduction of current parallel to the radial electric field. The net result is that the radial current density is proportional to the effective electric field and is independent of the Hall parameter, thereby allowing the conduction of current even in a region of very large Hall parameter.

We have studied the current flow and the motion of the fin in the context of an analytical model which neglects internal structure of the fin and nonuniformities in the plane of the fin. The dynamics of the fin have been considered in conjunction with generalized Ohm's law. An overall torque-angular momentum balance applied to the fin gives a lower bound on the rotation frequency which is compared with experimental data. Finally, the structure of the fin and factors related to efficiency are considered briefly.

Analytical Model

The experiments of Lovberg[12, 17, 18] showed that an argon arc which reached steady conditions during millisecond pulsed operation has an azimuthally localized current distribution which rotated with a single angular frequency. Later localized rotating current distributions were observed also in steady flow MPD arcs operated with ammonia,[19] argon and nitrogen[20] and hydrogen and lithium.[21] We consider the dynamics and current conduction in an idealization of the fin-like structure revealed by Lovberg's experiments. We suppose that the fin

is of uniform thickness and that all parts of the fin move with the same velocity. Radial mass motion in the interior of the fin is assumed to be zero, the centrifugal forces being supposed balanced by forces originating with solid surfaces or azimuthal currents outside the rotating fin. Nonuniformities of plasma variables in the plane of the fin will be neglected. In addition we will at first not consider the coaxial MPD arc geometry but study the rectilinear motion of the current density distribution under the influence of uniform crossed electric and magnetic fields employing the coordinate system shown below.
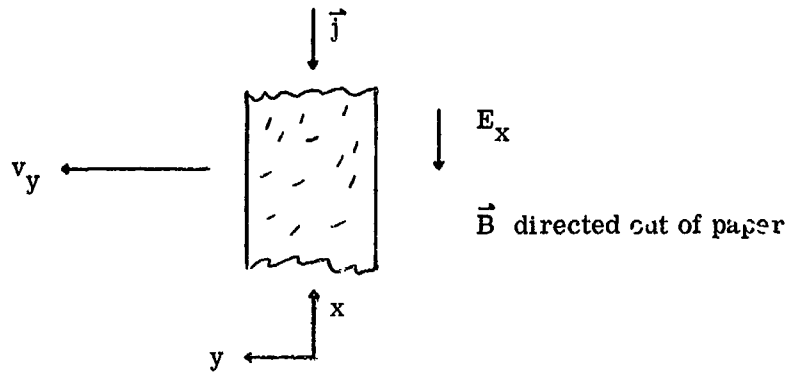
When the gas breaks down in a localized region, the crossed electric and magnetic fields generate a potential difference across the fin in much the same way as the Hall effect occurs in a solid conductor. The electrons, under the influence of the crossed fields and because of their small mass, attempt to escape the discharge region with a drift velocity E_x/B, and in so doing set up a charge distribution that is the source of a transverse field E_y, as illustrated below:
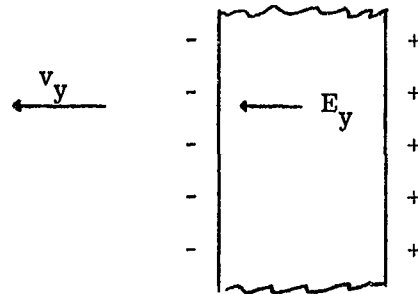
The discharge as a whole remains electrically neutral. We view the fin as a localized azimuthal distribution of ion (and electron) density which does not change as the fin moves. That is to say, each point of the ion density configuration moves with the same velocity so that the fin does not change its shape as it rotates. If the cold gas into which the fin moves

penetrates the fixed current density distribution with its background matrix of ions, the fin velocity and the mass velocity will not be equal or, said in another way, there will be neutra`-ion slip in the interior of the fin. If there is no ion-slip the gas outside the fin is accelerated without penetrating the fin. This condition could in principle be realized if a strong shock would stand near the leading surface of the fin. It turns out that the limited results obtained here in the approximate treatment of the problem are independent of the degree to which the gas penetrates the fin provided there is no mass flux through the trailing surface.

In accordance with our assumption of the undeformed motion of the ion and electron density distribution which determines the fin we take the velocity v_{iy} of the ions to be the same for all points of the fin. In our approximate treatment this represents the condition that in a coaxial geometry the rotation frequency is the same everywhere within the fin, and if there is no ion slip, v_{iy} and the mass motion are equal everywhere in the fin. In the case of rectilinear motion we have

$$\frac{\partial v_{iy}}{\partial y} = \frac{\partial v_{iy}}{\partial z} = 0 \ .$$ (1)

Because of the conservation of charge

$$\frac{\partial j_x}{\partial x} + \frac{\partial j_y}{\partial y} + \frac{\partial j_z}{\partial z} = - \frac{\partial \rho_e}{\partial t} \ .$$ (2)

For $j_z = 0$, and $\partial j_x / \partial x = 0$ (uniform in x). Our assumption of undeformed motion implies that the charge density viewed in a frame moving with the fin velocity is constant, i. e.,

$$\frac{\partial \rho_e}{\partial t} + v_{iy} \frac{\partial \rho_e}{\partial y} = 0 \ .$$ (3)

It follows that

$$\frac{\partial j_y}{\partial y} = v_{iy} \frac{\partial \rho_e}{\partial y} \ .$$ (4)

Since v_{iy} is uniform in the fin, we have

$$j_y = v_{iy} \rho_e \ .$$ (5)

This shows that the transverse component of the current is entirely a convection current. The charge density ρ_e is the source of the transverse electric field.

The charge density ρ_e produces an electric field which satisfies

$$\frac{\partial E_y}{\partial y} = \frac{\rho_e}{\epsilon_o} .$$

(6)

Combining (6) with (5) yields

$$j_y = \epsilon_o v_{iy} \frac{\partial E_y}{\partial y} .$$

(7)

Then, integrating across the fin gives

$$I_y = \int j_y \, dy = 0$$

(8)

as it should be. The magnitude of the transverse convective current density can be calculated with the aid of (7). Integrating over the current until the maximum value of the transverse field is reached we obtain

$$I_y' = \epsilon_o E_y v_{iy} .$$

Using $E_y = 200$ volts/meter, $v_{iy} = 5 \times 10^3$ meters/sec, which are experimental values, yields

$$I_y' = 8.85 \times 10^{-6} \text{ amps}$$

which is entirely negligible compared to the arc current.

Transient Motion of the Fin

Now let us consider the momentum balance on the fin. We imagine that the arc is formed while the plasma is stationary and that the fin accelerates as a rigid structure to a final velocity, which is determined by the pressure gradients, momentum flux and Lorentz forces acting on the fin. The y-component of the momentum equation for a continuum inviscid flow is

$$\rho \, \frac{d v_y}{d t} = - \frac{\partial p}{\partial y} \, , \tag{9}$$

which is coupled to the electric current equation. The generalized Ohm's law we shall employ is

$$\eta \, j_x + \frac{B}{e n_e} \, j_y = E_x^{\prime\prime\prime} \, , \tag{10}$$

$$- \frac{B}{e n_e} \, j_x + \eta \, j_y = E_y^{\prime\prime\prime} \, , \tag{11}$$

where

$$E_x^{\prime\prime\prime} = E_x + v_{iy} B + \frac{1}{e n_e} \, \frac{\partial p_e}{\partial x} \, , \tag{12}$$

$$E_y^{\prime\prime\prime} = E_y - v_{ix} B + \frac{1}{e n_e} \, \frac{\partial p_e}{\partial y} \, , \tag{13}$$

are the effective parallel and transverse electric field. η is the electrical resistivity, B is the magnitude of the axial bias field and n_e, p_e are the electron density and pressure. This form of the current equation neglects the partial time derivative of the current density and quadratic terms in $\vec{j}$ and $\vec{v}$. Solving (10) and (11) for the components of the current density yields

$$j_x = \frac{1}{\eta (1 + \Omega^2)} \left(E_x^{\prime\prime\prime} - \Omega E_y^{\prime\prime\prime} \right) \, , \tag{14}$$

$$j_y = \frac{1}{\eta (1 + \Omega^2)} \left(\Omega E_x^{\prime\prime\prime} + E_y^{\prime\prime\prime} \right) \, , \tag{15}$$

where

$$\Omega = \frac{e B}{\eta m_e} \tag{16}$$

If an azimuthally diffuse discharge forms and provides a continuous conduction path for the flow of an azimuthal current density, then charge separation cannot be sustained and E_y vanishes. If the Hall current j_y would also vanish then from generalized Ohm's law it follows that

$$j_x = e n_e v_{ix} , \qquad (17)$$

if

$$\frac{1}{e n_e} \frac{\partial p_e}{\partial x} = 0 ,$$

showing that the entire parallel conduction current is carried by the ions.

In contrast, in an azimuthally localized discharge, which is the case of interest here, the Hall current density j_y cannot flow because there is no continuous conduction path, but a transverse field E_y is sustained by charge separation. Generalized Ohm's law gives in this case the relation between the effective Hall and parallel fields,

$$E_y''' = - \Omega E_x''' , \qquad (18)$$

and the current density parallel to the arc field E_x is given by

$$j_x = \frac{1}{\eta} E_x''' . \qquad (19)$$

Returning to the momentum equation (9) and integrating across the fin gives

$$\int_{y_1}^{y_2} \left(\frac{\partial v_y}{\partial t} + v_y \frac{\partial v_y}{\partial y} \right) dy = - \int_{y_1}^{y_2} \frac{j_x B}{\rho} dy - \int_{y_1}^{y_2} \frac{dp}{\rho} \qquad (20)$$

where y_2 and y_1 are the coordinates of the leading and trailing surfaces of the fin. If the neutrals flow through the leading surface of the fin then $v_y(y_2) = 0$, and if there is no flux of neutrals through the trailing surface then $v_y(y_1) = v_{iy}$. We neglect the last term in (20), which would vanish if ρ is constant or, more generally, if p and ρ are related by a polytropic process. Then (20) simplifies to

$$\frac{\partial v_{iy}}{\partial t} = - \frac{v_{iy}^2}{2} - \frac{j_x B D}{\rho} , \qquad (21)$$

where D is the thickness of the fin and j_x and ρ are the average electric current density and mass density in the fin. Use of (19) in (21) yields

$$\frac{\partial v_{iy}}{\partial t} = - \frac{B^2}{\eta \rho} \left(\frac{E_x''}{B} + v_{iy} \right) - \frac{v_{iy}^2}{2D} , \qquad (22)$$

75

where

$$E_x'' = E_x + \frac{1}{e\,n_e}\frac{\partial p_e}{\partial x} \tag{23}$$

and η is to be understood as the average resistivity across the fin. For time independent η and ρ equation (22) can be integrated with the result

$$v_{iy} = 2D\lambda_+ \left[\frac{1 + e^{-(\lambda_+ - \lambda_-)t}}{1 - \frac{\lambda_+}{\lambda_-}e^{-(\lambda_+ - \lambda_-)t}}\right] , \tag{24}$$

where the characteristic roots λ_+ and λ_- are determined by

$$\lambda_\pm = -\frac{1}{2\tau} \pm \left[\frac{1}{(2\tau)^2} + \frac{1}{\tau}\frac{E_x''}{2DB}\right] . \tag{25}$$

In (25) the parameter τ has been introduced and it is defined by

$$\tau = \frac{B^2}{\eta\rho} . \tag{26}$$

It is a characteristic time in this problem. It is seen by inspection of (24) and with the aid of (25) that the characteristic time for the fin to approach steady motion may be written as

$$\frac{1}{\lambda_+ - \lambda_-} = \frac{\tau}{(1 - 2E_x''\tau/BD)^{1/2}} . \tag{27}$$

Since E_x'' is negative, it can be seen from (27) that $1/(\lambda_+ - \lambda_-)$ is less than τ. The magnitude of τ or $1/(\lambda_+ - \lambda_-)$ may be of some interest in pulsed arcs when there is some concern about whether steady motion is achieved in short times. In Lovberg's experiments τ is very small compared with the pulse duration and steady motion is obtained during the pulse.

The steady state velocity of the fin, v_f, is given by

$$v_f = -\frac{D}{\tau} + \left[\left(\frac{D}{\tau}\right)^2 - \frac{2E_x''D}{B\tau}\right]^{1/2} . \tag{28}$$

Alternatively we may relate the fin velocity to the transverse electric field by equating the right hand side of the momentum balance equation to zero and with the aid of (15) for $j_y = 0$,

obtain

$$\frac{B^2 E_y''}{\eta \rho \Omega} = \frac{1}{2} \frac{v_f^2}{D} \ .$$

With the definition (16) of the Hall parameter this equation is expressed as

$$E_y'' = \frac{1}{2} \frac{m_i v_f^2}{\epsilon e D} \ , \tag{29}$$

where ϵ is the ionization fraction. Equation (29) has a simple interpretation: $e E_y'' D$ is the effective Hall voltage required to bring a charged particle of mass m_i / ϵ moving with the fin velocity to rest.

There is some evidence that a radial mass flow develops near the leading surface of the fin, which suggests that the fin may accelerate part of the mass into which it moves without the gas having to pass through the fin. It is attractive to speculate that a strongly ionized fin could thus accelerate a gas in the manner of a propeller without the flow passing into the fin and reaching the same temperature and degree of ionization as the plasma in the interior. Carrying this idea to a limit an idealization is reached where a strong shock or pressure front of some kind stands at the leading surface of the fin and the hot flow is accelerated to the fin velocity at the leading surface and there is no mass flux into the interior of the fin. The momentum balance on the fin is then achieved by the equality of the Lorentz force density and the pressure gradient in the fin. In this case the pressure difference across the fin would be roughly $\rho v_f^2 / 2$ and if we take the pressure gradient to be this pressure difference divided by the fin thickness, the momentum balance, in steady motion, yields

$$0 = - j_x B - \frac{\rho v_f^2}{2 D} \ . \tag{30}$$

Thus in this very approximate treatment of the steady state momentum balance on the fin, we obtain the same results (30) for the impermeable fin as for the permeable fin, as can be seen by setting the time derivative in (21) equal to zero.

Numerical Values of Plasma Parameters

With (28) and (29) we are in a position to calculate the characteristic time τ and the ionization fraction ϵ from the data of Lovberg's experiments. If we knew the average values of τ and the ionization fraction ϵ we could compare the predictions of (28) and (29) with experiment and this would constitute a check on our theoretical analysis of the fin. Instead we must calculate values of τ and ϵ which are consistent with measured values of

E_x, E_y and v_f. According to (28)

$$\tau = - \frac{2D(E_x''/B + v_f)}{v_f^2}$$

(31)

Using $D = 3 \times 10^{-2}$ meters, $E_x''/B = -1.4 \times 10^4$ meters/sec, $v_f = 5 \times 10^3$ meters/sec, which represent conditions at the middle of the fin, and neglecting a possible contribution of the electron pressure gradient to the effective electric field we obtain

$$\tau = 2.2 \times 10^{-5} \text{ sec} .$$

From (29), using the argon ion mass and $E_y = 2 \times 10^2$ volts/meter, we find

$$\epsilon = 0.42 ,$$

which is a high value according to independent estimates of the degree of ionization in the fin. We have assumed that all the mass flow is accelerated to the fin velocity. If this assumption was modified to let some fraction of the mass pass through the fin without attaining the fin velocity, the ionization fraction calculated as above would be reduced.

With the aid of the experimentally determined values of B, j_x, E_x, E_y we may determine directly from generalized Ohm's law, independently of the fin dynamics, the Hall parameter, resistivity and the electron number density. The values found are

$$\eta = 1.9 \times 10^{-3} \text{ ohm-meters} ,$$

$$n_e = 3.8 \times 10^{20} \text{ electrons/meter}^3 ,$$

(32)

$$\Omega = 0.44 .$$

Now the plasma variables, η, n_e, Ω are not independent of the characteristic time τ and the ionization fraction ϵ, which appeared when we considered also the dynamics of the fin. In fact, τ may be expressed as

$$\tau = \frac{1}{\epsilon \, \omega_i \, \Omega} .$$

(33)

Hence, a weak experimental check on the analysis of the fin motion and current conduction can be obtained by calculating the Hall parameter Ω from (33) using the values of τ and ϵ computed above and then comparing with the value given by (32). We obtain

$$\Omega = 0.87 ,$$

and so there is a discrepancy of a factor two between the two values, which is not surprising in view of the approximations entering into the analysis and uncertainties in the experimental values. Collecting these results we have

TABLE 1

Resistivity, η	1.9×10^{-3} ohm-meter
Electron number density, n_e	3.8×10^{20} meter^{-3}
Hall parameter, Ω	0.44, 0.87
Ionization fraction, ϵ	0.42
Characteristic time, τ	2.2×10^{-5} sec

The experimentally determined quantities[12, 18] used in the above calculations are

TABLE 2

Parallel field, E_x	7×10^2 volts/meter
Transverse field, E_y	2×10^2 volts/meter
Current density, j_x	2.4×10^5 amps/meter^2
Magnetic field, B_z	5×10^{-2} tesla

Fin Rotation Frequency for Invisced Flow

Let us now consider the factors which determine the rotation frequency of the fin. Taking the cross product of the equation of motion for an inviscid flow with the radius vector $\vec{r}$, use of the conservation of mass, integration over a volume which contains the currents at all times, and application of Gauss' theorem gives

$$\int_A r v_\theta \, d\dot{m} = \int r j_\perp B r \, d\theta \, dz \, dr , \qquad (34)$$

where the integration on the left hand side is over an area bounding the volume of integration. The time derivative drops out when the fin reaches its steady velocity since in the periodic motion of the fin the total angular momentum of the system is independent of time. In (34) $j_\perp$ is the component of the current density perpendicular to the field lines and B is the magnitude of the magnetic field. If we integrate over surfaces of constant magnetic flux then we may rewrite (34) in the form[2]

$$\int_A r v_\theta \, d\dot{m} = \frac{1}{2\pi} \iint_{I \ \varphi} dI \, d\varphi \ , \tag{35}$$

where

$$dI = j_\perp r \, d\theta \, ds$$

is the current flowing through an infinitesimal area on a surface of constant flux and

$$d\varphi = 2\pi B_z r \, dr$$

is the flux through an infinitesimal annular area. We suppose that the maximum angular velocity which the gas can attain is the fin velocity. The maximum angular momentum flux is therefore obtained if the mass is ejected at the outer periphery of the fin with the fin angular velocity. Taking the left hand side of (35) equal to this maximum value we obtain

$$R^2 \omega \dot{m} \geq \frac{1}{2\pi} \iint_{I \ \varphi} dI \, d\varphi \ , \tag{36}$$

where ω in (30) is the angular velocity of the fin and R is the outer radius of the fin. In certain special cases the integral on the right hand side can be calculated exactly.[2] In general the integral is greater than $I\varphi/2$, where I is the total arc current and φ is the flux through an annular area which is bounded on the outside by a surface of revolution formed by field lines which intersect by the anode at the throat and field lines emanating from the outer boundary of the current attachment at the cathode. Hence we retain the inequality (36) if we replace the integral by $I\varphi/2$, with φ as defined above, yielding

$$R^2 \omega \geq \frac{I\varphi}{2\pi} \ . \tag{37}$$

If we assume the radial extension of the fin does not extend significantly beyond the anode attachment we may express the inequality (37) in the form

$$f_{exp} \geq f_{min} = \frac{I\bar{B}_z}{4\pi\dot{m}} \tag{38}$$

where $\bar{B}_z$ is the z-component of the field averaged over the throat area, and f is the cyclic frequency of rotation. The inequality shows agreement with experiment on several points; a linear increase in frequency with the product IB_z, and a decreasing frequency with increasing mass flow and linear dependence on I and B separately. The measured rotation frequency for a steady ammonia arc is shown in Figures 51 and 52 where the frequency is seen to decrease with increasing mass flow, the linear dependence on IB is observed and the data is in agreement with the theoretical lower bound given by (38).

Rotation Frequency with Viscosity

For the pulsed quasi-steady argon arc we still have agreement with the bilinear dependence of frequency on I and B, but this data violates the theoretical lower bound derived here as can be seen in Figure 53. We have replotted the data of reference 19 using the average value of B_z estimated from measurements given in reference 18. The discrepancy suggests that viscous forces may be important here. A rough measure of the significance of the viscous forces in this problem is given by the magnitude of the square of the Hartmann number

$$M^2 = \frac{B_z^2 R^2}{\eta\mu} \, ,$$

where μ is the viscosity. Using $\eta = 1.9 \times 10^{-3}$ ohm-meters as calculated above, $B = 5 \times 10^{-2}$ tesla and $\mu = 1.4 \times 10^{-4}$ kg/meter-sec and $R = 10^{-2}$ meters shows that M^2 is of the order of unity, indicating that viscous forces should be given some consideration.

The momentum equation, with the viscous force, may be expressed in the form

$$\rho\,\frac{d\vec{v}}{dt} = \vec{j}\times\vec{B} - \text{grad }p + \mu\,\text{div}\,\vec{\vec{\tau}} \, , \tag{39}$$

where $\vec{\vec{\tau}}$ is the viscous part of the stress tensor. Integrating over a cylindrical volume containing the currents at all times, use of Gauss' theorem and the boundary condition $v_r = v_\theta = 0$ at the anode surface and neglecting the contribution of the viscous stresses on the part of the cylinders not in contact with the anode yields

$$\int_A r v_\theta \, d\dot{m} = \frac{1}{2\pi}\int dI d\varphi + \mu \int_{A'} \frac{\partial v_\theta}{\partial r} R^2 d\theta dz \, , \tag{40}$$

81

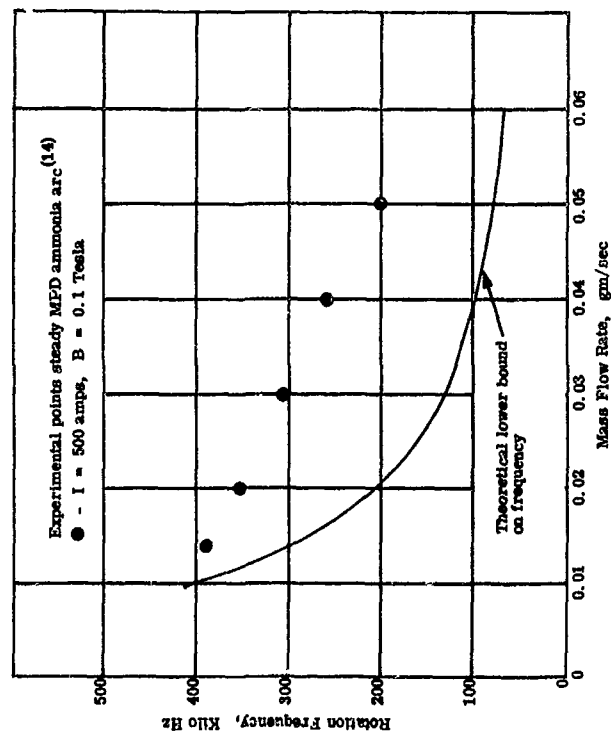Figure 51. Lower Bound on Rotation Frequency According to Theory Based on Fin Structure of Arc. Fixed Current and Magnetic Field Strength, Variable Mass Flow Rate

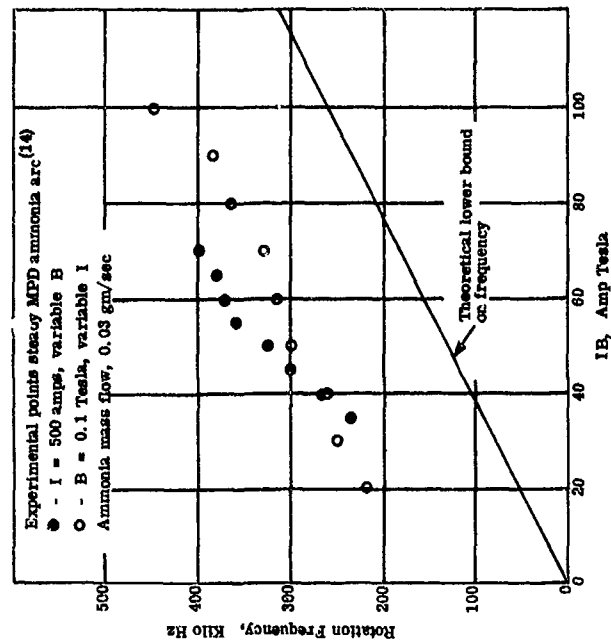Figure 52. Lower Bound on Arc Rotation Frequency According to Theory Based on Fin Structure of Arc
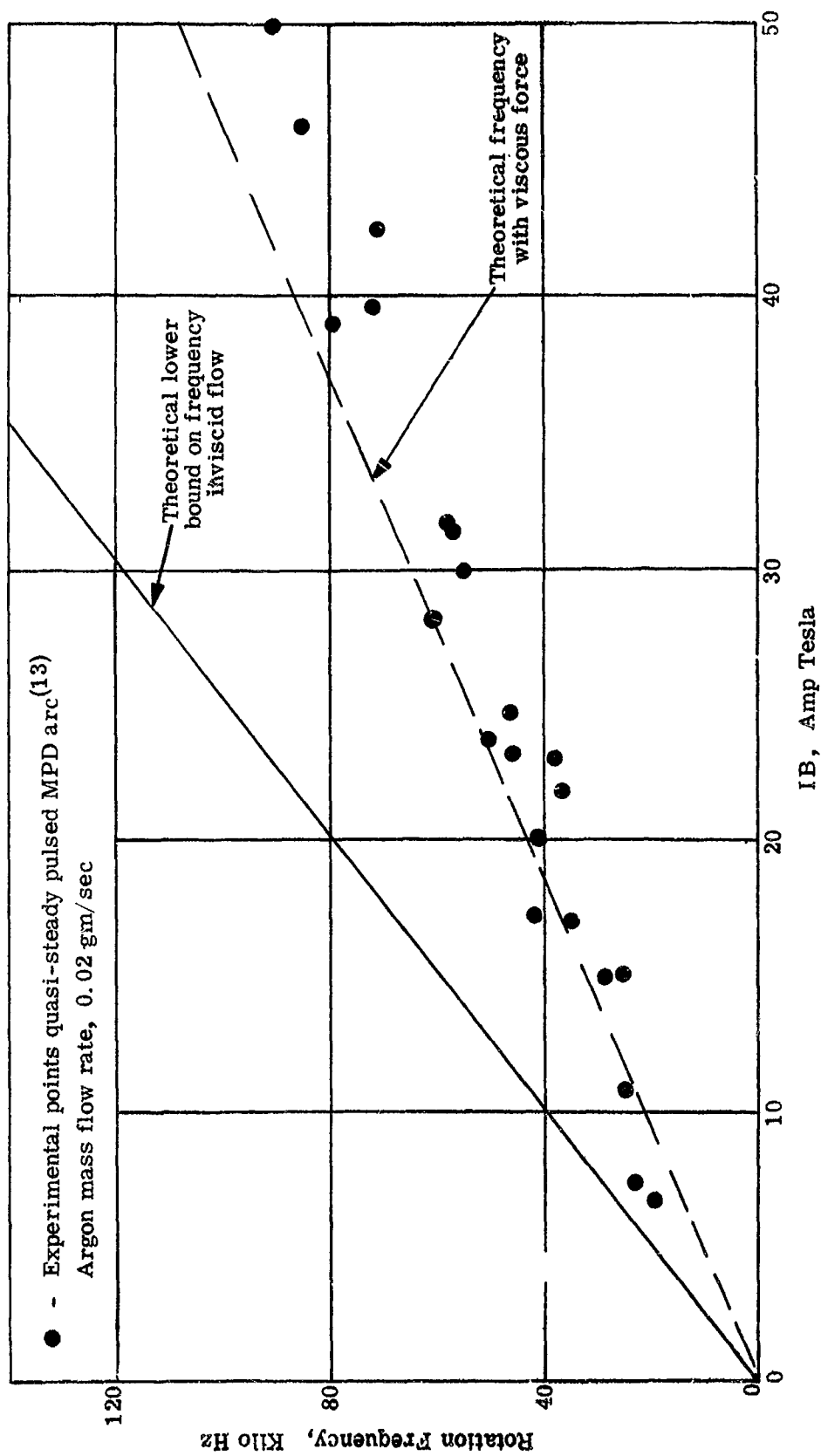
82

Figure 53. Theoretical Lower Bound on Arc Rotation Frequency According to Theory Based on Fin Structure of the Arc With Viscous Forces Neglected

where μ is the viscosity of the gas. In (40), A is the surface area bounding the current distribution and A' is the surface area over which the rotating gas makes contact with the anode. Supposing that the surface A has the anode radius R and that all the gas is ejected through this surface with the fin velocity $R\omega$, treating the Lorentz force on the gas as before and estimating the velocity gradient by $R\omega/\Delta R$ where ΔR is the thickness of the boundary layer yields

$$\omega \dot{m} + \mu \omega \frac{R}{\Delta R} \Delta \theta L = \frac{I \bar{B}_z}{2} \, ,$$

or

$$f = \frac{I \bar{B}_z}{4\pi (\dot{m} + \mu R \Delta \theta L / \Delta R)} \, , \tag{41}$$

where $f = \omega/2\pi$ and L is the axial dimension of the rotating gas in contact with the anode and $R\Delta\theta$ is the thickness of the fin.

To continue the calculation of the contribution of the viscous torque we need to make a numerical estimate of the quantity $\mu R \theta L / \Delta R$. We take the values displayed in the following table:

TABLE 3

Azimuthal dimension, $R\Delta\theta$	3×10^{-2} meters
Fin length at anode attachment in throat, L	3×10^{-2} meters
Boundary layer thickness, ΔR	1×10^{-2} meters
Argon viscosity, μ	1.4×10^{-4} kg/meter-sec
Argon mass flow rate, $\dot{m}$	2×10^{-5} kg/sec

The length L has been taken as the distance from the anode face to the tip of the cathode and represents an estimate of the axial length of the fin which is sweeping against the anode, an estimate which is based on the current distribution shown in Figure 52, Reference 19. The azimuthal dimension of the flow over which radial gradients of the azimuthal velocity are significant has been taken to be the fin thickness. The boundary layer is assumed to begin where the electric field intensity begins to increase sharply. The boundary layer could be smaller than 10^{-2} meter but not larger, as measurements have shown the angular velocity of the fin angular velocity to be constant up to radii of more than 3.5 centimeters. The

viscosity has been obtained from reference 22. Using the values listed in Table 3, the frequency given by (41) is computed and shown graphically in Figure 53 as a function of $I\bar{B}_z$ together with the experimental data.

Discussion

In the above analysis we have considered the fin motion where the leading surface is penetrated by neutrals and have also considered the motion where the fin acts as an impenetrable object, accelerating the flow without the cold gas penetrating the fin. The approximate treatments of the fin motion and current conduction do not distinguish between these two models. Moreover, the analysis giving the rotation frequency was based on the integral conservation of torque and angular momentum flux and it was not necessary to consider the internal structure of the fin. However, the internal fin structure is of interest with respect to efficiency since it has to do with the fraction of the total mass flow that penetrates the fin and is ionized and excited, and these losses can be dominant if the flow is ionized and excited at the level set by local thermal equilibrium conditions at the average stagnation enthalpy of the exit flow. It is attractive to speculate that a very strongly ionized fin could accelerate the gas in a manner of a propeller, without the flow passing into the fin and becoming ionized to the same degree as the plasma in the interior of the fin. We note the obvious fact that when the fin has achieved steady motion it does not pick up mass in the manner of an imploding current sheet as, for example, in a linear pinch discharge. The same amount of mass as is incident on the leading fin surface must also be ejected from the interior of the fin if it penetrates, or flow over and around the leading fin surface if it does not. The details of this acceleration are of course very important for a thruster application.

In connection with efficiency we consider the energy balance equation

$$IV_f = I^2 \mathcal{R} + IBRv_f \tag{42}$$

where $V_f = E_r R$ is the radial fin voltage, R is the radial extension of the fin, $v_f = \omega R/2$ is the fin velocity at the midpoint and $\mathcal{R}$ is the electrical resistance. Equation (42) is obtained from generalized Ohm's law by multiplying by j_r integrating over the fin volume and neglecting the volume integral of the term containing the radial electron pressure gradient. According to the experimental values for argon (which may not be representative of conditions for different thrusters and propellants) the total power is divided into about 70 percent ohmic heating and 30 percent nondissipative electromagnetic work. The dissipative part of the power must be accounted for by heat transfer from the fin and increasing the enthalpy of the part of the flow which penetrates the fin. In a thruster application, one is then faced, as in a purely thermal device, with the usual problem of the recovery of static enthalpy. For the operation point for argon considered above the partition of nondissipative to dissipative power does not appear favorable. In the lighter gases this power partition may be quite different.

85

REFERENCES

1. A. C. Ducati, R. G. Jahn, E. Muehlberger and R. P. Treat, "Exploratory Electromagnetic Thruster Research, Phase II," Semiannual Report, 2SS108-1513, Contract NASw-1513 (Oct. 1968).

2. A. C. Ducati, R. G. Jahn, E. Muehlberger and R. P. Treat, "Exploratory Electromagnetic Thruster Research," NASA CR 62047 (Feb. 1968).

3. A. C. Ducati, R. G. Jahn, E. Muehlberger and R. P. Treat, "Design and Development of a Thermo-Ionic Electric Thruster," NASA CR 54703 (May 1966).

4. A. C. Ducati, "Electrothermally Accelerated Plasma Jets," AFOSR Contract AF 49(638)-1572, Final Report (Sept. 1966).

5. A. C. Ducati, "Losses in Plasma Acceleration," AFOSR 68-0004 (Nov. 1967).

6. U. S. Department of the Interior, Geodetic Survey, Los Angeles, California, private communication.

7. H. S. W. Massey and E. H. S. Burhop, Electronic and Ionic Phenomena, Oxford Press (1952)

8. L. Spitzer, Jr., Physics of Fully Ionized Gases, John Wiley and Sons, 2nd ed., pp. 139-141 (1962).

9. H. Dreicer, Physics Review, 115, 238 (1959) and 117, 329 (1960).

10. T. F. Stratton, AIAA Journal, 3, 1961 (1965).

11. J. R. Pierce, Theory and Design of Electron Beams, D. van Norstrad Co., Inc., 2nd ed. (1954), Ch. IX.

12. R. Lovberg, "Physical Processes in the Magneto-Plasmadynamic Arc," Second Semiannual Report (Mar. 1967).

13. A. C. Ducati, "Losses in Plasma Acceleration," Annual Technical Report TR 117-1743, AFOSR Contract AF 49(638)-1743 (Nov. 1967).

14. A. C. Ducati, "Study of Factors Effecting the Efficiency of Thermal Acceleration of Propellants," Final Technical Report covering 1 May 1962 thru 30 April 1965, Contract AF 49(638)-1161 (Oct. 1965).

15. A. C. Ducati, R. G. Jahn, E. Muehlberger and R. P. Treat, "Design and Development of a Thermo-Ionic Thruster," NASA CR-54703, FR-056-968, Prepared for NASA under Contract NASw-968 (May 1966).

REFERENCES

16. John R. Wheaton, Robert C. Dean, Jr., "Anode Gas- ath Electrical Breakdown - A High Pressure Arc Plasma Generator," Research Report from Thayer School of Engineering, Dartmouth College, (Oct. 1961).

17. C. Ekdahl, R. Kribel and R. Lovberg, "Internal Measurements of Plasma Rotation in an MPD Arc," AIAA Paper No. 67-655 (Sept. 1967).

18. Third Semiannual Report, NASA Grant NGR-05-009-030, University of California, San Diego (Nov. 1967).

19. D. Connolly, et. al., "Low Environmental Pressure MPD Arc Tests," AIAA J. 6, 1271 (1968).

20. A. Larson, "Experiments on Current Rotation in an MPD Engine," AIAA Paper No. 67-689 (Sept. 1967).

21. G. I. Cann, et al., "Magneto-Plasmadynamic Thruster Research," Technical Report EOS 7223-IR-1 (Nov. 1967).

22. R. A. Suehla, "Estimated Viscosities and Thermal Conductivities of Gases at High Temperatures," NASA, Technical Report R-132 (1962).

DOCUMENT CONTROL DATA - R & D

(Security classification of title, body of abstract and indexing annotation must be entered when the overall report is classified)

1. ORIGINATING ACTIVITY *(Corporate author)*	2a. REPORT SECURITY CLASSIFICATION
Plasmadyne, a division of Geotel, Inc. 3839 South Main Street Santa Ana, California	UNCLASSIFIED
	2b. GROUP

3. REPORT TITLE

EXPLORATORY ELECTROMAGNETIC THRUSTER RESEARCH, PHASE II

4. DESCRIPTIVE NOTES *(Type of report and inclusive dates)*

Scientific   Annual

5. AUTHOR(S) *(First name, middle initial, last name)*

Adriano C. Ducati   Erich Muehlberger
Robert G. Jahn   Richard P. Treat

6. REPORT DATE	7a. TOTAL NO. OF PAGES	7b. NO. OF REFS
June 1969	87	22

8a. CONTRACT OR GRANT NO. NAS w-1513 b. PROJECT NO. c. d.	9a. ORIGINATOR'S REPORT NUMBER(S) FR-069-1513 9b. OTHER REPORT NO(S) *(Any other numbers that may be assigned this report)*

10. DISTRIBUTION STATEMENT

11. SUPPLEMENTARY NOTES	12. SPONSORING MILITARY ACTIVITY National Aeronautics and Space Adm. Headquarters Contracts Division Washington, D. C. 20546

13. ABSTRACT

This report describes work done to evaluate the performance of MPD Thrusters. A large fraction of the effort is concerned with the effect of environmental conditions on the plume. It is becoming clear that a sizable portion of the arc power is expended externally in the plume, and that ambient gas is rapidly entrained in the jet in a region very close to the thruster. This combination of conditions can affect the thrust produced in a different manner for a test environment than for the environment expected in space. An increased effort on studies of the plume region is therefore considered appropriate.

A vacuum chamber made of insulating material is used to eliminate conducting paths for stray electrical currents and to avoid influencing the magnetic field in the region of the plume. Weak ambient magnetic fields were introduced by wrapping coils around the outside of the test chamber so that the effects of a changing ambient field could be observed. This was found to be a useful diagnostic tool.